WARSAW UNIVERSITY
OF TECHNOLOGY

Faculty of Electronics and Information Technology

Ph.D. THESIS

Karol Paweł Klincewicz, M.Sc.

Methods of single-frequency network transmitters localisation and time desynchronisation estimation applied to passive radiolocation

Supervisor
Piotr Samczyński, Ph.D., D.Sc., Professor at WUT

Warsaw, 2023

Streszczenie

Wraz z rozwojem dziedziny radiolokacji pasywnej pojawiają się nowe wyzwania i potrzeby, które wymagają ulepszenia narzędzi planowania misji oraz rozwiązań wspomagających stabilną pracę radaru. Jedną z niezbędnych informacji dla systemów radarów pasywnych jest precyzyjna lokalizacja nadajników okazjonalnych. Kompleksowe przygotowania w tym zakresie nie zawsze są możliwe, zwłaszcza gdy miejsce rozmieszczenia systemu radarowego często się zmienia, infrastruktura lokalnych nadajników jest regularnie modyfikowana lub rozmieszczenie systemu jest przeprowadzane na terytorium, na którym użytkownik nie może potwierdzić dostępności i lokalizacji nadajników. Taka sytuacja może doprowadzić do efektu pracy nadajników okazjonalnych w sieci jednoczęstotliwościowej (ang. single frequency network, SFN). Aby sprostać tym wyzwaniom, autor proponuje dwie metody wspomagające działanie radaru pasywnego. Pierwszą z nich jest metoda lokalizacji drugorzędnych i nierozpoznanych nadajników pracujących w SFN wspólnie z silnymi nadajnikami, których istnienie było przewidywane lub znane a priori. Większość analiz pasywnych systemów radarów operujących w SFN skupia się na usuwaniu lub filtrowaniu efektów ubocznych pracy w SFN. Zaproponowany w niniejszej rozprawie algorytm konstruktywnie wykorzystuje, powszechnie uznawane za niepożądane, wykrycia w korelacji wzajemnej sygnałów z pary odbiorników systemu radarowego. Druga z zaproponowanych metod pozwala na estymację desynchronizacji czasowej nadajników DVB-T pracujących w SFN. Powszechnym założeniem w literaturze związanej z radiolokacją pasywną jest, że nadajniki w SFN są w pełni zsynchronizowane czasowo. W ramach niniejszej pracy autor podważa to założenie i przedstawia algorytm pozwalający na estymację wartości desynchronizacji czasowej, którą można wykorzystać w dalszym procesie przetwarzania sygnału w radarze pasywnym. Pokazano, że pomijanie problemu desynchronizacji w przetwarzaniu sygnału radaru pasywnego może prowadzić do istotnych błędów w pozycjonowaniu celu. Opisana metoda może pomóc ograniczyć te błędy. W niniejszej rozprawie porównano i oceniono różne algorytmy lokalizacji nadajników pod kątem ich możliwości i ograniczeń w rozwiązywaniu równań hiperbolicznych. Do weryfikacji wyników teoretycznych wykorzystano symulacje komputerowe, które wykazały dokładność analizy i przydatność dwóch zaproponowanych metod. Dodatkowo przedstawiono wyniki przetwarzania sygnałów pozyskanych z wykorzystaniem demonstratora radaru pasywnego opracowanego na potrzeby niniejszej pracy.

Słowa kluczowe: *radar, radar pasywny, sieci jednoczęstotliwościowe.*

Abstract

With the development of the field of passive radiolocation, new challenges and demands arise that require improvements in mission planning tools and solutions to support stable radar operation. One of the essential pieces of information for passive radar systems is the localisation of illuminators of opportunity. Exhaustive preparations in this matter are not always possible, especially when the radar system deployment position is frequently changed, or the local transmitter's infrastructure is often modified. This situation can introduce the effect of illuminators of opportunity working in a single frequency network (SFN). To address these challenges, the author proposes two methods to aid passive radar performance. The first of the two is a method for localising secondary and unidentified transmitters operating in SFN together with strong transmitters whose existence was anticipated. Most of the analyses of passive radar systems working in an SFN focus on removing or filtering the side effects of operating in an SFN. The algorithm proposed in this thesis constructively exploits detections, commonly considered undesirable, in the cross-correlation function of signals from a pair of radar system receivers. The second is a method for estimating the desynchronisation of DVB-T transmitters operating in SFN. A common assumption in passive radar signal processing is that SFN transmitters are fully time-synchronised. The author challenges that assumption and provides an algorithm that provides a desynchronisation estimate that can be used in further passive radar signal processing. The author shows that ignoring desynchronisation in passive radar processing may lead to substantial errors in target positioning. The described method can help alleviate those errors, significantly improving passive radar performance. In this thesis, different transmitter localisation algorithms have been compared and evaluated for their ability to solve the hyperbolic equations. Computer simulations were used to verify the theoretical findings, which demonstrated the accuracy of the analysis and the relevance of the two proposed innovative methods. Additionally, this dissertation presents the results of processing signals recorded using a passive radar demonstrator developed for the purposes of this work.

Keywords: *radar, passive coherent location, single frequency network.*

Acknowledgements

First and foremost, I am extremely grateful to my supervisor, Prof. Piotr Samczyński, for his continuous support, comprehensive assistance, and understanding, which I have experienced for many years.

My gratitude extends to all my colleagues in the Radiolocation Techniques Division, especially Dr. Karol Abratkiewicz, for his insightful comments and suggestions on the original version of the text, which resulted in the elimination of many errors.

Finally, I would like to thank my wife, Agnieszka. I would not have been able to get to the point where I am today without her love, encouragement, and undying support.

Contents

List of Acronyms

2-D	two-dimensional
3-D	three-dimensional
ADC	Analog-to-Digital Converter
AOA	Angle Of Arrival
CA-CFAR	Cell Averaging Constant False Alarm Rate
CFAR	Constant False Alarm Rate
COTS	Commercial off-the-shelf
CUT	Cell Under Test
DAB	Digital Audio Broadcasting
DAC	Digital-to-Analog Converter
DOA	Direction Of Arrival
DVB-T	Digital Video Broadcasting–Terrestrial
FM	Frequency Modulation
GSM	Global System for Mobile Communications
GPS	Global Positioning System
LS	Least Squares
LTE	Long-Term Evolution
OFDM	Orthogonal Frequency-Division Multiplexing
PC	Personal Computer
PCL	Passive Coherent Location
RF	Radio Frequency
RMS	Root Mean Square

RSS	Received Signal Strength
SDR	Software Defined Radio
SFN	Single Frequency Network
SNR	Signal-to-Noise Ratio
TDOA	Time Difference of Arrival
TOA	Time Of Arrival
USRP	Universal Software Radio Peripheral
UWB	Ultra WideBand
WLS	Weighted Least Squares

List of Symbols

c	speed of light in vacuum
D_{AB}	Cartesian two-dimensional distance between positions A and B
G_{AB}	Cartesian three-dimensional distance between positions A and B
I	identity matrix
f_s	sampling rate
$\mathbf{x}_{2D}$	two-dimensional source position
$\mathbf{x}_{3D}$	three-dimensional source position

1. INTRODUCTION

Radar technology has become an important part of modern technology, both civil and military. Today's use of radar has surpassed its original application. Even the original name of radar, derived from the meaning Radio Detection And Ranging, does not cover the full spectrum of today's applications. Radar is not only limited to ranging and detection. Its purposes include, among others, measurement of object speed, acceleration, and target identification, automotive sensing, as well as imaging of planetary surfaces and flying objects [1][2]. Even in military technology, its first and best-known field of application, it continues to evolve and improve with the ever-changing challenges of the battlefield.

Two of these are the growing presence of stealth technology and the importance of electronic countermeasure warfare. Both are critical elements in the effectiveness of air warfare and can radically change the outcome of military operations. To meet the challenges posed by these two capabilities, passive radar systems, also known as Passive Coherent Location (PCL) systems, have been proposed [3]. The central idea of PCL radars is to use existing transmissions rather than emitting their own radio wave. At any given time, there are several commercial transmissions, e.g. Frequency Modulation (FM) radio, Digital Video Broadcasting – Terrestrial (DVB-T), Digital Audio Broadcasting (DAB), Global System for Mobile Communications (GSM), Long-Term Evolution (LTE), covering significant parts of the lower airspace, especially over cities and populated areas.

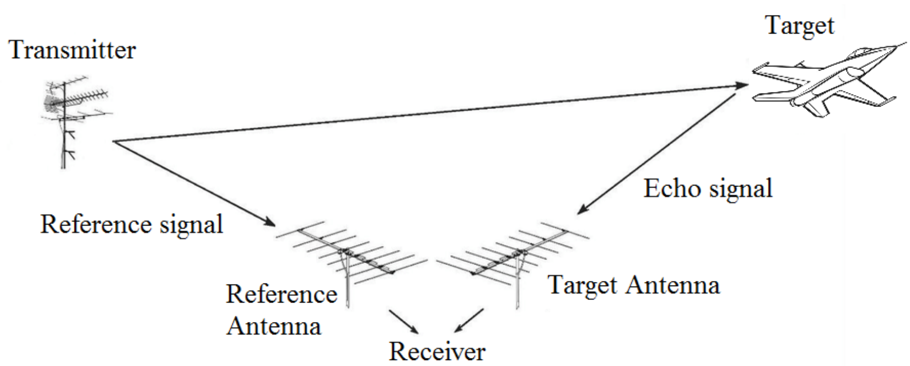

Figure 1. Passive radar principle visualization.

In the simplest design, passive radar, as shown in Figure **1**, has two receive channels. A "reference" channel collects the direct broadcast signal from a transmitting source, and a second called the surveillance channel, receives potential echoes of this broadcast.

The presence of such an echo indicates a possible target within the radar's range. If this is the case, the signal from the illuminator of opportunity will be reflected by the target and the echo received by the surveillance antenna will be shifted in time (due to the longer distance of wave propagation), shifted in frequency (due to the Doppler effect), and, of course, at orders of magnitude lower power level (due to the distance and target reflection losses). By comparing the direct signal with the surveillance signal and taking into account the relevant positions of the passive radar and the illuminator of opportunity, it is possible to determine the bistatic range. The target's position can be estimated from multiple bistatic ranges.

One of the greatest advantages of passive radar is its potential ability to detect stealth aircraft [4]. In stealth technology, the main concern is to design aircraft in such a way that, when illuminated by a radar, the incident signal is not reflected back in the direction from which it came but is scattered in some other direction. This technique is efficient with active radars, but the multistatic nature of passive radars mitigates this advantage in most cases. The fact that the transmitter and receiver are separated by a relatively large distance allows more situations where the geometry favours detection of the stealth target. In addition, most of the illuminators used by passive radar systems transmit at low frequencies compared to active radars. The wavelengths corresponding to these frequencies are comparable to those of most aircraft structures (e.g. wings, tail, stabilisers). As a result, resonance phenomena occur and the target's echo is amplified. Finally, the radar-absorbing material used in the coatings of stealth aircraft is designed to maximise its properties when absorbing shorter wavelengths and is less efficient at lower frequencies. This makes the task of hiding the aircraft from passive radars much more difficult.

Another important advantage of passive radars is their electromagnetic invisibility (covert sensing). The fact that such a system does not emit any radiation makes all modern countermeasures or self-protection systems useless. Passive radar stations are virtually impervious to jamming and decoy techniques and cannot be targeted by anti-radiation missiles. The absence of transmitters or any moving parts can significantly reduce production, operation and maintenance costs. Because passive radar receivers operate at low frequencies (typically below 1GHz [5][6][7][8]), they eliminate many complicated and costly radio frequency (RF) components. With recent advances in RF sampling technology, it is possible to further reduce the cost and simplify the design of passive radar analog front-ends.

On the other hand, passive radar technology has its challenges and disadvantages. The most important and unavoidable is the dependence on external transmitters. The radar user cannot control key characteristics of the transmitter such as its position, power and antenna radiation pattern. Geometry and radiation pattern of most emitters of opportunity determine the inability of passive radars to detect targets at higher altitudes (emitters tend to transmit signals parallel to the earth's surface). In addition, the signals themselves are designed for telecommunications or data transmission, not for radiolocation. This presents a number of challenges that add to the already complicated digital signal processing of passive radar. This complexity is the main obstacle to overcome in the development of passive radar systems, since in addition to the classical radar digital signal processing tasks, many problems that do not occur in active radars have to be overcome. The list includes problems such as adaptive filtering, cartesian localisation from bistatic data sets, as well as the reconstruction of transmitted signals [9][10], and the synchronisation of separated receivers. Despite these problems and difficulties, passive radiolocation systems could and should be developed and used as a natural complement to a network of low frequency active radars. A passive system would enhance and, in favourable circumstances, exceed the performance of its active counterpart.

1.1. Motivation

The author's motivations for working on the topic of passive radar systems in a Single Frequency Network (SFN) environment stem from several considerations. The first of these was the desire to gain an insight into contemporary trends in of one of the most dynamically developing radiolocation techniques in the world, i.e. the techniques of signal processing in passive radars. Frequent contact with the subject during his education and career has led the author to take a broader interest in the passive coherent location radar systems.

The second consideration is the scarcity of publications in the literature on the challenges faced by passive radars operating in single frequency networks. The vast majority of publications dealing with the problem of passive radars are based on the assumption of full knowledge of the transmitters in the radar operating environment [11][12][13][14]. Another common assumption is full synchronisation of illuminators of opportunity operating in SFN [15][16][17][18][19]. The author's aim is to draw attention to those issues.

Passive radar technology, after nearly three decades, has reached a stage of maturity in recent years and become an attractive addition to their active counterparts in world of electronic warfare and surveillance [20]. Passive radars are facing multiple challenges such as complex signal processing algorithms, inevitable multistatic nature or dependency on external sources of signal. With growing number and complexity of a passive radar applications and prototypes [3][5][6][7][8] so does the demand for better tools necessary for thorough mission planning, proper setup and stable radar operation. One of the essential information for passive radar systems is localisation of illuminators of opportunity. Exhaustive preparations in this matter is not always possible, especially when radar system deployment position is frequently changed or local transmitter infrastructure is often modified. Such changes may affect both transmitters localisation and frequency of operation. On top of steady growth of commercial emitter complexity used as possible illuminators of opportunity force passive radars to operate with transmitters working in SFN configuration. SFN is commonly used in uplands and urban regions when additional transmitters are needed to fully cover entire area of interest. This situation can introduce previously unexpected, but impactful effects and challenges in signal processing or, if no countermeasures are taken, false positives target detections. The constantly evolving reality of commercial transmitters such as DVB-T networks, and particularly the increasing use of single-frequency transmitters, will compel designers and users of passive radars to develop new solutions and tools necessary to maintain the proper functioning of these radars. The author of this thesis, who is involved in research projects closely related to passive radiolocation is trying to highlight and address some of these challenges.

Taking into account such situation, the author presents two novel methods that are crucial for passive radar system using illuminator of opportunity working in SNF. First of them is the method of calculating desynchronisation value of SFN transmitters. The second one is the method of localisation of additional previously unknown transmitter working in SFN with expected or known receiver. The methods proposed by the author are based on Time Difference of Arrival (TDOA) technique and do not require any additional hardware beyond classical passive radar receivers.

1.2. Goal and Aims of the Thesis

This thesis has two main objectives. The first goal is to contribute to passive radar systems by providing a reliable mechanism for estimating the desynchronisation of transmitters operating in SFN. This mechanism will improve the localisation accuracy and overall performance of passive radars in new, previously unexplored areas. Second objective is to assist passive radars by presenting a novel method for localising weak and unidentified transmitters operating in SFN together with strong transmitters whose existence was anticipated.

Both methods are useful tools for passive radar users during the mission planning phase and during radar operation. Both objectives have been achieved through the development and field testing of the algorithms described in detail in this thesis.

The theses of this dissertation are as follows:

It is possible to estimate the value of time desynchronisation of DVB-T transmitters operating in single frequency network using only the time difference of arrival measurements.

It is possible to localise secondary DVB-T transmitter operating in single frequency network using only the time difference of arrival measurements from pair of receivers.

1.3. Contributions Made by this Thesis

The author's innovative achievements are as follows:

- Conducting a comprehensive TDOA transmitter localisation techniques analysis;
- Development of a novel algorithm for estimating desynchronisation of transmitters operating in single frequency network [21];
- Development of a novel algorithm for localising secondary transmitters operating in Single Frequency network;
- The design and construction of a system comprising synchronized portable receivers and a central processing station. System was built using Commercial Off-The-Shelf (COTS) components and is capable of processing data in real time [22];
- Verification of the developed algorithms on simulated and experimental data [21].

1. Layout of the Thesis

The thesis is structured into seven chapters.

Chapter 2 provides the fundamentals of passive radars, including the bistatic geometry, the bistatic radar range equation, and the cross-ambiguity function. This chapter lays the foundation for the localisation techniques and SFN discussed in later chapters.

Chapter 3 focuses on various localisation techniques used in passive emitter localisation, including received signal strength, angle of arrival, time of arrival, and time difference of arrival. The chapter then dives into TDOA based source-localisation algorithms, discussing methods such as Friedlander's, Taylor-Series, Fang's, Chan's and Ho's, Spherical-Intersection, and Spherical-Interpolation. This chapter also provides a conclusion for the TDOA localisation techniques.

Chapter 4 discusses SFN in passive emitter localisation. The chapter begins with a description of the localisation of an unknown SFN transmitter algorithm. A detailed description includes all the algorithm steps: signal conditioning and cross-correlation, TDOA detection, cross-correlation results permutation, and curves intersection. The chapter then delves into SFN desynchronisation and its impact on passive radar. Finally, the time desynchronisation value calculation algorithm and all its steps are presented.

Chapter 5 covers simulations, where a signal model is presented, and various scenarios are simulated to test TDOA localisation, localisation of an unknown SFN transmitter, and desynchronisation calculation.

Chapter 6 discusses trials and experiments carried out to validate the simulation results. The chapter details the hardware used, the geometry of the transmitters, and two scenarios tested. The signal analysis, TDOA peak detection, localisation of an unknown SFN transmitter, and desynchronisation calculation are also discussed.

Finally, chapter 7 provides a summary of the thesis, highlighting the main contributions, and outlining future work that can be carried out in this field.

2. PASSIVE RADARS FUNDAMENTALS

2.1. Bistatic geometry

Passive radar operates on a different basis than active radar. In a traditional, active radar system, the signals transmitting and receiving modulus share the same antenna array, so by definition, both the transmitter and receiver are located in the same place. This configuration can be described as a radar monostatic geometry. In classical active radar, the position of the target is determined by measurements of its relative position in range, azimuth angle, and elevation angle. Constant-range measurement define the circle (two dimensions) or sphere (three dimensions) on which the target is located. After considering measured angles, it is possible to find precise spherical coordinates for the target.

In case of passive radars situation is far more complicated. In passive systems transmitter, also known as illuminator of opportunity, works independently of radar system. This creates a pair of receiver (Rx) and transmitter (Tx) working in` bistatic configuration.

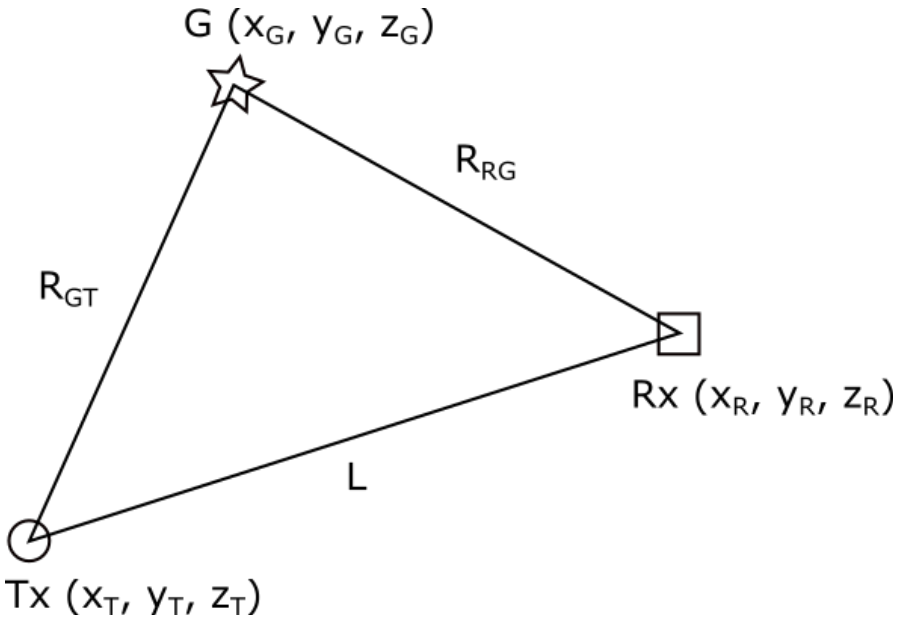

Figure 2. Bistatic geometry example.

Let us consider such geometry as shown in Figure **2** with a single target G described in cartesian coordinates as $(x_G,\ y_G,\ z_G)$. Assuming that receiver Cartesian coordinates are (x_{Rx}, y_{Rx}, z_{Rx}) and transmitter Cartesian coordinates are (x_{Tx}, y_{Tx}, z_{Tx}), both not changing in time, the distance between receiver and target is equal to

$$R_{RxG} = \sqrt{(x_G - x_{Rx})^2 + (y_G - y_{Rx})^2 + (z_G - z_{Rx})^2}, \tag{1}$$

the distance between transmitter and target is equal to

$$R_{GTx} = \sqrt{(x_G - x_{Tx})^2 + (y_G - y_{Tx})^2 + (z_G - z_{Tx})^2}, \tag{2}$$

and the distance between transmitter and receiver, often called the baseline, is equal to

$$L = \sqrt{(x_R - x_{Tx})^2 + (y_R - y_{Tx})^2 + (z_R - z_{Tx})^2}. \tag{3}$$

The range measured by passive radar is known as the bistatic range and is defined as

$$R_B = R_{RxG} + R_{GTx} - L. \tag{4}$$

In monostatic geometry, a constant range measured by radar defines a sphere (or circle in two-dimensional geometry) with the radar position as the centre [23]. In the case of bistatic geometry, a constant bistatic range defines an ellipsoid (or ellipse circle in two-dimensional geometry) with transmitter and receiver positions as the focal points. Moreover, it is much more complicated to find azimuth and elevation angles. Passive radiolocation is restricted by the available illuminators and the bands on which they operate. Most of them use relatively low frequencies [3], ranging from about 80 MHz (FM) to 940 MHz (upper DVB-T channels and GSM [8][24]). Operating at such wavelengths forces passive radar antennas to have considerable size and limits the use of phased-array antennas with narrow main lobes due to challenging mechanical design. Because of this, it is common for passive radars to experience big angle measurement errors (when a couple antenna elements are used) or not measure angles of arrival at all (in the case of only one antenna). There are, of course, a wide range of papers that take other frequencies into account [25], but they don't provide the long-range capabilities of high-power, low-frequency illuminators.

2.2. The bistatic radar range equation

The radar range equation is a useful tool in radar design as it links the specification of the main operating parameters with detection performance in a concise fashion. It relates the range of a radar to the characteristics of the transmitter, receiver, antenna, target, and distance. In bistatic radar geometry, the range equation is similar to its monostatic equivalent but must be adjusted for the fact that the transmitter and receiver are not located in the same place. The signal emitted by the transmitter illuminates the target and is then reflected, scattering in all directions. A portion of the reflected signal power is then acquired by the radar receiver and can be stated as [4]

$$P_{Rx} = \frac{P_{\mathrm{Tx}} G_{\mathrm{Tx}} G_{\mathrm{Rx}} \sigma_b \lambda^2 L_{\mathrm{add}}}{(4\pi)^3 R_{\mathrm{TxG}}^2 R_{\mathrm{RxG}}^2}, \tag{5}$$

where P_{Tx} is the power radiated by the transmitter, G_{Tx} is the antenna gain of the transmitter, G_{Rx} is the antenna gain of the receiver, σ_b is the bistatic radar cross section (RCS) of the target, λ is transmitter wavelength, and L_{add} stands for all additional losses in the radar system (due to transmission lines, antenna losses, additional atmospheric losses, etc.).

Based on the equation (5), it is possible to find a formula for the signal-to-noise ratio (SNR):

$$\mathrm{SNR} = \frac{P_{\mathrm{Rx}}}{P_N} = \frac{P_{\mathrm{Tx}} G_{\mathrm{Tx}} G_{\mathrm{Rx}} \sigma_b \lambda^2 L_{\mathrm{add}}}{(4\pi)^3 R_{\mathrm{TxG}}^2 R_{\mathrm{RxG}}^2 k_B T_0 B_{\mathrm{Rx}}}, \tag{6}$$

where P_N is noise power, k_B is Boltzmann's constant, T_0 is reference temperature, and B_{Rx} is receiver bandwidth.

Signal detection is possible only when the power of the received signal is greater than the noise power, i.e., when the SNR is positive. In order to increase SNR, it is common to use coherent integration. This technique allows for an increase in SNR by a factor of BT , where B is the signal bandwidth and T is the signal integration time.

2.3. Cross-ambiguity function

One of the most important stages in passive radar signal processing is calculating the cross-ambiguity function of the measured signal x_{ef} and the reference signal x_r. Cross-ambiguity function provides a measure of the similarity between those signals in time and doppler domains and plays a crucial role in radiolocation by enabling radar systems to detect and locate objects in a reliable and accurate manner. In practice, it is equivalent to calculating the correlation between time- and phase-shifted reference signals and measured signals. In signal processing, the cross-ambiguity function between any two signals $x(t)$ and $y(t)$can be defined as

$$\psi(\tau, f) = \int_{-\infty}^{\infty} y(t) x^*(t-\tau) e^{-j2\pi f t} \mathrm{dt}, \tag{7}$$

where * denotes conjugation, f is frequency shift, τ is the relative time delay.

To properly relate this equation to radar signal processing, some changes must be made. Firstly, signals x(t) and y(t) must be redefined as actual signals gathered by a bistatic pair: x_{ef} and x_r respectively. Secondly, conversion of the time delay τ into the bistatic range was made. Finally, because the signals under consideration are discrete, the equation can be rewritten as

$$\psi(R_B, V_B) = \sum_{n=-\frac{N_s}{2}}^{\frac{N_s}{2}-1} x_{ef}(n) {x_r}^* \left(n - \frac{R_B f_s}{c}\right) e^{-j2\pi \frac{V_B}{\lambda f_s} n}, \tag{8}$$

where N_s is number of samples of signals and f_s is the signal sampling rate.

3. Localisation techniques in passive emitter localisation

Passive emitter localisation has been a subject of great interest for decades and still receives great interest in the signal processing research community, including radiolocation. Many indoor and outdoor applications benefit from constant advancements in this field. Different proposed position estimation algorithms make use of different measurements of the transmitted signal's characteristics, such as received signal strength (RSS), angle of arrival (AOA), or time of signal propagation. The latter can be divided into TDOA and Time of Arrival (TOA) techniques.

3.1. Received signal strength

The most basic technique of localising the source of the signal It is commonly used for localising sensor nodes in wireless networks. Since RSS requires only the ability to measure the strength of the received signal, it is easily implementable in Wi-Fi [26], Ultra WideBand (UWB) [27], infrared data association Zigbee [25], and Bluetooth [28] technologies. The RSS technique benefits from the fact that RF signals diminish with the square of the distance from the signal source. By measuring the power of the received signal and comparing it to the power of the transmitted signal, the receiver can calculate its distance from the transmitter. In order to measure distance correctly, an accurate signal attenuation model needs to be chosen.

Of course, a single measurement is not enough to localise the source of emission. Therefore, multiple receivers must be employed. By measuring corresponding transmitter power levels at receivers and using triangulation techniques, it is possible to calculate the emitter's position (Figure **3**). When wave propagation is taking place in free space, a simple direct line of sight (LOS) propagation model may be enough to measure RSS properly. However, when wave encounter any obstacle, the attenuation model must be modified accordingly.

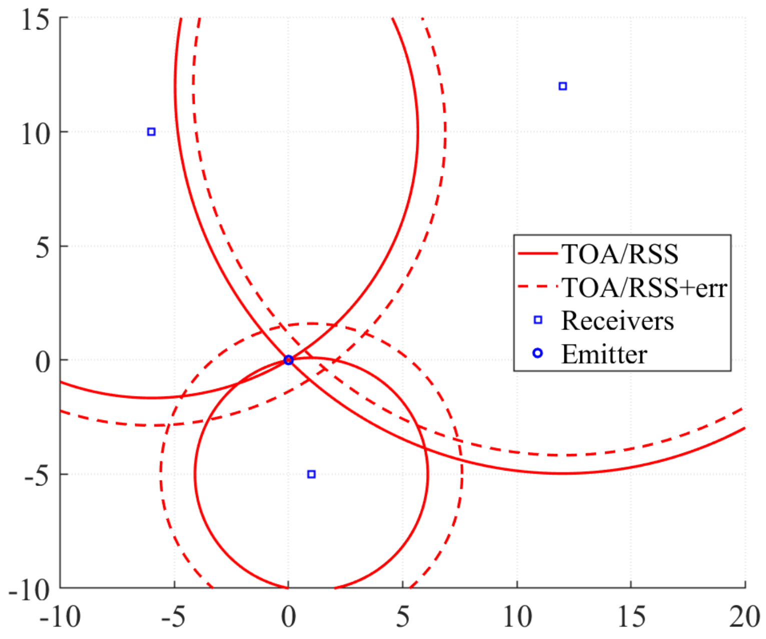

Figure 3. TOA/RSS geometry visualization.

RSS localisation method is a simple and inexpensive. It does not require any kind of time synchronization and performs well in small, controlled environments. Unfortunately, due to its low accuracy, lack of a reliable attenuation model, and susceptibility to multipath and shadow fading, it is utterly useless in large-scale passive radar systems.

3.2. Angle of arrival

Another method of locating the source of emission is to find the angle of arrival (AOA), also known as the direction of arrival (DOA). Most of the applications utilizing AOA are based on one of two possible solutions: beamforming or a rotating antenna.

Beamforming is a signal processing technique that controls the phase and relative amplitude of the signal at each receiver to achieve directional signal transmission or reception [4][29][30]. The general concept of beamforming is to create a pattern of interferences: constructive at the desired angle and destructive in all other directions. This technique comes down to designing a phased-array antenna and can be archived by either analog or digital means. In the case of an analog beamformer, there is an analog front-end composed of a phase shifter and gain control (combination of high power and low noise amplifiers) behind every antenna element. Every channel's front end introduces different phase shift and gain, therefore forming the desired radiation pattern. Then signals from all channels are summed in an analog RF combiner and sampled. Depending on the character of the used elements, analog beamforming can form a single beam (fixed values of phase shifters) or the direction of a phased array can be steered by controlling the RF phase of each element prior to combining all signals.

If there is a possibility to use receiver with ADCs for every antenna in the array, beamforming can be done in the digital domain, phase shifts and amplitude weighting are applied digitally on each channel. The digital sum of the signals from those channels forms the antenna pattern. This solution is superior due to the possibility of forming multiple beams simultaneously. Both analog and digital solutions require carefully designed and constructed antenna arrays that are relatively large and expensive. Simplified visualisation of antenna array block diagram for beamforming is presented on Figure **4**.

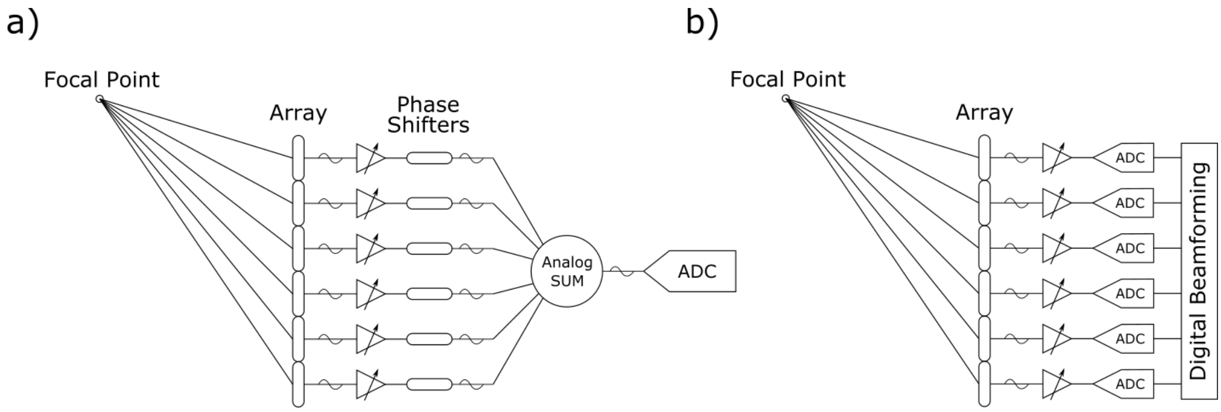

Figure 4. Block diagram of a) analog beamforming b) digital beamforming.

Use of a rotating directional antenna (e.g., a high-gain antenna) is an alternative to beamforming. A robust AOA measurement can be made by mounting a directional antenna onto a rotator and periodically scanning the horizon. The best results can be achieved by combining those two approaches. By rotating an analog or digital beamformer, it is possible to cover the entire horizon with a narrow phased array antenna and achieve a precise AOA estimate. Further improvements of the measurement precision, regardless of the chosen method, can be made by digital signal processing [31][32][33].

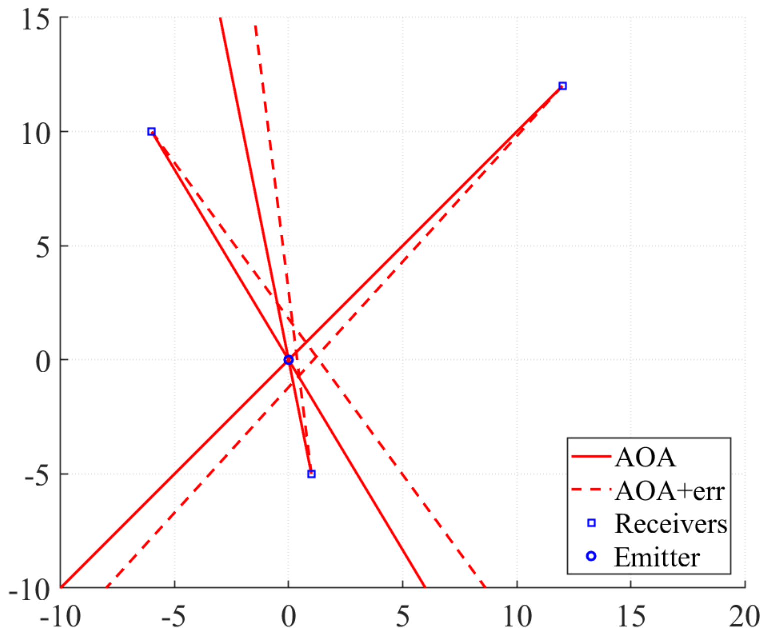

Figure 5. AOA geometry visualization.

The measured angle forms a straight line on which the target can be found (Figure **5**). Two such measurements from two receivers need to be acquired to locate the source of emission (considering 2D). The transmitter is located at the intersection of AOA lines. In practical solutions, where signals are corrupted by noise and other measurement errors, the estimated localisation of the emitter will differ from the actual localisation (dotted red line in Figure **5**).

3.3. Time of arrival

The TOA technique is a method used to estimate the location of a transmitter by measuring the time it takes for a wave to travel from the transmitter to a receiver. This technique is commonly used in wireless communication systems and radar systems to locate the position of an emitter. Ranges are calculated by multiplying TOA by the speed of light in the appropriate medium (e.g., air or vacuum).

In a two-dimensional space, TOA from each sensor, similarly to classical active radar, determines a circle. If measured with high accuracy and assumed to be free of noise, at least three such measurements from different receivers are needed to estimate the source's location. The position of the source is at a single point where all three circles intersect. Just as in the case of AOA, when signals are corrupted by noise and other measurement errors, there can be no such triple intersection (see dotted red lines in Figure **3**). In such a case, simple multilateration will yield only multiple double intersections. The estimated emitter position can then be obtained by solving for an optimal solution. Analogously, in a three-dimensional space, the emitter location locus for each TOA is the surface of a sphere. Three TOA sphere surfaces intersect at two points; therefore, a fourth TOA is needed to find the position of the emitter. Though TOA techniques offer high accuracy, time synchronization of the emitter, and all receivers are needed for one-way ranging. The requirement of any kind of cooperation from the source of emission discredits TOA as a legitimate technique in passive radars.

3.4. Time difference of arrival

The time difference of arrival (TDOA) localisation method is based on the difference in signal propagation time between an unknown emitter and two or more receivers. Time difference is calculated by comparing signals collected by sensors and finding corresponding time shifts. In the case of continuous transmission, a single TDOA measurement can be made by cross-correlating the signals received at two different sensors. Alternatively, when impulse signals are considered, TOA measurements can be gathered at the receivers and converted into TDOA measurements by calculating the differences. Regardless of method, once TDOA estimates are gathered, they are recalculated into range differences using the wave velocity equation. Next, these measurements can be converted into nonlinear hyperbolic (2-D) or hyperboloid (3-D) equations. Each pair of receivers defines the foci of a corresponding hyperbola (or hyperboloid), and the source of emission is located at the intersection of those curves (or surfaces) as shown in Figure **6**.

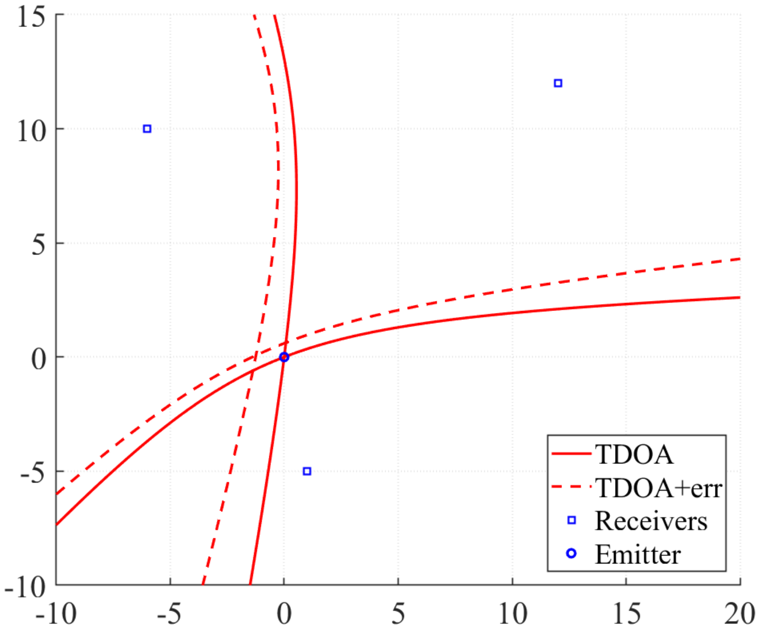

Figure 6. TDOA geometry visualization

Just as in the case of previously discussed localisation methods, in the presence of measurement error (dotted red line in Figure **6**) curves intersection point will deviate from the real position of emitter. A detailed analysis of this phenomenon using simulation data is given in Chapter 5.2.

A major advantage of this TDOA method is that it does not require any knowledge of the transmission timing from the source, as in TOA. Consequently, no synchronization between the transmitter and receivers is required. As a result, it is a viable method of localising emitters in passive radiolocation. However, strict synchronization is required of all used receivers. In both 2-D and 3-D case mentioned equations are non-linear and solving them is not a trivial operation. Multiple algorithms were proposed throughout the years to solve this problem. In chapter 3.5 some of popular TDOA based source-localisation algorithms will be briefly described. General idea behind each of them will be presented and advantages as well as disadvantages will be presented.

3.5. TDOA based source-localisation algorithms

Before presenting different algorithms, let us explore the two-dimensional geometry of TDOA. The distance between positions A (x_A, y_A) and B (x_B, y_B) can be defined as

$$D_{AB} = \sqrt{(x_A - x_B)^2 + (y_A - y_B)^2}. \tag{9}$$

A general model for two-dimensional emitter localisation estimation using N receivers is developed. Referring all TDOAs to the first receiver Rx_1, which can be picked at random, let's refer to the rest of the receivers with index $i = 2, \dots, M$. The unknown source location will be defined as $Tx(x_{Tx}, y_{Tx})$ and the known location of i-th receiver will be defined as $Rx_i(x_{Rxi}, y_{Rxi})$. Knowing that the distance between the transmitter and the i-th receiver is D_{Rx_iTx}, let the range difference between the i-th receiver with respect to the first receiver be

$$\Delta D_{i,1} = c\Delta t_{i,1} = D_{TxRx_i} - D_{TxRx_1}, \tag{10}$$

where c is the signal propagation speed and $\Delta t_{i,1}$ is TDOA between receivers Rx_1 and Rx_i. Considering multiple pairs of receivers create the set of nonlinear hyperbolic equations whose solution gives the 2-D coordinates of the transmitter. Solving this linear system is an exigent task. One common approach is to linearise them through the use of Taylor-series expansion and retaining the first two terms. Another approach is to rearrange (10) to

$$D_{TxRx_i}{}^2 = (\Delta D_{i,1} + D_{TxRx_1})^2, \tag{11}$$

and after expanding using (9)

$$\Delta D_{i,1}^2 + 2\Delta D_{i,1} D_{TxRx_1} + D_{TxRx_1}^2 = x_{Rx_i}^2 + y_{Rx_i}^2 - 2x_{Rx_i}x_{Tx} - 2y_{Rx_i}y_{Tx} + x_{Tx}^2 + y_{Tx}^2 \, . \tag{12}$$

Subtracting $D_{TxRx_1}^2$ from both sides

$$\Delta D_{i,1}^2 + 2\Delta D_{i,1} D_{TxRx_1} = K_i - 2x_{i,1}x_{Tx} - 2y_{i,1}y_{Tx} - K_1, \tag{13}$$

where $x_{i,1} = x_{Rx_i} - x_{Rx_1}$, $y_{i,1} = y_{Rx_i} - y_{Rx_1}$ and

$$K_i = x_{Rx_i}^2 + y_{Rx_i}^2. \tag{14}$$

This new set of equations with the transmitter location Tx and the range of the first receiver to the source D_{TxRx_1} as the unknowns are more easily handled. In case of 3-D approach all equations above can be easily extended by z-factor.

3.5.1. Friedlander's method

Friedlander's method [34] utilizes a Least Squares (LS) and a Weighted LS (WLS) error criterion to solve for the position location. First step is to transform (13) into

$$x_{i,1}x_{Tx} + y_{i,1}y_{Tx} = \frac{\left(K_i - K_1 - \Delta D_{i,1}^2\right)}{2} - \Delta D_{i,1} D_{TxRx_1}, \tag{15}$$

or using matrix notation for N receivers

$$\boldsymbol{S}\boldsymbol{x_{2D}} = \boldsymbol{u} - D_{TxRx_1}\boldsymbol{d} \, , \tag{16}$$

where

$$\boldsymbol{S} \triangleq \begin{bmatrix} x_{2,1} & y_{2,1} \\ \vdots & \vdots \\ x_{N,1} & x_{N,1} \end{bmatrix}, \tag{17}$$

$$\boldsymbol{x_{2D}} \triangleq [x_{Tx} \quad y_{Tx}]^T, \tag{18}$$

$$\boldsymbol{u} \triangleq \frac{1}{2}\begin{bmatrix} K_2 - K_1 - \Delta D_{2,1}^2 \\ \vdots \\ K_N - K_1 - \Delta D_{N,1}^2 \end{bmatrix}, \tag{19}$$

$$\boldsymbol{d} \triangleq [\Delta D_{2,1} \quad \cdots \quad \Delta D_{N,1}]\,. \tag{20}$$

In order to eliminate a second term of (16), which require position of Tx, it is necessary to multiply (16) by matrix **M** that fulfils the condition $\boldsymbol{Md} = 0$. The matrix

$$\boldsymbol{M^k} = (\boldsymbol{I} - \boldsymbol{Z}^k)\boldsymbol{D}\,, \tag{21}$$

where

$$\boldsymbol{Z} = \begin{bmatrix} 0 & 1 & & \\ & \ddots & \ddots & \\ & 0 & \ddots & 1 \\ 1 & & & 0 \end{bmatrix} \tag{22}$$

is a circular shift matrix and

$$\boldsymbol{D} = (diag\{\boldsymbol{d}\})^{-1}\,, \tag{23}$$

has this property for any value of k because $\boldsymbol{Dd} = \boldsymbol{I}$ and $(\boldsymbol{I} - \boldsymbol{Z}^k)\boldsymbol{I} = 0$. Let us use singular value decomposition (SVD) on $(\boldsymbol{I} - \boldsymbol{Z}^k)$:

$$\left(\boldsymbol{I} - \boldsymbol{Z^k}\right) = [\boldsymbol{U}_k, \boldsymbol{u}_k]\begin{bmatrix} \eta_1^k & & & 0 \\ & \ddots & & \\ & & \eta_{N-2}^k & \\ 0 & & & 0 \end{bmatrix}[\boldsymbol{V}_k, \boldsymbol{v}_k]^T = \\ \boldsymbol{U}_k diag\{\eta_1^k, \cdots, \eta_{N-2}^k\}\boldsymbol{V}_k^T\,, \tag{24}$$

where $\{\eta_1^k, \cdots, \eta_{M-2}^k\}$ are the non-zero singular values. Since $(\boldsymbol{I} - \boldsymbol{Z}^k)\boldsymbol{I} = 0$ it can be stated that $V_k^T I = 0$ and consequently the matrix M to eliminate the second term of (16) is then given by

$$\boldsymbol{M} = \boldsymbol{V}_k^T\boldsymbol{D}\,. \tag{25}$$

Multiplying (16) by matrix $\boldsymbol{M}$ results in N-2 linear equations

$$\boldsymbol{MSx_{2D}} = \boldsymbol{Mu}\quad. \tag{26}$$

A closed form solution to find the transmitter position can be computed using the LS solution of equation

$$\boldsymbol{x_{2D}} = (\boldsymbol{S}^T\boldsymbol{M}\boldsymbol{M}^T\boldsymbol{S})^{-1}\boldsymbol{S}^T\boldsymbol{M}\boldsymbol{M}^T\boldsymbol{u} \ . \tag{27}$$

As an alternative to LS solution Friedlander propose WLS solution. It can be used when zero-mean Gaussian noise is present in range difference measurements. Is such case, the transmitter position is given by

$$\boldsymbol{x_{2D}} = (\boldsymbol{S}^T\boldsymbol{M}\boldsymbol{W}\boldsymbol{M}^T\boldsymbol{S})^{-1}\boldsymbol{S}^T\boldsymbol{M}\boldsymbol{W}\boldsymbol{M}^T\boldsymbol{u} \ . \tag{28}$$

The weighting matrix $\boldsymbol{W}$ is given as

$$\boldsymbol{W} = [\boldsymbol{M}(diag\{\boldsymbol{d}\} + D_{TR_1}\boldsymbol{I})\boldsymbol{Q}(diag\{\boldsymbol{d}\} + D_{TR_1}\boldsymbol{I})\boldsymbol{M}^T]^{-1} \ , \tag{29}$$

where Q is the covariance matrix of the range difference measurements. Since **W** is a function of unknown parameter of D_{TxRx_1} Friedlander proposed to estimate its value by

$$D_{TxRx_1} = \frac{\boldsymbol{d}^T\boldsymbol{P}\boldsymbol{u}}{\boldsymbol{d}^T\boldsymbol{P}\boldsymbol{d}} \ , \tag{30}$$

where

$$\boldsymbol{P} = \boldsymbol{I} - \boldsymbol{S}(\boldsymbol{S}^T\boldsymbol{S})^{-1}\boldsymbol{S} \ . \tag{31}$$

Friedlander's method provides localisation of emitter for both minimal required number of sensors and over-determined systems. Simulation results suggests that when using minimal number of receivers, the LS and WLS solutions were identical [34]. However, for more than four base stations, the WLS localisation solution was superior to the LS solution. The main disadvantage of this method is a requirement of a priori knowledge of measurement variances.

3.5.2. Taylor-Series method

Taylor-series method is another method of passive emitter localisation [35]. What is interesting in this method is its flexibility. It can be successfully used in solving multiple measurement mixed mode location problems typical of any navigational applications including but not limited to TDOA geometry. The Taylor-series method linearizes (10) by Taylor-series expansion, then uses an iterative method to solve the system of linear equations:

$$\begin{bmatrix}\Delta x_{Tx}\\ \Delta y_{Tx}\end{bmatrix} = (\boldsymbol{G}_t^T\boldsymbol{Q}^T\boldsymbol{G}_t)^{-1}\boldsymbol{G}_t^T\boldsymbol{Q}^{-1}\boldsymbol{h}_t \ , \tag{32}$$

where

$$\boldsymbol{h}_t = \begin{bmatrix} D_{Rx_2Rx_1} - \Delta D_{2,1} \\ D_{Rx_3Rx_1} - \Delta D_{3,1} \\ \vdots \\ D_{Rx_NRx_1} - \Delta D_{N,1} \end{bmatrix}, \tag{33}$$

$$G_t = \begin{bmatrix} \frac{x_{Rx_1}-x_{Tx}}{D_{TxRx_1}} - \frac{x_{Rx_2}-x_{Tx}}{D_{TxRx_2}} & \frac{y_{Rx_1}-y_{Tx}}{D_{TxRx_1}} - \frac{y_{Rx_2}-y_{Tx}}{D_{TxRx_2}} \\ \frac{x_{Rx_1}-x_{Tx}}{D_{TxRx_1}} - \frac{x_{Rx_3}-x_{Tx}}{D_{TxRx_3}} & \frac{y_{Rx_1}-y_{Tx}}{D_{TxRx_1}} - \frac{y_{Rx_3}-y_{Tx}}{D_{TxRx_3}} \\ \vdots & \vdots \\ \frac{x_{Rx_1}-x_{Tx}}{D_{TxRx_1}} - \frac{x_{Rx_N}-x_{Tx}}{D_{TxRx_N}} & \frac{y_{Rx_1}-y_{Tx}}{D_{TxRx_1}} - \frac{y_{Rx_N}-y_{Tx}}{D_{TxRx_N}} \end{bmatrix}, \tag{34}$$

and **Q** is the covariance matrix of the TDOA measurements. In the first iteration the values of x_{Tx} and xy_{Tx} are given initial guess (x_0, y_0) and in next iterations are set to x_{Tx}=$x_0 + \Delta$x and y_{Tx}=$y_0 + \Delta$y. The algorithm keeps iterating until Δx and Δy are sufficiently small. Final values of x_{Tx} and xy_{Tx} are final estimates of transmitter position.

Taylor-series method provide accurate results and is robust but due to requirement of initial guess is prone to converge to local minima. Yet, with close initial location guess it will deliver reliable results even with presence of reasonable noise levels. This method is sensible to bad geometric dilution of precision i.e. when transmitter is located on a portion of hyperbola curve far away from both receivers. In such case relatively small TDOA measurement error can result in a large position location error. Taylor-Series method can also make use of redundant measurements further improving final solution. Since its iterative algorithm, this method can be computationally demanding.

3.5.3. Fang's method

Fang [36] proposed a specific 2-D coordinate system where first receiver is located in $(0, 0)$, the second in $(x_{Rx_2}, 0)$ and the third receiver in (x_{Rx_3}, y_{Rx_3}). Introducing these positions into (13) for $i = 2$ and $i = 3$, two equations takes form of

$$2\Delta D_{2,1} D_{TxRx_1} = -\Delta D_{2,1}^2 + x_{Rx_2}^2 - 2x_{2,1}x_{Tx}\,, \tag{35}$$

$$2\Delta D_{3,1} D_{TxRx_1} = -\Delta D_{3,1}^2 + K_3 - 2x_{3,1}x_{Tx} - 2y_{3,1}y_{Tx}\,. \tag{36}$$

Equating the two equations and simplifying results in

$$y_T = dx_{Tx} + e\,, \tag{37}$$

where

$$d = \frac{\frac{\Delta D_{3,1} x_{Rx_2}}{\Delta D_{2,1}} - x_{Rx_3}}{y_{Rx_3}}\,, \tag{38}$$

$$e = \frac{K_3 - \Delta D_{3,1}^2 + \Delta D_{3,1}\Delta D_{2,1}\left[1 - \left(\frac{x_{Rx_2}}{\Delta D_{2,1}}\right)^2\right]}{2 y_{Rx_3}}\,. \tag{39}$$

Substituting (37) into (35) results in

$$a{x_{Tx}}^2 + b x_{Tx} + c = 0\,, \tag{40}$$

where

$$a = \left(\frac{x_{Rx_2}}{\Delta D_{2,1}}\right)^2 - d^2 - 1\,, \tag{41}$$

$$b = x_{Rx_2}\left[1 - \left(\frac{x_{Rx_2}}{\Delta D_{2,1}}\right)^2\right] - 2de\,, \tag{42}$$

$$c = \frac{\Delta D_{2,1}^2}{4}\left[1 - \left(\frac{x_{Rx_2}}{\Delta D_{2,1}}\right)^2\right]^2 - e^2\,, \tag{43}$$

Solving (40) results in two possible values for x_{Tx}

$$x_{Tx} = \frac{-b \pm \sqrt{b^2 - 4ac}}{2a}\,. \tag{44}$$

One of roots can be eliminated by use of additional information or by fact that its value is out of measurements area of interest. With solution ambiguity resolved the other coordinate of the transmitter's position estimate can be found by putting correct value of x_{Tx} into (37).

Fang's method provides a closed form and exact solution and it is also computationally less intensive than the Taylor-series method. The major disadvantages of this method is the solution ambiguity and no utilization of redundant measurements (with additional receivers there is no improvement of position location accuracy).

3.5.4. *Chan's and Ho's method*

In Chan's and Ho's method [37], two situations are considered. First one is when three sensors are used resulting in two TDOA measurements. Similarly to Friedlander's method, Chan transforms (13) for $N = 3$ to find transmitter position:

$$\boldsymbol{x_{2D}} = -\boldsymbol{S}^{-1}\left(\boldsymbol{d}D_{TxRx_1} + \boldsymbol{h}\right), \tag{45}$$

where

$$\boldsymbol{h} = \frac{1}{2}\begin{bmatrix} \Delta D_{2,1}^2 - K_2 + K_1 \\ \vdots \\ \Delta D_{N,1}^2 - K_N + K_1 \end{bmatrix}, \tag{46}$$

and $N = 3$.

Next by inserting this result into (13) at $i = 1$ gives a quadratic equation in D_{TxRx_1}. Substitution of the positive root back into (45) produces the solution. In some geometries, there may be two positive roots that produce two distinct answers. Similarly to Fangs method, the solution ambiguity can be resolved by use of a priori information about transmitters position or by restricting the transmitter to lie within the region of interest. Chan and Ho stated that this solution is an equivalent to spherical-intersection method proposed by Schau and Robinson presented in chapter 3.5.5.

Second situation address the case when more than three sensors are available, thus number of TDOA measurements is greater than the number of variables (x_{Tx} and xy_{Tx}). In the presence of any measurement error, the results of the equations in (13) will have multiple points of intersection and the proper answer is the $\boldsymbol{x_{2D}}$ that best fit these equations.

First step is to define the unknown vector as

$$\boldsymbol{z} = [x_{Tx} \quad y_{Tx} \quad D_{TxRx_1}]^T . \tag{47}$$

It is also necessary to redefine the squared distance between the source and the sensor from a geometrical point of view:

$$D_{TR_i}{}^2 = \left(x_{Rx_i} - x_{Tx}\right)^2 + \left(y_{Rx_i} - y_{Tx}\right)^2 = \tag{48}$$

$$K_i - 2x_{Rx_i}x_{Tx} - 2y_{Rx_i}y_{Tx} + x_{Tx}{}^2 + y_{Tx}{}^2 .$$

With TDOA measurement noise, the error vector derived from (13) is

$$\boldsymbol{\psi} = \boldsymbol{h} - \boldsymbol{G}_a\boldsymbol{z}^{\boldsymbol{F}} , \tag{49}$$

where $\boldsymbol{z}^{\boldsymbol{F}}$ is noise free value of $\boldsymbol{z}$ and

$$\boldsymbol{G}_a = -\begin{bmatrix} x_{2,1} & y_{2,1} & \Delta D_{2,1} \\ x_{3,1} & y_{3,1} & \Delta D_{3,1} \\ \vdots & \vdots & \vdots \\ x_{N,1} & y_{N,1} & \Delta D_{N,1} \end{bmatrix}. \tag{50}$$

Remembering that the range difference between receivers are not noise-free since they are directly calculated from TDOA measurements. Chan's and Ho's method proved that when the SNR is high covariance matrix of (49) can be reduced to

$$\boldsymbol{\Psi} = \boldsymbol{E}[\boldsymbol{\psi}\boldsymbol{\psi}^{\boldsymbol{T}}] = c^2\boldsymbol{BQB}\ , \tag{51}$$

where $\mathbf{Q}$ is covariance matrix of the estimated TDOA vector $[\Delta t_{2,1}, \Delta t_{3,1}, \dots, \Delta t_{N,1}]^T$ and

$$\boldsymbol{B} = diag\{D_{TxRx_2}{}^F, D_{TxRx_3}{}^F, \dots, D_{TxRx_N}{}^F\}\,. \tag{52}$$

The components of $\boldsymbol{z}$ are related according to (48), implying that (49) represents a set of nonlinear equations in two variables x_{Tx} and y_{Tx}. To address this nonlinear problem, an initial assumption is made that there is no relationship between x_{Tx}, y_{Tx} and D_{TxRx_1}, which can then be solved using the least squares method. The resulting solution is applied to (48) through another least squares computation. This two-stage process approximates a true maximum likelihood estimator for transmitter position.

By treating the components of $\boldsymbol{z}$ as independent, the maximum likelihood estimate of $\boldsymbol{z}$ is

$$\boldsymbol{z} = \arg\min\{(\boldsymbol{h} - \boldsymbol{G}_a\boldsymbol{z})^T\boldsymbol{\Psi}^{-1}(\boldsymbol{h} - \boldsymbol{G}_a\boldsymbol{z})\} = (\boldsymbol{G}_a^T\boldsymbol{\Psi}^{-1}\boldsymbol{G}_a)^{-1}\boldsymbol{G}_a^T\boldsymbol{\Psi}^{-1}\boldsymbol{h}\ , \tag{53}$$

which can also be identified as the Generalized Least Squares solution of (49). The remaining problem is that the covariance matrix $\boldsymbol{\Psi}$ is unknown, since $\boldsymbol{B}$ contains noise-free distances between transmitter and receivers. To solve this problem, another approximation is required. Chan and Ho consider two situations. First when the transmitter is far from the receiver array i.e. each $D_{TxRx_i}^F \approx D_A$ and therefore (52) become

$$\boldsymbol{B} \approx D_A\, \boldsymbol{I}_{N-1}, \tag{54}$$

where $\boldsymbol{I}_{N-1}$ is identity matrix of size $N-1$ and D_A is distance between transmitter and array of receivers.

As the scaling of $\boldsymbol{\Psi}$ does not impact the result, an approximation of (53) can be made:

$$\boldsymbol{z} \approx (\boldsymbol{G}_a^T \boldsymbol{Q}^{-1} \boldsymbol{G}_a)^{-1} \boldsymbol{G}_a^T \boldsymbol{Q}^{-1} \boldsymbol{h}\,. \tag{55}$$

The second situation when the transmitter is close from the receiver array. In such a case (55) can be used to estimate $\boldsymbol{B}$ from (52). Next using that estimate followed the final answer can be found using (53) completing the first part of transmitter position estimation.

In their analysis, Chan and Ho used the perturbation approach to compute the covariance matrix of $\boldsymbol{z}$ as

$$cov(\boldsymbol{z}) = (\boldsymbol{G}_a^{FT} \boldsymbol{\Psi}^{-1} \boldsymbol{G}_a^F)^{-1}, \tag{56}$$

where cov is covariance.

The solution of **z** presented in (55), the assumption is that x_{Tx}, y_{Tx}, and D_{TxRx_1} are independent. However, at $i = 1$, these variables are related by (48). Thus, the challenge is to integrate this relationship and improve the estimation. When considering small noises in the TDOA measurement, bias can be disregarded. Under this assumption, the mean of the random vector $\boldsymbol{z}$ is centered at the true value. Consequently, the components of the vector $\boldsymbol{z}$ can be formulated as follows:

$$\boldsymbol{z} = \begin{bmatrix} x_{Tx}^F + e_1 \\ y_{Tx}^F + e_2 \\ D_{TxRx_1}^F + e_3 \end{bmatrix}, \tag{57}$$

where e_1, e_{12} and e_3 are estimation errors of $\boldsymbol{z}$. By subtracting the first two components of $\boldsymbol{z}$ with respect to x_{Rx_1} and y_{Rx_1} and taking the square of each element, a new set of equations can be obtained:

$$\boldsymbol{\psi}' = \boldsymbol{h}' - \boldsymbol{G}_a' \boldsymbol{z}', \tag{58}$$

where

$$\boldsymbol{h}' = \begin{bmatrix} (x_{Tx}^F + e_1 - x_{Rx1})^2 \\ (y_{Tx}^F + e_2 - y_{Rx1})^2 \\ \left(D_{TxRx_1}^F + e_3\right)^2 \end{bmatrix}, \tag{59}$$

$$\boldsymbol{G}_a' = \begin{bmatrix} 1 & 0 \\ 0 & 1 \\ 1 & 1 \end{bmatrix}, \tag{60}$$

$$\boldsymbol{z}' = \begin{bmatrix} (x_{Tx} + x_{Rx1})^2 \\ (y_{Tx} + y_{Rx1})^2 \end{bmatrix}, \tag{61}$$

where $\boldsymbol{\psi}'$ represents a vector indicating deviations in the elements of $\boldsymbol{z}$. Substituting (57) into (58) gives

$$\begin{aligned} \psi_1' &= 2(x_{Tx}^F - x_{Rx1})e_1 + e_1^2 \approx 2(x_{Tx}^F - x_{Rx1})e_1 , \\ \psi_2' &= 2(y_{Tx}^F - y_{Rx1})e_2 + e_2^2 \approx 2(y_{Tx}^F - y_{Rx1})e_2 , \\ \psi_3' &= 2D_{TxRx_1}^F e_3 + e_3^2 \approx 2D_{TxRx_1}^F e_3 . \end{aligned} \tag{62}$$

This is another approximation to the true maximum likelihood procedure. It can be made since the assumption regarding errors e_i, $i = 1,2,3$ was that measurement errors are small. The covariance matrix of $\boldsymbol{\psi}'$can be expressed as

$$\boldsymbol{\Psi}' = \boldsymbol{E}[\boldsymbol{\psi}'\boldsymbol{\psi}'^{\boldsymbol{T}}] = \boldsymbol{4B}'cov(\boldsymbol{z})\boldsymbol{B}', \tag{63}$$

where

$$\boldsymbol{B}' = diag\{x_{Tx}^F - x_{Rx1}, y_{Tx}^F - y_{Rx1}, D_{TxRx_1}^F\} . \tag{64}$$

Given that $\boldsymbol{\psi}$ is a Gaussian distribution, it follows that $\boldsymbol{\psi}'$ is also a Gaussian distribution. Therefore, the maximum likelihood estimate of $\boldsymbol{z}'$ is

$$\boldsymbol{z}' = (\boldsymbol{G}_a'^T \boldsymbol{\Psi}'^{-\boldsymbol{1}} \boldsymbol{G}_a')^{-1} \boldsymbol{G}_a'^T \boldsymbol{\Psi}'^{-\boldsymbol{1}} \boldsymbol{h}' . \tag{65}$$

The matrix $\boldsymbol{\Psi}'$ is not known since it contains the true values. Firstly, $\boldsymbol{B}'$ from (63) can be approximated by $\boldsymbol{B}$ constructed based on values in $\boldsymbol{z}$ from (55). After that $\boldsymbol{G}_a^F$ in (56) can be approximated by $\boldsymbol{G}_a$. Lastly $\boldsymbol{B}$ can be approximated by values calculated based on values in $\mathbf{z}$ from (55). Similarly as before, if the transmitter is distant from receivers it is possible to express (56) as

$$cov(\boldsymbol{z}) = c^2 D_A^2 (\boldsymbol{G}_a^{FT} \boldsymbol{Q}^{-1} \boldsymbol{G}_a^F)^{-1}, \tag{66}$$

and (65) can be reduced to

$$\boldsymbol{z}' \approx (\boldsymbol{G}_a'^T \boldsymbol{B}'^{-1} \boldsymbol{G}_{\boldsymbol{a}} \boldsymbol{Q}^{-1} \boldsymbol{G}_{\boldsymbol{a}} \boldsymbol{B}'^{-1} \boldsymbol{G}_a')^{-1} (\boldsymbol{G}_a'^T \boldsymbol{B}'^{-1} \boldsymbol{G}_{\boldsymbol{a}} \boldsymbol{Q}^{-1} \boldsymbol{G}_{\boldsymbol{a}} \boldsymbol{B}'^{-1}) \boldsymbol{h}' . \tag{67}$$

The final estimate of transmitter position can be calculated from $\boldsymbol{z}'$ as

$$\begin{bmatrix} x_{Tx} \\ y_{Tx} \end{bmatrix} = \begin{bmatrix} x_{Rx1} \\ y_{Rx1} \end{bmatrix} \pm \sqrt{\boldsymbol{z}'} . \tag{68}$$

In order to obtain a valid solution, it is necessary to choose one that falls within the relevant area of interest. If any of the components of $\boldsymbol{z}'$ are in proximity to zero, the square root in (24) may become imaginary. To address this issue, the imaginary component should be set to zero.

To summarize, the solution equations are given by (53), (65), and (68). However, since the weighting matrices in (53) and (65) are not known, an appropriate approximation is required to obtain the answer. If the source is far from the array, (53), (67), and (68) are used. On the other hand, for a situation when the transmitter is relatively close to the receivers (55) is initially used to provide an approximation of $\boldsymbol{B}$. The solution is then obtained using equations (53), (65), and (68).

3.5.5. Spherical-intersection method

Alternative method of localising source of emission was proposed by H. C. Schau and A. Z. Robinson [38]. It was based on intersecting spheres, and by design was a 3-D analysis of localisation problem. It delivered a closed-form solution for the case of four receivers. To present this method, equations from Chapter 3.2 need to be expanded by third dimension.

First of all, in 3-D geometry distance between position A (x_A, y_A, z_A) and B (x_B, y_B, z_B) can be defined as

$$G_{AB} = \sqrt{(x_A - x_B)^2 + (y_A - y_B)^2 + (z_A - z_B)^2}\ , \tag{69}$$

and range difference between i-th receiver with respect to the first receiver become

$$\Delta G_{i,1} = G_{TxR_{xi}} - G_{TxRx_1}. \tag{70}$$

As a result, a set of equation (12) can be redefined as

$$\begin{aligned}\Delta G_{i,1}^2 + 2\Delta G_{i,1} G_{TxRx_1} + G_{TxRx_1}^2 = x_{Rx_i}^2 + y_{Rx_i}^2 + z_{Rx_i}^2 - 2x_{Rx_i}x_{Tx} \\ - 2y_{Rx_i}y_{Tx} - 2z_{Rx_i}z_{Tx} + x_{Tx}^2 + y_{Tx}^2 + z_{Tx}^2\end{aligned} \tag{71}$$

for $i = 2,3,4$. Similarly as in 2-D case, by subtracting $G_{TxRx_1}^2$ from both sides and assuming Rx_1 as origin ($x_1 = 0, y_1 = 0, z_1 = 0$) (71) takes on the form:

$$\begin{gathered}\Delta G_{i,1}^2 + 2\Delta G_{i,1} G_{TxRx_1} = \\ x_{Rx_i}^2 + y_{Rx_i}^2 + z_{Rx_i}^2 - 2x_{Rx_i}x_{Tx} - 2y_{Rx_i}y_{Tx} - 2z_{Rx_i}z_{Tx}\ .\end{gathered} \tag{72}$$

Based on (72) H. C. Schau and A. Z. Robinson provide equation for all four receivers

$$\boldsymbol{\delta} - 2G_{TxRx_1}\Delta\boldsymbol{G} = 2\boldsymbol{L}\boldsymbol{x_{3D}}\ , \tag{73}$$

where

$$\boldsymbol{\delta} \triangleq \begin{bmatrix} x_{Rx_2}^2 + y_{Rx_2}^2 + z_{Rx_2}^2 - \Delta G_{2,1}^2 \\ x_{Rx_3}^2 + y_{Rx_3}^2 + z_{Rx_3}^2 - \Delta G_{3,1}^2 \\ x_{Rx_4}^2 + y_{Rx_4}^2 + z_{Rx_4}^2 - \Delta G_{4,1}^2 \end{bmatrix}, \qquad \Delta\boldsymbol{G} \triangleq \begin{bmatrix} \Delta G_{2,1} \\ \Delta G_{3,1} \\ \Delta G_{4,1} \end{bmatrix},$$
$$\boldsymbol{x_{3D}} \triangleq \begin{bmatrix} x_{Tx} \\ y_{Tx} \\ z_{Tx} \end{bmatrix}, \qquad \boldsymbol{L} \triangleq \begin{bmatrix} x_{Rx_2} & y_{Rx_2} & z_{Rx_2} \\ x_{Rx_3} & y_{Rx_3} & z_{Rx_3} \\ x_{Rx_4} & y_{Rx_4} & z_{Rx_4} \end{bmatrix}. \tag{74}$$

Equation (73) features an unknown values that are present on both sides of the equation. On the right-hand side, it appears as the source position $\boldsymbol{x_{3D}}$, while on the left-hand side, it is represented by the source radius G_{TxRx_1}. Assuming that the source radius G_{TxRx_1} is a known, the solution to equation (73) can be rewritten as

$$\boldsymbol{x_{3D}} = \frac{1}{2}\boldsymbol{L}^{-1}(\boldsymbol{\delta} - 2G_{TxRx_1}\Delta\boldsymbol{G}) \tag{75}$$

Solution (53) contains the variable G_{TxRx_1}which is still unknown. In order to resolve this issue, it is necessary to revisit the problem and remember that

$$G_{TxRx_1} = (\boldsymbol{x_{3D}}^T\boldsymbol{x_{3D}})^{\frac{1}{2}} \tag{76}$$

Upon substitution of (53) into (76), expansion of the resulting expression takes the form

$$\begin{aligned} &G_{TxRx_1}^2[4 - 4(\Delta\boldsymbol{G})^T(\boldsymbol{L}^{-1})^T\boldsymbol{L}^{-1}\Delta\boldsymbol{G}] \\ &\qquad + G_{TxRx_1}[2(\Delta\boldsymbol{G})^T(\boldsymbol{L}^{-1})^T\boldsymbol{L}^{-1}\boldsymbol{\delta} + 2\boldsymbol{\delta}^T(\boldsymbol{L}^{-1})^T\boldsymbol{L}^{-1}\Delta\boldsymbol{G}] \\ &\qquad - [\boldsymbol{\delta}^T(\boldsymbol{L}^{-1})^T\boldsymbol{L}^{-1}\boldsymbol{\delta}] = 0 \end{aligned} \tag{77}$$

This equation solely pertains to the unknown source radius R, with all other parameters being known quantities obtained from the sensor locations $\boldsymbol{L}$, measured time delay differences $\Delta\boldsymbol{G}$, or a combination of both $\boldsymbol{\delta}$. Solving equation (77) results in

$$G_{TxRx_1} = \frac{-b_{SI} \pm \sqrt{b^2 - 4a_{SI}c_{SI}}}{2a_{SI}};\ G_{TxRx_1} \geq 0\ , \tag{78}$$

where

$$a_{SI} = 4 - 4(\Delta\boldsymbol{G})^T(\boldsymbol{L}^{-1})^T\boldsymbol{L}^{-1}\Delta\boldsymbol{G}\,, \tag{79}$$

$$b_{SI} = 2(\Delta\boldsymbol{G})^T(\boldsymbol{L}^{-1})^T\boldsymbol{L}^{-1}\boldsymbol{\delta} + 2\boldsymbol{\delta}^T(\boldsymbol{L}^{-1})^T\boldsymbol{L}^{-1}\Delta\boldsymbol{G}\,, \tag{80}$$

$$c_{SI} = \boldsymbol{\delta}^T(\boldsymbol{L}^{-1})^T\boldsymbol{L}^{-1}\boldsymbol{\delta}\,. \tag{81}$$

Consequently, equations (75) and (78) collectively offer a two-step approach to tackle the passive source localisation problem. The initial step involves solving (78) to determine the source radius, which is subsequently substituted into (75) to derive the source position. Occasionally, (78) might yield two feasible solutions ($G_{TxRx_1} \geq 0$), leading to two possible source locations that could reproduce the measured data. In such instances, these locations tend to be far apart from each other, thus enabling the correct solution to be determined based on other physical reasoning, such as one solution being outside the relevant domain.

3.5.6. Spherical-Interpolation method

Yet another approach of the problem was presented by Smith, J. O. and Abel, J. S. [39]. They introduced equation error vector $\boldsymbol{\varepsilon}$ into equation (73) to represent imprecise measurements:

$$\boldsymbol{\varepsilon} = \boldsymbol{\delta} - 2G_{TxRx_1}\Delta\boldsymbol{G} - 2\boldsymbol{L}\boldsymbol{x_{3D}}\,. \tag{82}$$

It is noteworthy that the vector of equation errors (82) exhibits linearity in $\boldsymbol{x_{3D}}$ given by $G_{TxR_{x1}}$ and simultaneously exhibits linearity in G_{TxRx_1} given by $\boldsymbol{x_{3D}}$**.** Error vectors which are linear in the unknowns yield closed form least-squares solutions. The precise solution via least-squares approach for $\boldsymbol{x_{3D}}$ considering a known G_{TxRx_1} is expressed as:

$$\boldsymbol{x_{3D}} = \frac{1}{2}\,\boldsymbol{L}_W^*(\boldsymbol{\delta} - 2G_{TxRx_1}\Delta\boldsymbol{G})\,, \tag{83}$$

where

$$\boldsymbol{L}_W^* \triangleq (\boldsymbol{L}^T\boldsymbol{L})^{-\boldsymbol{1}}\boldsymbol{L}^T\,, \tag{84}$$

yields the minimiser of $\boldsymbol{\varepsilon^T}\boldsymbol{\varepsilon}$.

The proposed closed-form solution involves substituting (83) into (82) and then minimizing the resulting equation error with respect to G_{TxRx_1}. This approach results in a linear least-squares problem that can be used to identify the value of G_{TxRx_1}. Once the minimizing G_{TxRx_1} value is determined using this new linear equation, the corresponding value of $\boldsymbol{x_{3D}}$, as per (82), automatically serves as a minimiser of the squared equation-error norm in relation to $\boldsymbol{x_{3D}}$, considering this value of G_{TxRx_1}.

As a result of substituting (83) into (82), a new equation error (linear in G_{TxRx_1}) is given

$$\boldsymbol{\varepsilon}' = \boldsymbol{\delta} - 2G_{TxRx_1}\Delta\boldsymbol{G} - \boldsymbol{L}\boldsymbol{L}_W^*\left(\boldsymbol{\delta} - 2G_{TxRx_1}\Delta\boldsymbol{G}\right) = (\boldsymbol{I} - \boldsymbol{L}\boldsymbol{L}_W^*)(\boldsymbol{\delta} - 2G_{TxRx_1}\Delta\boldsymbol{G}) . \tag{85}$$

For the needs of further analysis, two $N - 1$ by $N - 1$ symmetric matrices are defined:

$$\boldsymbol{P_S} \triangleq \boldsymbol{L}\boldsymbol{L}_W^* , \tag{86}$$

$$\boldsymbol{P}_S^{\perp} \triangleq \boldsymbol{I} - \boldsymbol{P_S} . \tag{87}$$

The matrix $\boldsymbol{P_S}$ is constructed as a rank 3 projection matrix that removes components orthogonal to the space spanned by the columns of $\boldsymbol{L}$. This leads to the property of $\boldsymbol{P_S}$ being idempotent $\left(\boldsymbol{P_S^2} = \boldsymbol{P_S}\right)$. Additionally, the matrix $\boldsymbol{P}_S^{\perp}$ is another idempotent projection matrix, which removes components in the space spanned by the columns of $\boldsymbol{L}$.

In the specific scenario of having only four sensors (i.e., the three-range-difference case), the projection matrix $\boldsymbol{P_S}$ reduces to the identity matrix $\boldsymbol{I}$, and consequently, the equation error $\boldsymbol{\varepsilon}'$ becomes zero regardless of the values of G_{TxRx_1}. As a result, the proposed method is not applicable for estimating explicit range of the source, and instead, it provides a source location estimate with one degree of ambiguity. In the context of a more general case involving N sensors

$$\boldsymbol{\varepsilon}' = \boldsymbol{P}_S^{\perp}\left(\boldsymbol{\delta} - 2G_{TxRx_1}\Delta\boldsymbol{G}\right), \tag{88}$$

so that

$$\boldsymbol{\varepsilon}'\boldsymbol{V}\boldsymbol{\varepsilon}' = \left(\boldsymbol{\delta} - 2G_{TxRx_1}\Delta\boldsymbol{G}\right)^{\boldsymbol{T}}\boldsymbol{P}_S^{\perp}\boldsymbol{V}\boldsymbol{P}_S^{\perp}\left(\boldsymbol{\delta} - 2G_{TxRx_1}\Delta\boldsymbol{G}\right) . \tag{89}$$

Minimizing (89) with respect to G_{TxRx_1}, is a form of weighted least squares in which the weighting matrix $\boldsymbol{P}_S^{\perp}\boldsymbol{V}\boldsymbol{P}_S^{\perp}$ is of rank $N - 4$. The removal of three degrees of freedom in this matrix corresponds to the substitution of the least-squares solution (83) for the three spatial source coordinates. The solution is given by

$$\tilde{G}_{TxRx_1} = \frac{\Delta \boldsymbol{G}^T \boldsymbol{P}_S^{\perp} \boldsymbol{V} \boldsymbol{P}_S^{\perp} \boldsymbol{\delta}}{2\Delta \boldsymbol{G}^T \boldsymbol{P}_S^{\perp} \boldsymbol{V} \boldsymbol{P}_S^{\perp} \Delta \boldsymbol{G}}. \tag{90}$$

Upon substitution of this solution into (83), the estimate of the source location is obtained:

$$\hat{\boldsymbol{x}}_{\boldsymbol{3D}} = \frac{1}{2} \boldsymbol{L}_W^* \left(\boldsymbol{\delta} - 2\tilde{G}_{TxRx_1} \Delta \boldsymbol{G} \right). \tag{91}$$

If the goal is to achieve the lowest possible variance and bias through iterative nonlinear minimization, the initial value provided by (90) serves as an excellent starting point for a descent method.

3.5.7. Conclusion

Let us define $\mathbf{x}$ as source coordinate vector (depending on geometry, equal to $\boldsymbol{x}_{\boldsymbol{2D}}$ **or** $\boldsymbol{x}_{\boldsymbol{3D}}$) and $\boldsymbol{C}_{\boldsymbol{i}}$ as coordinate vector of sensor i,

$$\begin{gathered} \boldsymbol{C}_{\boldsymbol{i}} = [x_{Rx_i} \quad y_{Rx_i}], \quad \boldsymbol{x} = \boldsymbol{x}_{\boldsymbol{2D}} \text{ in case of 2-D,} \\ \boldsymbol{C}_{\boldsymbol{i}} = [x_{Rx_i} \quad y_{Rx_i} \quad z_{Rx_i}], \quad \boldsymbol{x} = \boldsymbol{x}_{\boldsymbol{3D}} \text{ in case of 3-D.} \end{gathered} \tag{92}$$

The general LS cost function for TDOA measurements is

$$J_{LS} = \sum_{i=2}^{N} \left(\Delta D_{i,1} - \|\boldsymbol{x} - \boldsymbol{C}_{\boldsymbol{i}}\| + \|\boldsymbol{x} - \boldsymbol{C}_{\boldsymbol{1}}\| \right)^2. \tag{93}$$

The general maximum likelihood cost function for TOA measurements and TDOA measurements are

$$J_{ML} = \sum_{i=2}^{N} \frac{\left(\Delta D_{i,1} - \|\boldsymbol{x} - \boldsymbol{C}_{\boldsymbol{i}}\| + \|\boldsymbol{x} - \boldsymbol{C}_{\boldsymbol{1}}\| \right)^2}{\sigma_i^2}, \tag{94}$$

where σ_i^2 is the variance of TDOA measurement at receiver i. The objective of all presented algorithms is to estimate the source coordinate vector **(**$\boldsymbol{x}_{\boldsymbol{2D}}$ or $\boldsymbol{x}_{\boldsymbol{3D}}$**)** that minimizes the cost function.

Method presented in Chapter 3.5.2 is representing group of iterative nonlinear minimization techniques. Those iterative algorithm based on an initial position estimate obtained using (as in case of method from Chapter 3.5.2) the Gauss-Newton method or other methods such as the steepest descent method or the combined Levenberg-Marquardt method [40]. To achieve the global minimum, it is necessary to have a reliable initial source position estimate. The Taylor series method is commonly utilized to linearize nonlinear equations by updating the least square solution. This iterative procedure refines the initial guess and estimates location errors. Taylor series methods are better than least square methods that ignore measurement errors, as they can provide accurate location estimation at reasonable noise levels. Nevertheless, a reasonably accurate initial estimate of the source location is still required, and there is no assurance of convergence on a source location estimate.

To avoid iterative algorithms, two-stage, closed-form least square estimators have been widely developed for maximum likelihood approximation. This family of solutions is represented by methods described in Chapters 3.5.1, 3.5.4, 3.5.5 and 3.5.6. These least squares solutions can provide results that can be treated as sufficient source localisation or can be used as initialization for iterative estimators, which converge with less computational effort to a source position estimate with higher accuracy.

To complete analysis, a representative of direct solutions is presented in Chapter 3.5.3. The source position can be directly calculated from different sets of geometric equations. Although the computational complexity of this approach to source localisation is low, it does not always result in a source location solution when TDOA measurement errors exist. Furthermore, in an over-determined system with additional measurements, the source position needs to be estimated by averaging all possible source locations calculated from sets of three receivers.

Summary with short a description, advantages, and disadvantages of all the methods is presented in Table **1**.

Table 1. TDOA localisation methods summary.

Chapter	Authors	Description	Advantages	Disadvantages
3.5.1	Friedlander, B	2-D,Weighted LS method	Works both for minimal required number of sensors and over-determined system, non-iterative	Suboptimal – ignore relationship (48) at i=1

3.5.2	Foy, W. H.	2-D, Taylor-series, iterative Gauss-Newton method, LS solution	Useful in solving multiple-measurement; mixed-mode problems	Iterative, convergence is not proved; Requires an initial guess
3.5.3	Fang, B. T.	2-D, An exact solution to the hyperbolic TDOA equations	Closed form and exact solution	Does not make use of redundant measurements; ambiguous result
3.5.4	Chan, Y. T. Ho, K. C.	2-D, Two-stage weighted LS method	Non-iterative, explicit solution	Requires high SNR and a priori knowledge of the second-order statistics of the TDOA measurement errors
3.5.5	Schau, H. C. Robinson, A. Z.	3-D, Spherical intersection method	Non-iterative; closed form	Requires a priori solution for the source range; solution only for four sensors
3.5.6	Smith, J. O. Abel, J. S.	3-D, Spherical interpolation method; closed-form two-step LS method	Non-iterative	Suboptimal – ignore relationship (48) at i=1

4. Single Frequency Network in passive emitter localisation

A single frequency network (SFN) is a collection of transmitters that broadcast the same signal at the same frequency. DVB-T and FM radio broadcast networks, as well as other digital broadcast networks, can and commonly do operate in this manner. The aim of creating such networks is to utilize radio spectrum more efficiently, allowing for a greater number of radio or TV channels. In certain geographically difficult areas like cities, highlands, or country borders, broadcasters will have much better success covering voids by using smaller, usually weaker satellite transmitters in addition to their main tower. The use of the SFN technique has one major downside, namely self-interference of the network. If transmitters are located at significantly different distances from receiver [41], some of the signals may cause interference due to the excessive delay. Such an effect can be considered as a form of multipath propagation. To counter this effect, in order to control self-interference designers of SFNs have to manipulate transmitters' location, power, antenna height, antenna pattern, and broadcast time delay. For example, transmitters located near the edge of the service area transmit slightly earlier to improve the overall quality of reception in the service area. Another method of counteracting multipath is the use of guard interval. The guard interval is a period in broadcast during which no data is transmitted, but the carrier signal is still present. The length of the guard interval is typically a fraction of the symbol duration, and in SFN using Orthogonal Frequency-Division Multiplexing (OFDM) (e.g., DAB, DVB-T), the beginning of each symbol is preceded by a delay longer than the maximum delay spread of the channel. The guard interval ensures that all the delayed signals arrive before the start of the next symbol, and hence there is no inter-symbol interference.

Naturally, the presence of SFN can have a tremendous impact on a passive radar. Two of the main difficulties in target detection using passive radar systems are the lack of control over waveform structure and the strong multipath interferences. Multiple works have been dedicated to this topic [10][11][42][43]. In comparison, there are only a few scientific works in the literature that focus on the problems of passive localisation systems operating with SFN [18][19].

Let us consider two transmitters used as illuminators of opportunity (Tx_1 and Tx_2) and two passive radar receivers (Rx_1 and Rx_2) with omni-directional antennas.

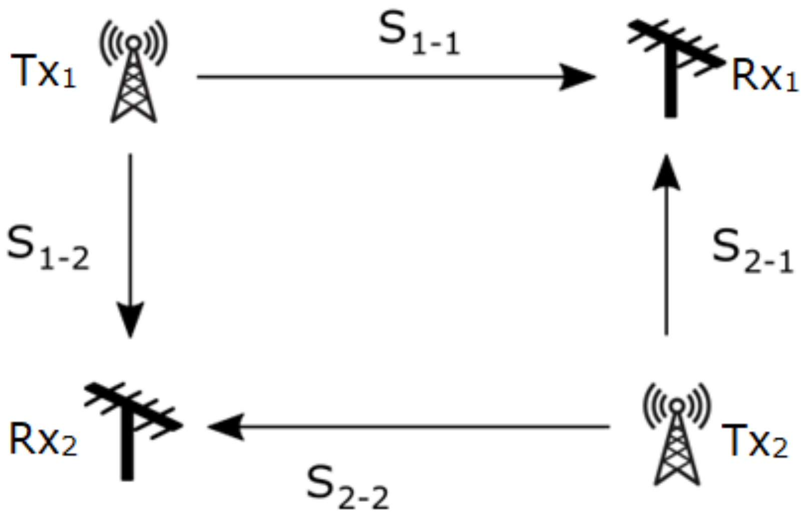

Figure 7. SFN signal propagation in two receiver and two transmitter configuration.

The signal gathered by each receiver is the sum of two transmissions:

- Rx_1 will capture the signal from Tx_1 ($S_{1\text{-}1}$) and the signal from Tx_2 ($S_{2\text{-}1}$).
- Rx_2 will capture the signal from Tx_1 ($S_{1\text{-}2}$) and the signal from Tx_2 ($S_{2\text{-}2}$).

The next step is to calculate the cross-correlation of those signals. It can be done by using (8) described in Chapter 2.3 at zero velocity which is equivalent to:

$$Xcorr(m) = \sum_{n=-\frac{N_s}{2}}^{\frac{N_s}{2}-1} x_{Rx1}(n) x_{Rx2}{}^{*}(n-m), \tag{95}$$

where x_{Rx1} and x_{Rx2} are signals gathered by Rx_1 and Rx_2 respectively.

If Tx_1 and Tx_2 broadcast different signals (not correlated in any way), two peaks[1] will occur:

- Peak 1 (P_1): Correlation between $S_{1\text{-}1}$ and $S_{1\text{-}2}$. This peak is the result of the TDOA for the signal emitted by Tx_1.
- Peak 2 (P_2): Correlation between $S_{2\text{-}1}$ and $S_{2\text{-}2}$. This peak is the result of the TDOA for the signal emitted by Tx_2.

For the purposes of further discussion, P_1 and P_2 will be referred to as TDOA peaks.

[1] The term *peak* will be used throughout the thesis. It denotes a distinctive local maximum in the cross-correlation diagram as shown in Figure **8**.

On the other hand, if Tx_1 and Tx_2 work in SFN (signals are identical and fully time-synchronized), four peaks will occur: the two described above and two further peaks. Those additional peaks are:

- Peak 3 (P_3): Correlation between S_{1-2} and S_{2-1}. This peak is a ghost detection.
- Peak 4 (P_4): Correlation between S_{1-1} and S_{2-2}. This peak is also a ghost detection.

For the purposes of further discussion, P_3 and P_4 will be referred to as ghost peaks.

Example plot of cross-correlation of signals gathered in the presence of two transmitters working in SFN in presented in Figure **8**.

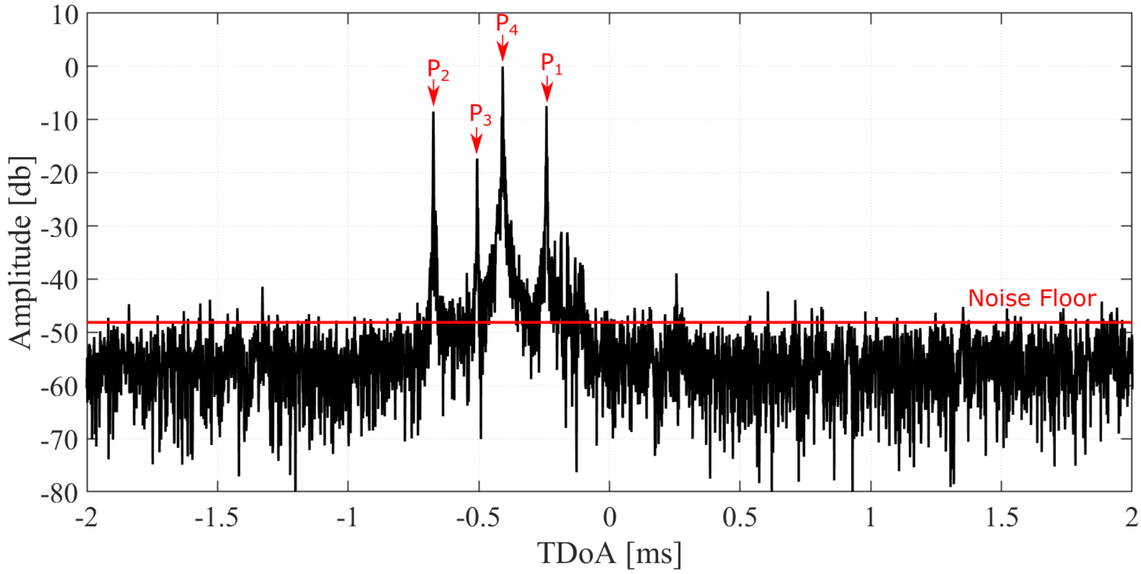

Figure 8. Cross-correlation of two signal gathered in the presence of SFN.

Amplitudes of all peaks depend on many variables, such as the initial power of signals or the relative positions of transmitters and receivers (signal power dissipates with square of distance). Additionally, in real-life situations, there are even more factors influencing the signal strength. Since antennas are not perfectly omni-directional, their radiation patterns will change the received signal's amplitude. Any obstacle between receivers and transmitters can introduce additional interferences. Considering those factors alone, it is possible that in measurements some cross-correlation peaks may not be visible—hidden in noise or in the side lobes of another peak.

4.1. Localisation of unknown SFN transmitter

One of the proposed constructive uses of ghost peaks in cross-correlation is the localisation of unknown emitters. In a scenario where only one emitter is anticipated (Tx_1) but an additional SFN emitter (Tx_2) is present, it is possible to use both TDOA and ghost measurements to locate a previously unknown SFN transmitter. Let's consider the 2-D geometry described in Chapter 4. Another assumption is that the positions of the receivers (Rx_1 and Rx_2) and the anticipated transmitter are known. Finally, all four peaks described in Chapter 4 are possible to identify.

Let us use (9) to analyze cross-correlation peaks in terms of geometrical distance. Peak 1 (P_1) is a result of TDOA for the signal emitted by Tx_1 and is equal to

$$P_1 = D_{Tx_1Rx_1} - D_{Tx_1Rx_2} \,. \tag{96}$$

Since all factors are known, it is possible to calculate this value and identify P_1 on cross-correlation. It can be discarded leaving 3 more peaks. One of them is a result of TDOA for the signal emitted by Tx_2:

$$P_2 = D_{Tx_2Rx_1} - D_{Tx_2Rx_2} \,. \tag{97}$$

As describer in Chapter 3.4, TDOA measurement define hyperbola with receivers as foci. Remaining two peaks (P_3 and P_4) are ghost peaks. By analyzing them in the same manner as previously

$$P_3 = D_{Tx_1Rx_2} - D_{Tx_2Rx_1} \,, \tag{98}$$

$$P_4 = D_{Tx_1Rx_1} - D_{Tx_2Rx_2} \,. \tag{99}$$

Looking for position of Tx_2, those two equations can be easily rearranged to form circle equations:

$$(x_{Tx_2} - x_{Rx_1})^2 + (y_{Tx_2} - y_{Rx_1})^2 = (D_{Tx_1Rx_2} - P_3)^2 \tag{100}$$

$$(x_{T_{x2}} - x_{Rx_2})^2 + (y_{Tx_2} - y_{Rx_2})^2 = (D_{Tx_1Rx_1} - P_4)^2 \tag{101}$$

The first equation defines a circle around Rx_1 with radius equal to $D_{Tx_1Rx_2} - P_3$. Similarly, the second equation defines a circle around Rx_2 with radius equal to $D_{Tx_1Rx_1} - P_4$. Because position of Tx_1, Rx_1, and Rx_2 is known, both $D_{Tx_1Rx_2}$ and $D_{Tx_1Rx_1}$can be easily calculated. By subtracting corresponding peaks both circle radiuses and can be found. Tx_2

is located on the intersection of all three described curves. That is because the intersection of three surfaces equivalent (two spheres and one hyperboloid) to described curves is a circle. This method cannot be directly used in 3-D scenarios by expanding calculations by third dimension (z-axis in Cartesian space). That is because the intersection of three surfaces equivalent to described curves (two spheres and one hyperboloid) is a circle. To find the explicit 3-D solution, an additional measurement is needed. Based on the considerations set out above, the algorithm for localisation of unknown SFN transmitter is proposed. In Figure **9**, a visualization of the proposed algorithm is presented and then each of the steps is further explained.

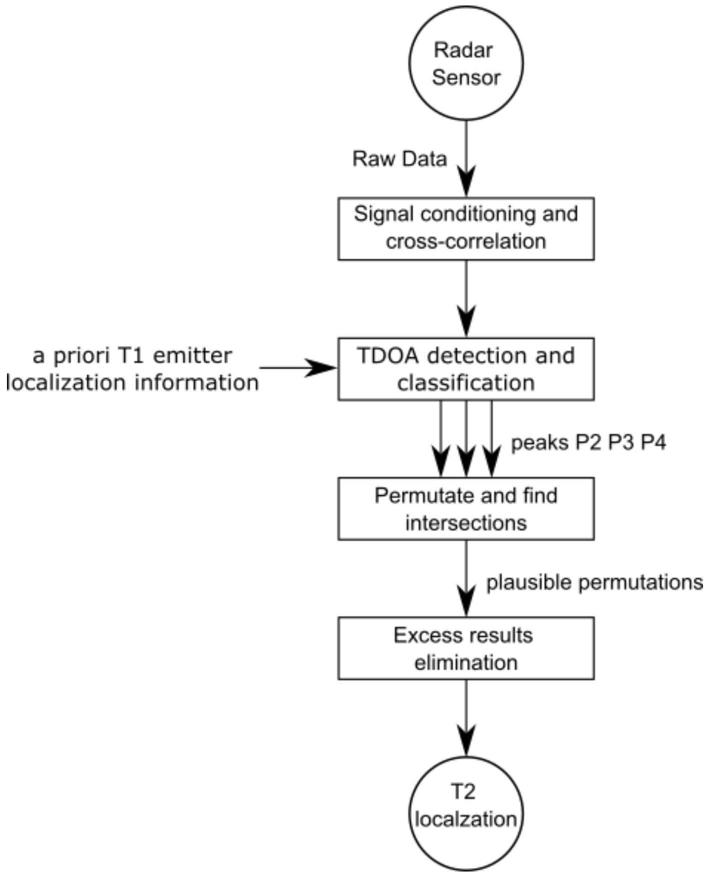

Figure 9. Proposed method of localisation of unknown SFN transmitter.

4.1.1. Signal conditioning and cross-correlation

Depending on the circumstances, the signals gathered from radar sensors may need initial conditioning [44]. It is advisable to maximize SNR by removing as much noise from signal as possible. For example, if signal sampling frequency is higher than the signal bandwidth, decimation and/or filtration may be needed. After conditioning is done, cross-correlation of two signal is calculated. Possible results of cross-correlation in presented in Figure **8**.

4.1.2. TDOA detection

The second step is to identify all peaks on cross-correlations amplitude plot. Detection method is arbitrary and highly depends on the emitted signals autocorrelation function shape. For signal autocorrelation with a narrow main lobe and low side lobe level, such as white noise autocorrelation, a simple amplitude threshold cut-off is sufficient detection method. In situations where signal autocorrelation function is more complex, signals are corrupted with non-Gaussian noise, or other phenomena drastically modify cross-correlation function, more sophisticated methods of detection may be necessary to extract peak values. In Chapter 5.3.1, such a situation occurred and is thoroughly discussed along with used method of TDOA detection. Regardless of the used method, the next step after acquiring peak values is to identify peak that corresponds with TDOA measurement of Tx_1. This peak can be ignored, as it holds no information about Tx_2.

4.1.3. Peak permutation and curves intersection

The remaining three peaks correspond to TDOA for the signal emitted by Tx_2 (and associated with its hyperbola) and two ghost detections with no physical interpretation (and associated with them circles). However, with no additional information, there is no way of knowing which peaks are ghost detections and how to assign them to the peaks described in Chapter 4. Therefore, all six possible permutations need to be explored simultaneously. As shown in Chapter 5.4.1 depending on the geometry of receivers and transmitters, there are up to two out of six combinations that yield a possibly valid solution, i.e., where all three curves share an intersection. Each plausible combination gives two intersection points, totalling two or four possible locations of Tx_2.

4.1.4. Excess results elimination

Unfortunately to find the explicit 2-D position of Tx_2, additional information is needed. It can be a priori information about the area of a possible Tx_2 location, a posteriori information (e.g., confronting possible transmitter locations with satellite images), a measurement from a third receiver, or, most realistically, an AOA measurement from either of the receivers.

If the latter is the case, it is advisable to use a directional antenna and make a series of measurements. In each measurement, change antenna angle only in one receiver, so it would point towards the next plausible Tx_2 location. To verify where the true position of Tx_2 is, it is not recommended to compare measured signal strength since that measurement will be equal to the sum of the signals from Tx_1 and Tx_2 transmitters. The recommended method is to compare the cross-correlation results instead. More precisely, to compare the power level of a peak that corresponds with TDOA for the signal emitted by transmitter Tx_2 if it was located in the position under test with its equivalents in other measurements. The power levels of the remaining three peaks can be ignored in this step. The measurement where the level of the peak in question is the highest, is the one that Tx_2's assumed location is true.

4.2. Time desynchronisation in SFN

The second of the proposed constructive use of ghost peaks in cross-correlation is to use them to calculate desynchronisation between transmitters working in SFN. A common assumption in passive radar signal processing is that SFN transmitters are time-synchronized. In reality, this condition is almost never fulfilled, and most SNF illuminators are not perfectly synchronized by design. Taking DVB-T standard [41] as an example, it is possible to formulate two main reasons for desynchronisation:

- The design of SFN utilizes a time-delay between transmitters to minimize network self-interference in an area of interest.
- The usage of the big guard interval, which determines a smaller emphasis on precise system synchronization.

As was presented in Chapter 4, ghost peaks (P_3 and P_4) are a product of correlation between two transmitters. Synchronization accuracy information can be extracted due to the fact that the peaks at t_3 and t_4 are the results of the correlation of two signals each from two different transmitters. Assuming that position of transmitters is known (either as an a priori knowledge or acquired via TDOA techniques using P_1 and P_2), it is possible to calculate where on cross-correlation P_3 and P_4 should be. If there is any difference between that calculation and actual position of the peaks on cross-correlation function of measured data, it may suggest there is a desynchronisation present. Based on this fact, an algorithm to determine the desynchronisation time between DVB-T transmitters have been proposed.

4.3. Impact of SFN desynchronisation on passive radar

Let us consider a scenario where a passive radar is operating in an SFN environment and only one reference signal is gathered. Such a case is realistic when the quality of a reference signal from the second transmitter is poor due to a lack of an unobstructed line of sight between the emitter and the receiver, a strong leak of the dominant transmitter into a weaker transmitter reference signal, or other causes. Assuming that the radar signal processing algorithm takes into account the time delay between the two reference signals reaching the receiver, it is perfectly valid to gather only one reference signal when utilizing transmitters in SNF. In such a scenario, it is even possible to localise a target with a single receiver. However, this approach is highly susceptible to any transmitter desynchronisation. The impact of desynchronisation on target location in passive radar is studied in Chapter 6.7.

4.4. Time desynchronisation calculation algorithm

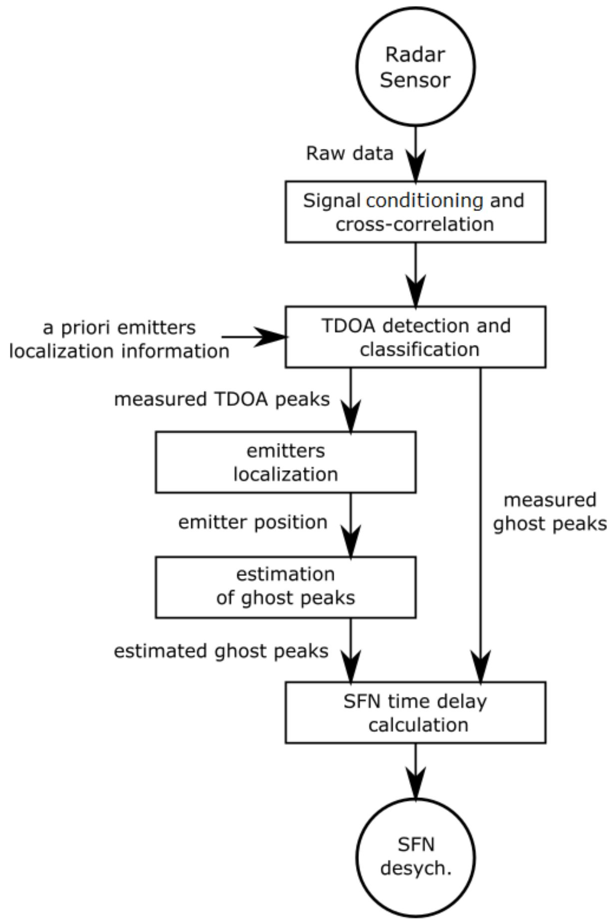

Figure 10. Proposed method of calculating desynchronisation of transmitters working in SFN.

To mitigate all errors and challenges that accompany desynchronisation of illuminators author propose algorithm for calculating the desynchronisation of DVB-T transmitters in SFN. In this work, a simple scenario with multiple radar sensors and two SFN transmitters is considered, but the algorithm can be easily expanded to bigger number of receivers and transmitters. In Figure **10**, a visualization of the proposed algorithm is presented and below each of the steps is further explained.

4.4.1. Signal conditioning and cross-correlation

Similar to the situation presented in Chapter 4.4.1, conditioning should be done if it is needed. After conditioning is done, signals are grouped into pairs and the cross-correlation of each pair is calculated. The next step is performed for each pair.

4.4.2. TDOA detection and classification

Just as in 4.1.2 next step is to identify all peaks on cross-correlations function result. After identifying peaks and acquiring their values it is necessary to classify them into two groups: TDOA peaks and ghost peaks.

In the best-case scenario, the algorithm can be presented with the exact Cartesian position of the emitter. To classify peaks, a set of four Cartesian distance equations (P1, P2, P3, and P4 from Chapter 4.1) must be solved and the results recalculated into the time domain by dividing by the speed of light. Final results should be used for peak classification. By taking into account measurement and system errors, pairing calculated values of peaks with their detected counterparts should be a trivial task reduced to finding the closest match. It is possible, but not recommended, to skip the next two steps (emitter localisation described in Chapter 4.4.3 and estimation of ghost peaks shown in Chapter 4.4.4), and use calculated ghost peak positions as estimated ghost peaks in SFN time delay calculation (see Chapter 4.4.5).

If only an approximate position of the transmitters is available, no such shortcut can be taken. An expected value of TDOA must be calculated using the approximate location of the emitter in (10) After that, finding calculated values within cross-correlation results needs to be done.

Another possibility is that only one emitter's location is known, such as when SFN was not expected. In such a case, it is possible to use the algorithm described in Chapter 4.1 to find an approximation of the second emitter position. Then one can use this rough estimate to identify the TDOA peak and move on to the next step.

In the worst case, if no a priori information about the transmitters localisation is available, it is possible with enough redundant receivers to perform an expanded analysis similar to the one in Chapter 4.1.3 to find permutation that have a geometric solution across all cross-correlation results from all pairs of receivers. This last method should be used as a last resort, but it is not applied or further discussed in this work.

4.4.3. Emitter localisation

The next step is to localise emitters after identifying TDOA peaks on the cross-correlation function. This can be done using any of the algorithms presented in Chapter 3.5. The selection of a specific algorithm depends on the requirements of the end user. When selecting an algorithm, parameters such as the number of receivers used, the desired geometry (2-D or 3-D), the available calculation capabilities, and the desired accuracy of the results, among others, will be important.

The end result of this point, regardless of the algorithm used, is to estimate the positions of emitters. One should bear in mind that this estimation is not perfect as it has an estimation error due to a number of reasons. Measurement error, projection error (3-D to 2-D), receiver synchronization error, and so on are a few examples.

4.4.4. Estimation of ghost peaks

With estimated emitter localisation, it is possible to use equations (98) and (99) to calculate estimated positions of ghost peaks.

4.4.5. SFN time delay calculation

The last step is to compare estimated positions of ghost peaks with their actual positions on the cross-correlation function result. The difference between those estimates and measured values can be explained as the sum of multiple causes: transmitter desynchronisation, receiver synchronization error, the positioning error of receivers and transmitters, measurement inaccuracies, rounding errors, etc.

If the exact Cartesian positions of the emitters are known, it is possible to minimize the impact of all of those errors except for desynchronisation. In order to do that, an additional step needs to be taken. A comparison should be made between measured TDOA peaks and the TDOA value calculated from the transmitter's exact position. Any differences between TDOA estimates and measurements are burdened with the same errors as ghost peaks, except for transmitter desynchronisation. The result of subtraction the difference between the calculated TDOA peak and the measured TDOA value from difference between the calculated ghost peak and the measured ghost peaks is the estimate of emitter desynchronisation. Errors originating from other causes are minimized in this estimate. To strengthen this effect, multiple measurements can be taken over some time, and averages should be calculated and then substituted.

5. Simulations

To verify the algorithms presented in this thesis, a series of experiments using both simulated and real-life data were held. In this chapter, the results of simulations are presented.

5.1. Signal model

Both algorithms expect unprocessed data (also known as raw data) collected directly from analog-digital converter (ADC) as an input. In order to avoid any modification of the implemented algorithms, a data generator was created. The main task of the generator was to provide a series of signals that were a good approximation of the data gathered by receivers from a single DVB-T channel. A signal generator is also capable of generating received signals when a number of transmitters working in SFN are present.

The first step in creating such a generator is to establish a satisfying signal model. For the purpose of this thesis, the signal from a single channel of DVB-T was approximated with white noise filtered by a digital filter to acquire 7.8 MHz of bandwidth and sampled at 10 MHz frequency (see Figure **11**). Such an approximation was made on the premise that DVB-T signals are used with success in passive noise radars as illuminators of opportunity [45].

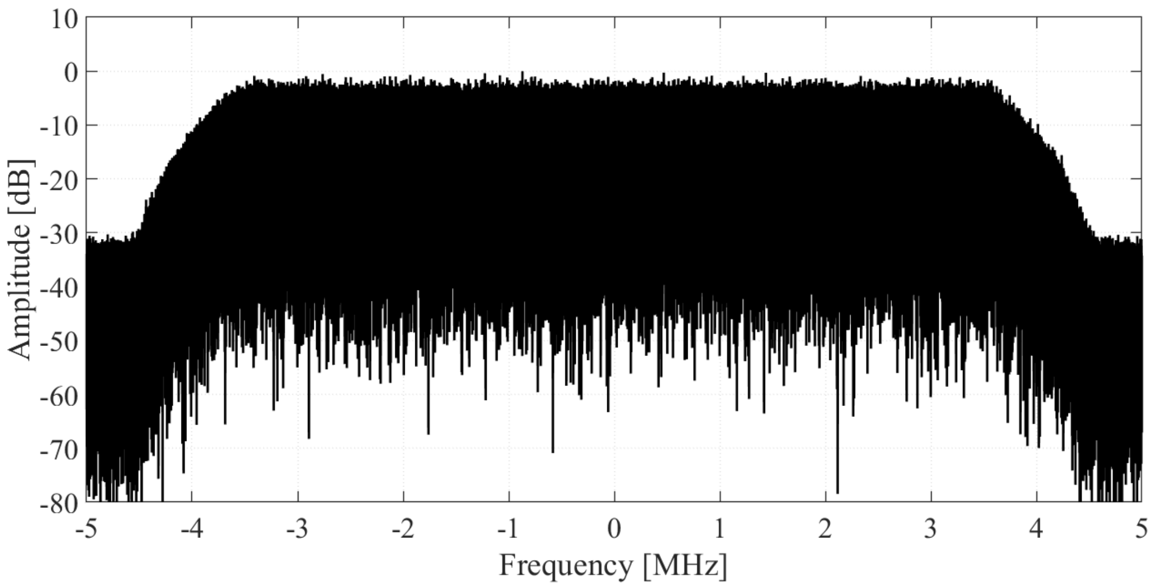

Figure 11. Spectral density of the simulated transmitter signal.

In general, the discrete signal gathered by a single receiver is a sum of time- and phase-delayed, attenuated signals from transmitters and can be described as:

$$s_R(n) = \sum_{m=1}^{M} \left(s_{T_m} \left(n - \left\lfloor \frac{f_s D_{RT_m}}{c} \right\rfloor \right) e^{j\left[\left(2\pi \frac{f_s D_{RT_m}}{c} - \pi\right) mod\ 2\pi\right]} \Big/ {D_{RT_m}}^2 \right) + s_N \tag{102}$$

where M is the number of transmitters in SFN, s_{T_m} is the signal emitted from the m transmitter, f_s is the sampling rate, s_N is white Gaussian noise and $\lfloor\ \rfloor$ is the rounding down operator.

Because all receivers and transmitters are stationary, there is no Doppler effect. In this thesis, DVB-T signals broadcasted by transmitters are approximated as a Gaussian noise. This approach will be incorrect when applied to a scenario with moving nodes since DVB-T signals introduce multiple peaks in range-velocity analysis (cross-ambiguity function) generated by pilot peaks [46]. Such peaks are absent in simple range analysis (via the cross-correlation function). The example of autocorrelation with two transmitters in SFN is presented in Figure **12**. The result is symmetric, which is due to the nature of autocorrelation. The middle peak with a maximum value in time shift equal to zero, is always present in autocorrelation regardless of the signal character. The peak on the left and its symmetric counterpart on the right are the results of SFN. Both of them appear when the autocorrelation input signal consists of two copies of the same signal, one shifted in time relative to the other.

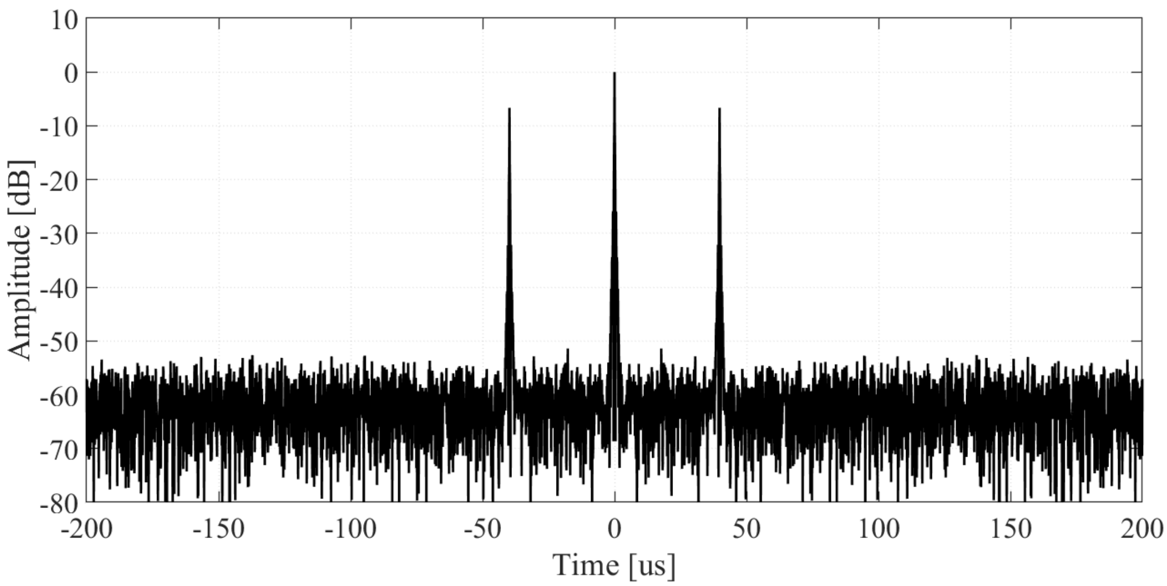

Figure 12. Autocorrelation of the signal from the receiver gathering signal from two transmitters.

This signal model is a rather simple one. It only emulates the most basic propagation effects: signal time delay and phase shift due to the distance travelled by radio waves and signal amplitude loss due to propagation in a free space. Those are the key factors needed to properly test all the algorithms presented in this work. The presented model does not take into consideration the signal multipath problem, obstructions in line-of-sight propagation, transmitter and receiver antenna apertures, atmospheric attenuation, or the atmospheric refraction effect.

5.2. Scenarios

An important aspect of the simulation is the arrangement of transmitters and receivers in the space. While it is possible to test algorithms using any array, this is not practical for passive radars. This is because the deployment of transmitters and receivers determines the layout of radar curves (e.g., hyperbolas in the case of TDOA) relative to each other and the distribution of peaks on the cross-correlation function. It is worth noting that analyzing the impact of measurement errors on algorithm performance only makes sense for one selected geometry and cannot be approximated for other geometries. This can be seen in the example below. It is important to note that every scenario and calculation in this and the next chapter are done in three-dimensional geometry. Flat, two-dimensional geometry is only used as an easy way to visualise problems and the results.

For the purposes of further analysis, a TDOA localisation algorithm described in Chapter 3.5.5 was chosen. This algorithm was selected because it fulfils all the requirements for simulation and measurement experiments. The main requirements were: three-dimensional localisation; utilisation of four sensors; and non-iterative calculations (important for signals distorted by random noise, where a large number of simulations are made).

To test the chosen localisation algorithm's performance, a set of measurements was made. In every measurement, a random value from a Gaussian distribution with known variance (value ranging from 0 to 30 m^2) representing measurement error was added to the TDOA value. Then, after a set of 10^4 measurements, a mean value of Tx localisation error was noted, and the next set of 10^4 measurements was carried out for another value of a Gaussian distribution variance.

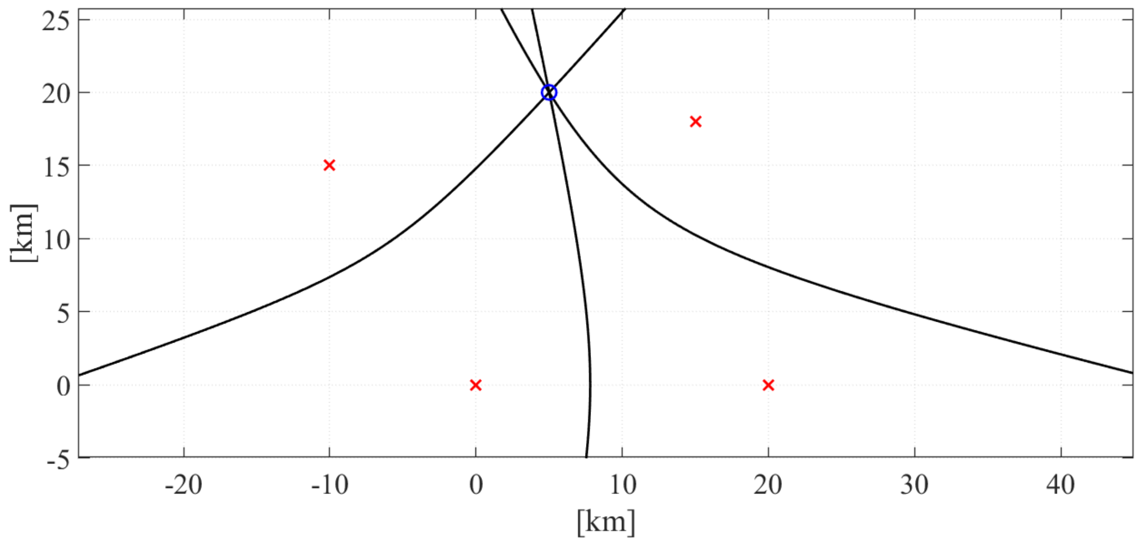

Figure 13. Example of TDOA geometry.

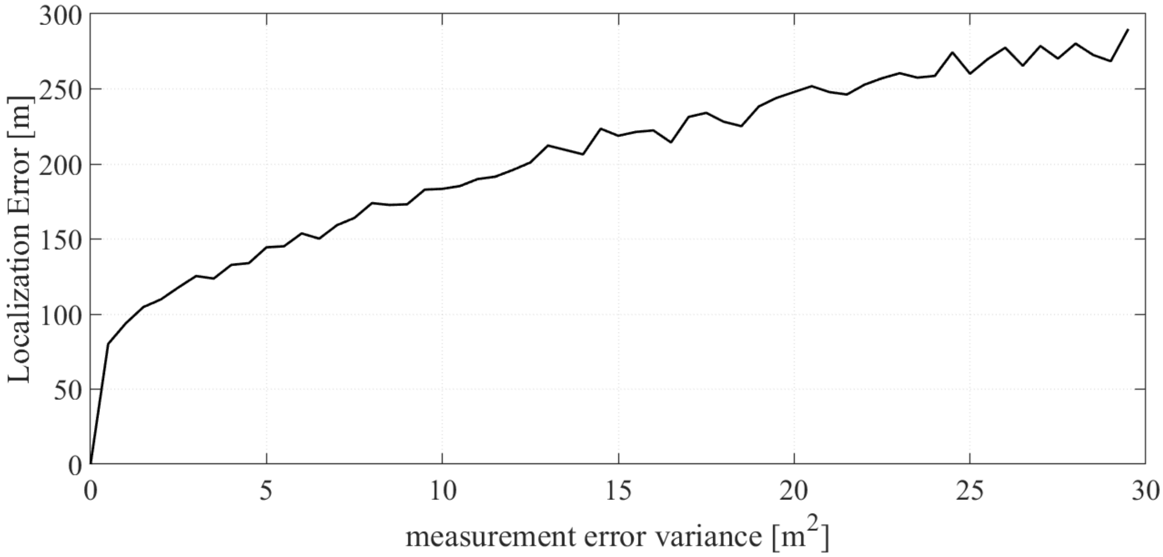

Figure 14. Relation between TDOA location method error and the variance of the TDOA measurement error

Figure **13** shows an example of the geometry, while

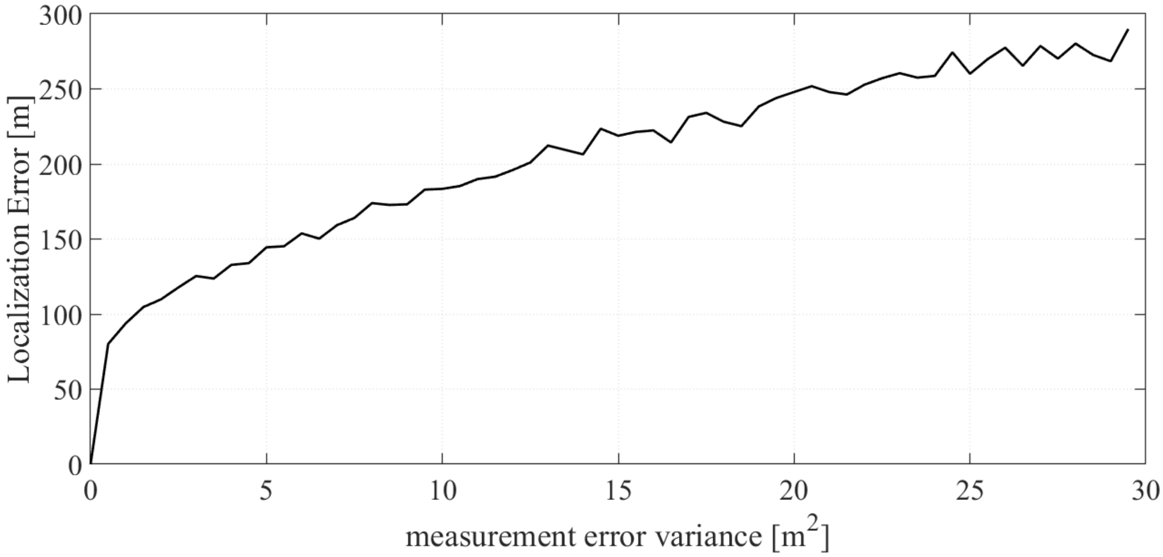

Figure **14** plots the dependence of the location error in the TDOA method on the variance of the random additive measurement error for this geometry. The geometry plot shows the distribution of the receivers (represented by red x) and the hyperbola (represented by a black line) at the intersection of which the transmitter will be located (represented by a blue o).

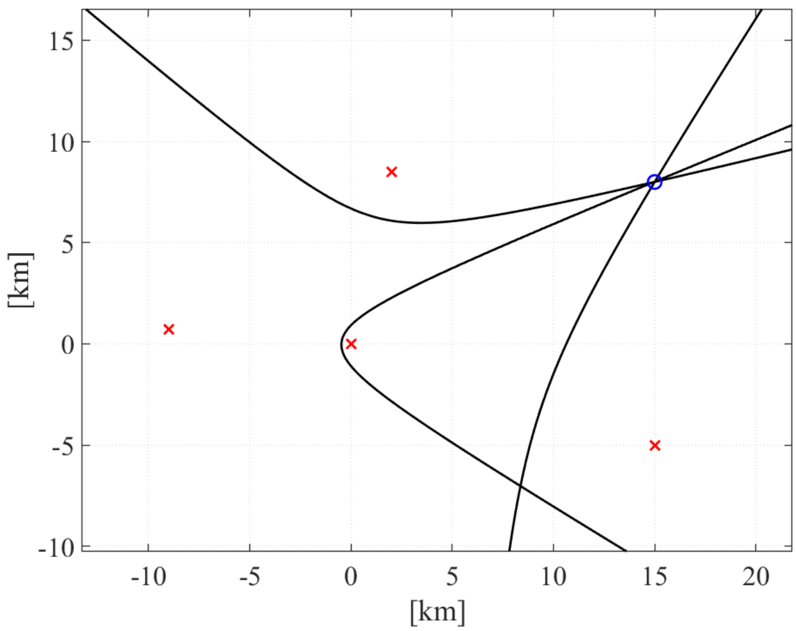

Figure 15. Example of another TDOA geometry

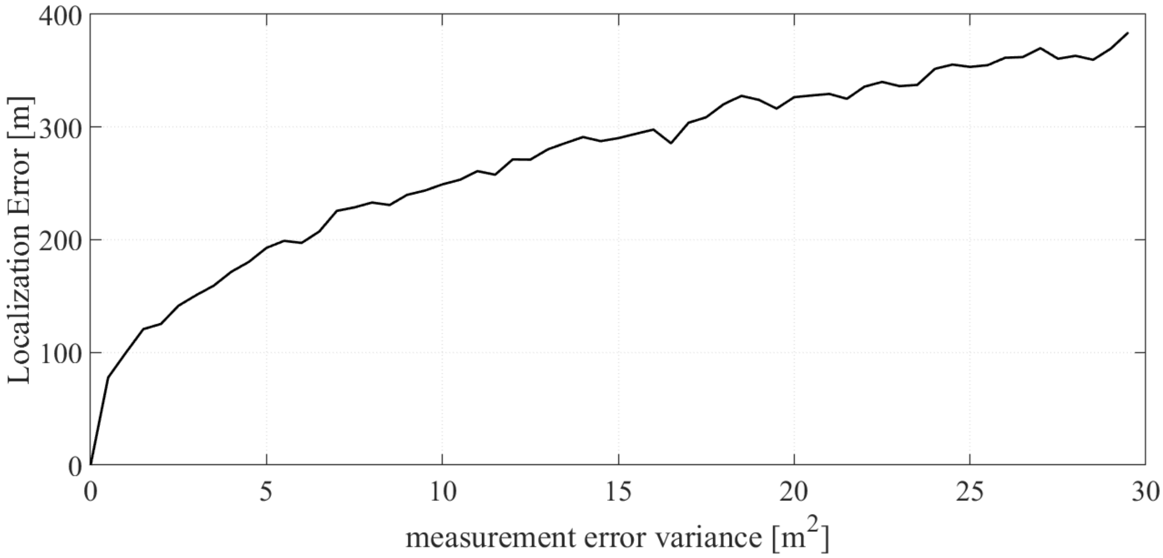

Figure 16. Relation between TDOA location method error and the variance of the TDOA measurement error

In contrast, the next two figures (Figure **15** and Figure **16**) show a different geometry and the associated location error graph. As shown, the localisation error differs in each case and is closely related to the geometry, which is typical for passive radiolocation. This necessitates further analysis being limited to specific scenarios with a geometry as close as possible to that assumed in experiments with real-life data. For this thesis, two measurement campaigns were planned corresponding to two simulation scenarios.

5.2.1. Scenario 1

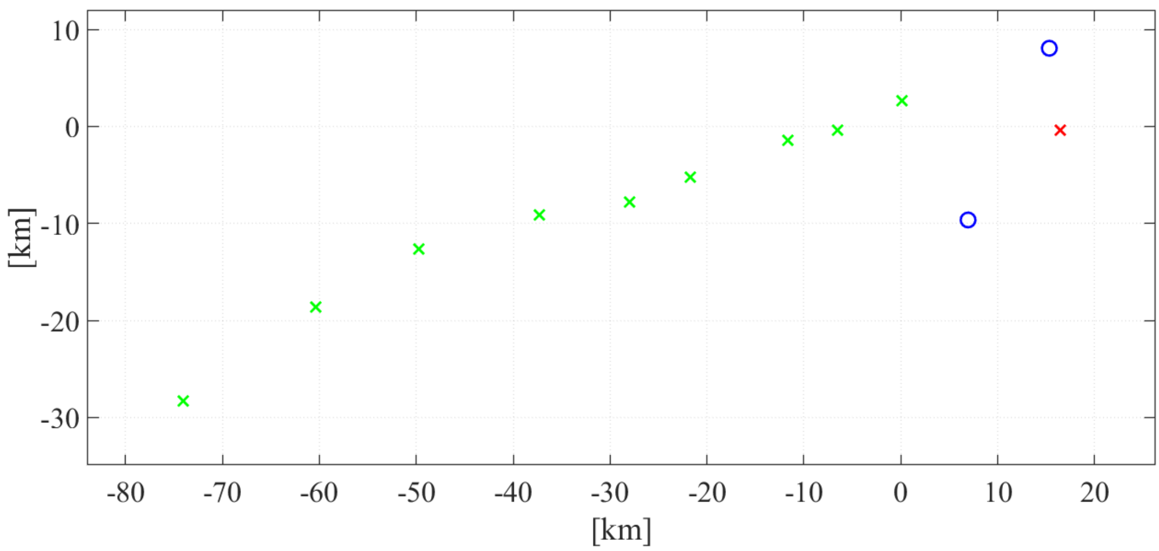

Figure 17. Geometry of scenario 1

The first scenario was planned to analyse the impact of long-range measurements on the receiver's performance and test the method of locating an unknown SFN transmitter. It consists of two transmitters working in SFN and two receivers: one stationary (represented by a blue x) placed between the transmitters and one mobile (represented by a green x). A two-dimensional visualization of this geometry is shown in Figure **17**. A total of nine measurements were planned, with the mobile receiver gradually moving further away from the transmitters. Since only one pair of receivers can be considered at the same time, one hyperboloid can be determined. This means no localisation of transmitters within a single measurement can be made.

5.2.2. Scenario 2

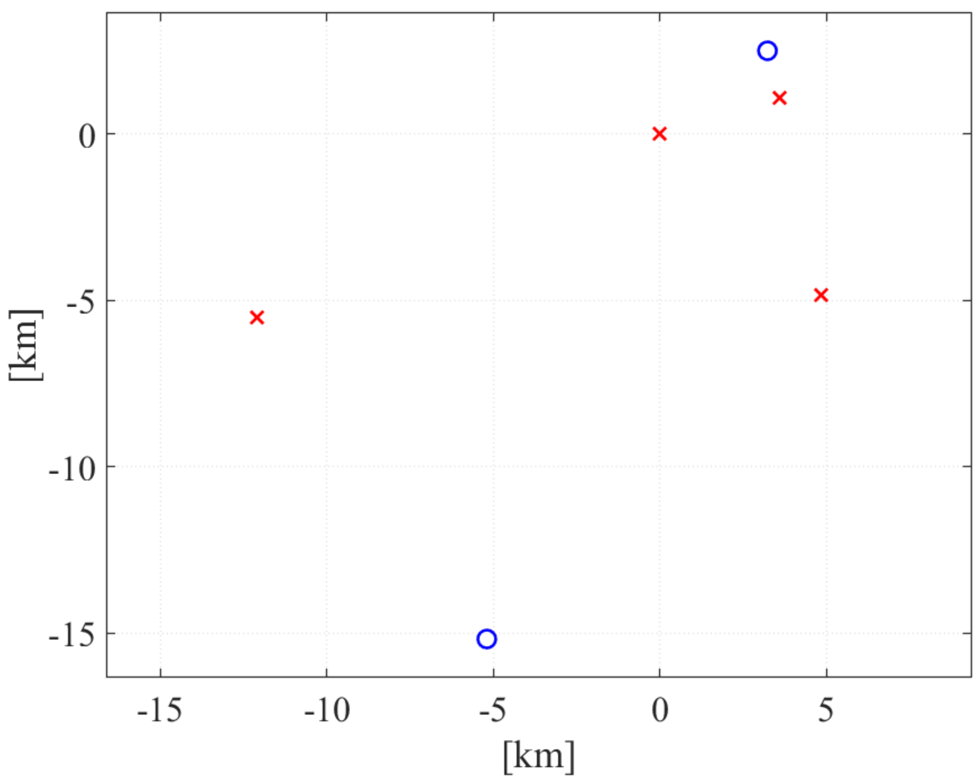

Figure 18. Geometry of scenario 2.

The second scenario was planned with a method of calculating desynchronisation between transmitters in mind. Four receivers (blue x) and two transmitters (red o) guaranteed a setup capable of supporting both algorithms presented in this thesis. Moreover, three pairs of receivers is enough for the calculation of TDOA localisation for both emitters, allowing for a precise estimate of measurement errors. A two-dimensional visualisation of this geometry is shown in Figure **18**.

5.3. TDOA localisation

To validate the correctness of the performance of the simulation tools, a TDOA localisation was conducted using geometry from scenario 2. Four receivers made it possible to form three pairs: Rx_4–Rx_1; Rx_4– Rx_2; Rx_4–Rx_3. In such a combination, three cross-correlation functions were calculated. At this point, it was necessary to develop a tool to detect and differentiate any peaks in cross-correlations plots and, at the same time, automate the entire process.

5.3.1. TDOA peak detection

As mentioned in Chapter 4.1.2, detection of TDOA peaks in cross-correlation results can be problematic. Especially in real-life data, where multipath effect is common. In most cases, there is no single distinct peak, and to extract the exact position of every peak, additional signal processing is required. In order to automate the detection process in this work, the Cell Averaging Constant False Alarm Rate (CA-CFAR) [1][47][48][49] detection technique is used to achieve this goal. CFAR is a family of adaptive detection algorithms based on determining the noise power level around a tested signal sample (also known as cell) called Cell Under Test (CUT). In CA-CFAR, the estimator of noise power level is found by measuring the arithmetic mean value of reference cells (grouped in two windows: the leading window and the lagging window). Then the CUT value is compared with the detection threshold, calculated as a multiplication of the mean value of reference cells and the threshold multiplier α given by [1]

$$\alpha = {P_{FA}}^{-\frac{1}{N}} - 1, \tag{103}$$

where N is the total number of reference cells (in both windows), and P_{FA} is the desired probability of a false alarm. If the value in CUT is greater than the threshold, CUT is considered to be a detection.

When the anticipated size of the peak is greater than one sample, it is common practice to introduce a gap (called guard cells) between the CUT and windows. This technique prevents the noise power level from being overestimated by the peak itself. The CA-CFAR block diagram is presented in Figure **19**. The example of autocorrelation and CA-CFAR threshold is presented in Figure **20**.

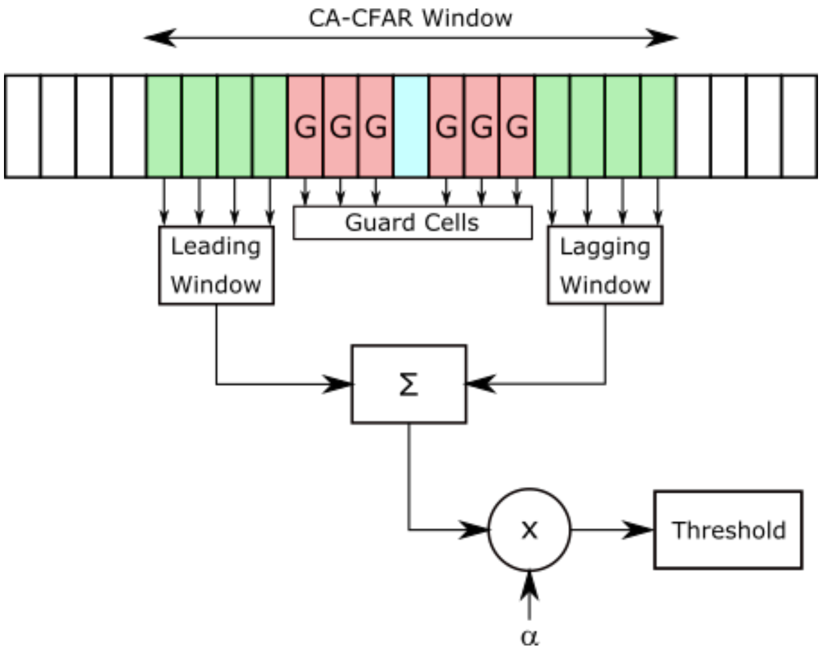

Figure 19. CA-CFAR block diagram.

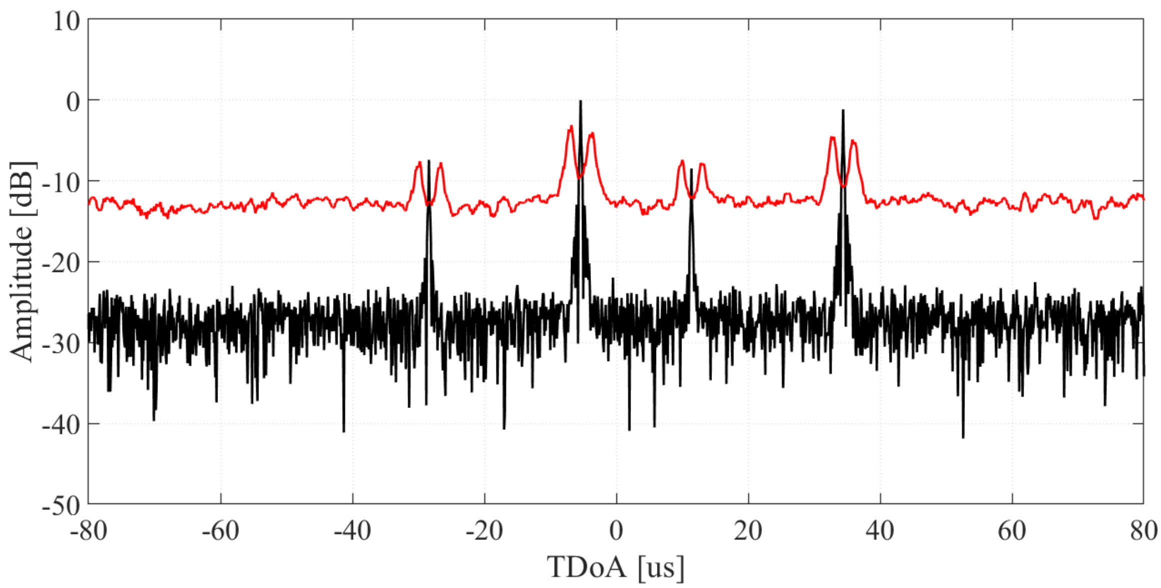

Figure 20. Example of cross-correlation function (black) and CA-CFAR threshold (red).

At this stage of processing, four areas of interest are found, each containing one TDOA peak. The ultimate CA-CFAR parameters used in simulations were as follows:

- number of guard cells: 11,
- number of cells in the reference window: 10,
- α: 15 dB.

The final step in peak detection is to extract the exact value of the estimated peak position. This was done simply by finding the TDOA value for the maximum amplitude within each area.

5.3.2. Transmitter localisation

Now equipped with a reliable peak detection tool, it was possible to locate all peaks within cross-correlation plots in an automated manner. Since the main goal of this simulation was to show the correctness of the chosen localisation algorithm, it was presumed that no peak identification was needed. In a real-world scenario, such an approach can be compared to situations where there is a priori information about the approximate position of emitters. Based on this assumption, peaks corresponding with the TDOA of one transmitter were found (red arrows in Figure **21**) and recalculated into distance using (10). Results are shown in Table **2** and the two-dimensional visualisation of localisation results using those results is shown in Figure **22**.

To complete the analysis of the performance of the chosen localisation algorithm, a random measurement error, in a form of the Gaussian noise with known distribution, was introduced in the TDOA measurement. As in Chapter 5.2, each data point on the error graph was calculated as the mean of 10^4 measurements. In each of those trials, a random disturbance value was added to the TDOA measurement generated using a normal distribution with a known variance. Results are presented in Figure **23**.

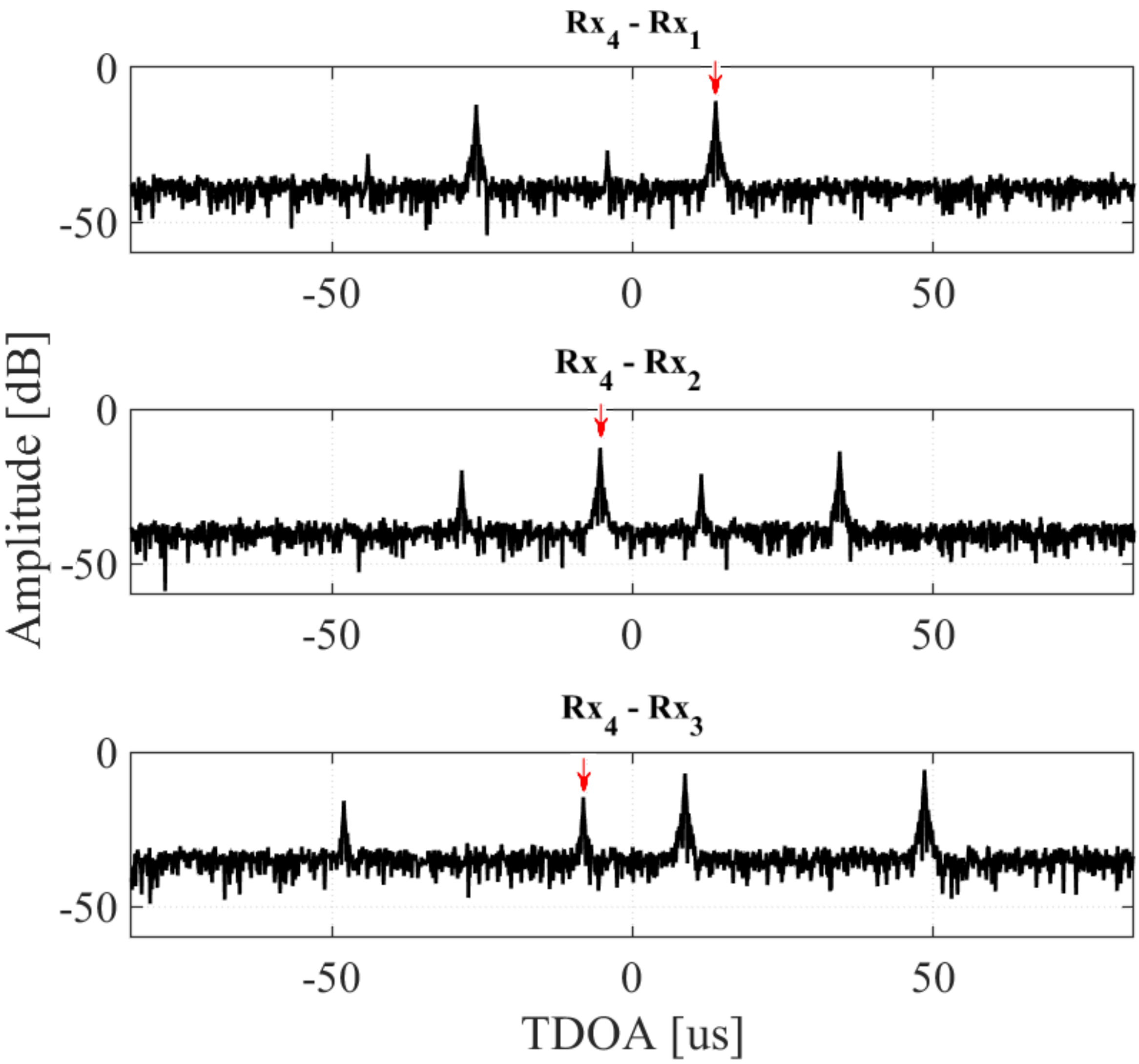

Figure 21. Cross-correlation plots of three receiver pairs with a visible peak. The red arrow indicates the peak corresponding to the TDOA value of the transmitter of interest.

Table 2. TDOA distance difference values.

Pair	TDOA [µs]	Distance difference [m]
$Rx_4 - Rx_1$	13.85	4155
$Rx_4 - Rx_2$	-5.38	-1615
$Rx_4 - Rx_3$	-8.14	-2443

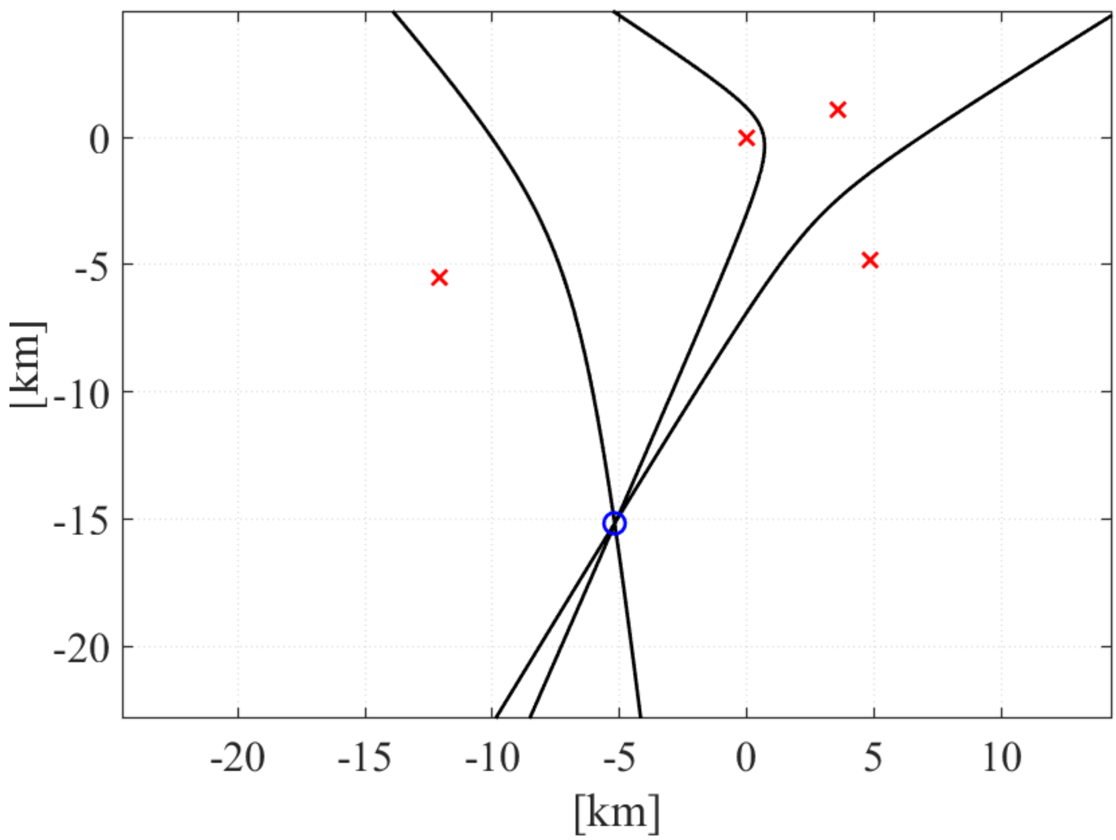

Figure 22. Visualization of location of transmitter of interest.

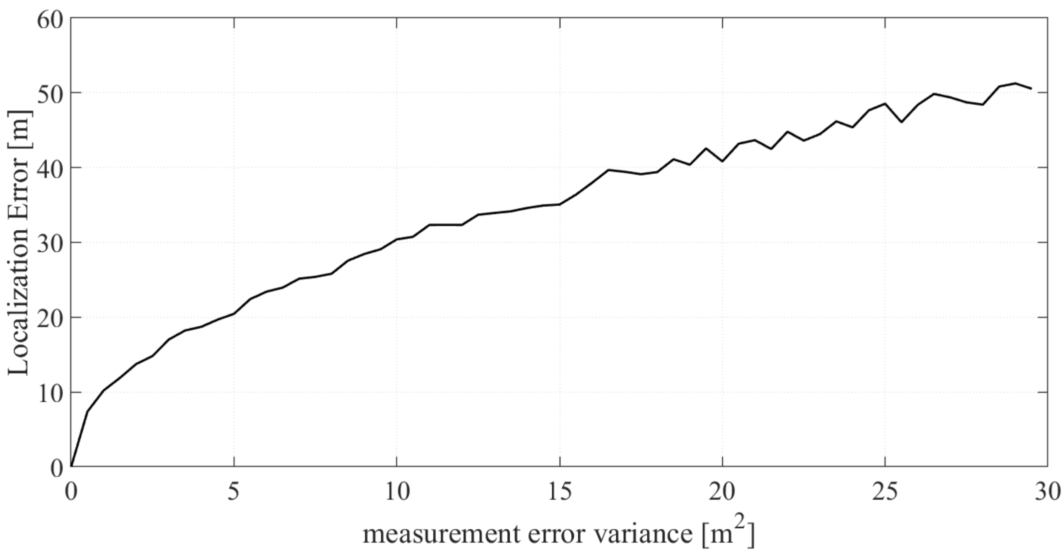

Figure 23. Relation between TDOA location method error and the variance of the TDOA measurement error.

The simulation results confirmed the reliability of the tools created for the study. The signal generator, peak detector, and transmitter localisation method described in Chapters 5.1, 5.3.1, and 3.5.5, respectively, proved to be reliable and suitable for further simulations.

5.4. Localisation of unknown SFN transmitter

In this chapter, the method from Chapter 4.1 is verified using simulated data.

5.4.1. Curve Intersections

In Chapter 4.1.3, it was mentioned that there are only two out of six permutations that include triple intersection points of all location curves (two circles and one hyperbole). To validate the claim that there are limited combinations of matching cross-correlation peaks with said curves, a Monte Carlo simulation was created. A total of 10^5 scenarios were created. In each of them, the 2-D positions of two receivers and two transmitters were randomly chosen within a 100 km x 100 km box. Next, based on the randomised positions, the values of P_2, P_3, and P_4 peaks described in Chapter 4.1 were calculated, and all possible combinations of matching peaks with curves were explored. For each combination, an algorithm searched for a three-curve intersection point. Since no noise was introduced to the peak estimates, only the numerical error of the intersection point-finding algorithm had to be taken into account. After repeating this procedure for 10^5 iterations, in 41.22% of them only one combination resulted in valid triple intersection points. For the rest (58.78%) of the scenarios, two combinations were valid. It is worth mentioning that in the case of 41 scenarios, no combinations were valid. This is because of the strict requirements for the Euclidean distance between a valid intersection point and Tx_2, so the actual positions (<1m) were not met by the intersection-finding algorithm. There were no scenarios in which more than two combinations were valid. Each plausible combination gives two solutions, totalling two or four possible locations for Tx_2 (in the worst-case scenario).

5.4.2. Scenario 1

In scenario 1, there are two receivers that can form a single pair. However, there are a total of nine measurements with different Rx_2 positions; three of these were chosen as a representative sample. For each measurement number of steps were taken:

- A cross-correlation was calculated (algorithm step from Chapter 4.1.1).

- All four peaks were identified in the plot via the peak detection method described in Chapter 5.3.1. Then peak corresponding with TDOA caused by a known transmitter (Tx_1) was discarded (algorithm step from Chapter 4.1.2).
- Six permutations of the three remaining peaks were determined. In every permutation, each of the peaks was assumed to have a different role, i.e., one peak was assigned as the second TDOA peak (caused by Tx_2) and the other two as ghost peaks. In this geometry, some pairs had two permutations with triple intersections, totalling four possible Tx_2 locations per measurement (algorithm step from Chapter 4.1.3).
- Since the simulation tools developed for this work do not include any way of simulating use of a directional antenna, no AOA measurements were made, and hence no further elimination of a plausible solution was possible (algorithm step from Chapter 4.1.4).

Measurements number 1 and 4 had triple intersection points in two permutations (see Figure **24** and Figure **25** for measurement number 1; Figure **26** and Figure **27** for measurement number 4). Measurements number 7 had triple intersection points in only one permutation (see Figure **28**). Blue asterisk indicates position of Tx_1, blue circle Tx_2 and red x marks position of the receivers.

To reduce the possible Tx_2 location, a comparison between measurements was made. This allowed for possible Tx_2 localisation to be reduced to a single, common for all measurements, triple intersection point. This location nearly perfectly reflected the initial Tx_2 position, with a localisation error below 1 metre. Such a good performance was possible due to the fact that no time disturbance in TDOA measurement was introduced (such errors may be added to imitate, e.g., synchronisation errors between receivers or receiver positioning error). The only source of noise in this simulation was random noise added to each signal gathered by receivers (SNR = 1). This does not affect localisation error in any major way as long as the peaks in the cross-correlation plot are above the noise floor. Of course, comparing multiple measurements is equivalent to standard TDOA localisation. That is why, in the case of a single measurement, to eliminate any plausible solutions, either AOA measurement or another verification method (e.g., confronting results with satellite images of the terrain to locate the transmitter) is necessary.

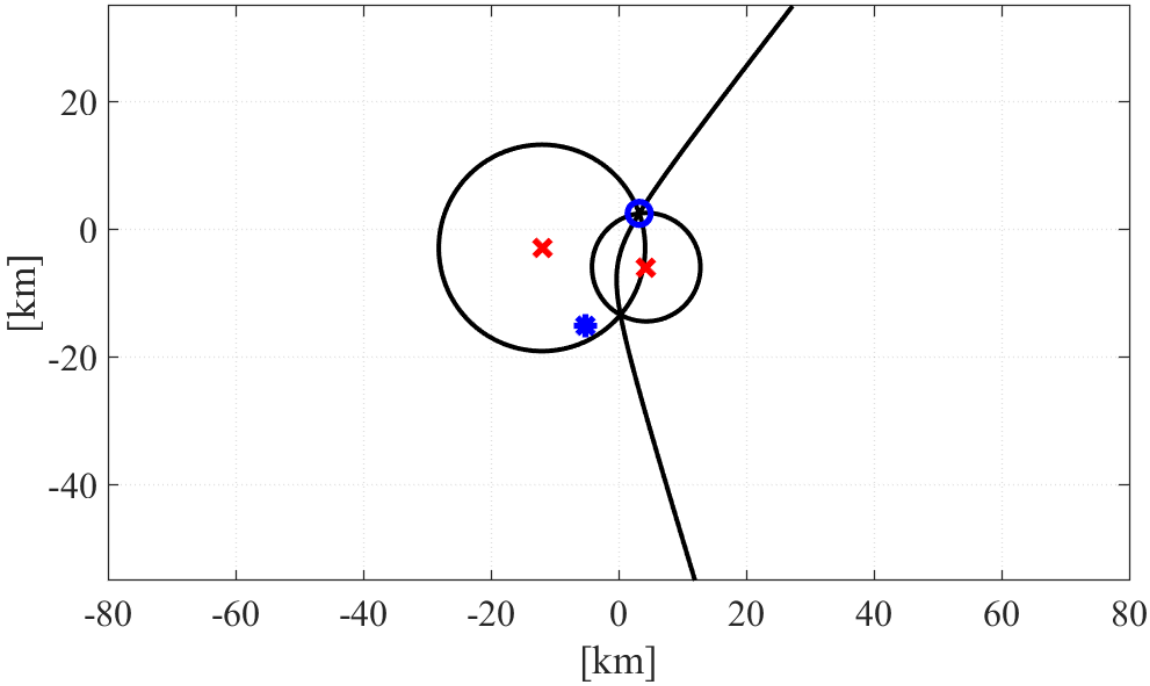

Figure 24. Localisation curves with triple intersection points with true Tx_2 position for the measurement number 1.

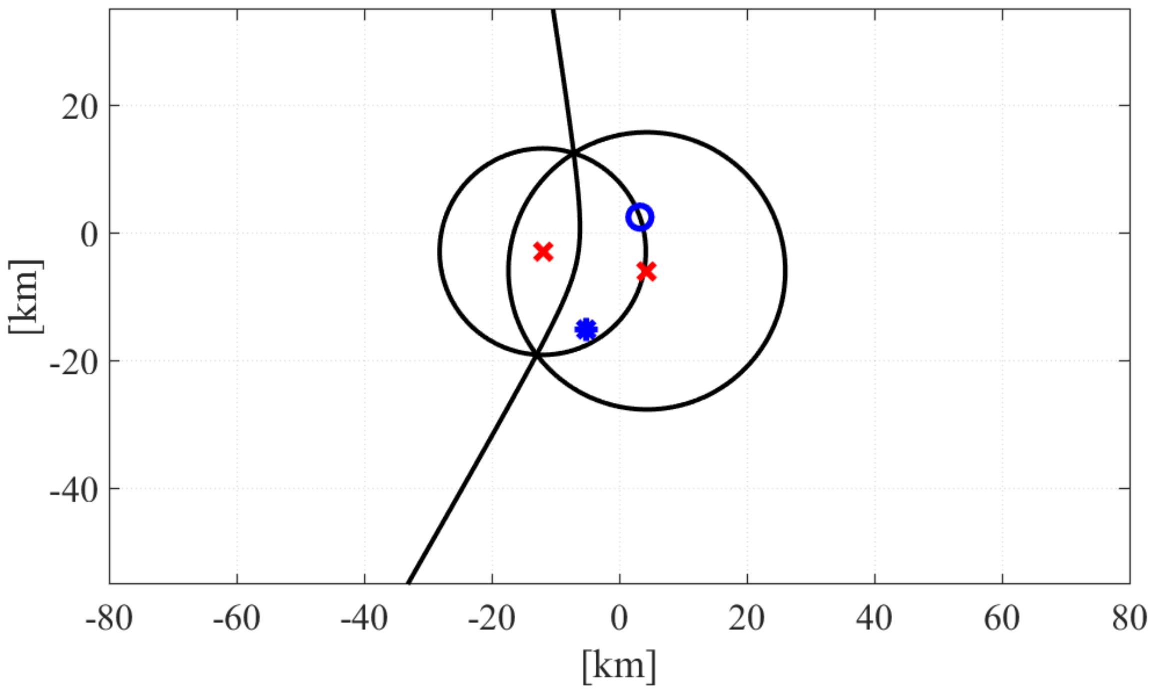

Figure 25. Localisation curves with triple intersection points with bogus Tx_2 position for the measurement number 1.

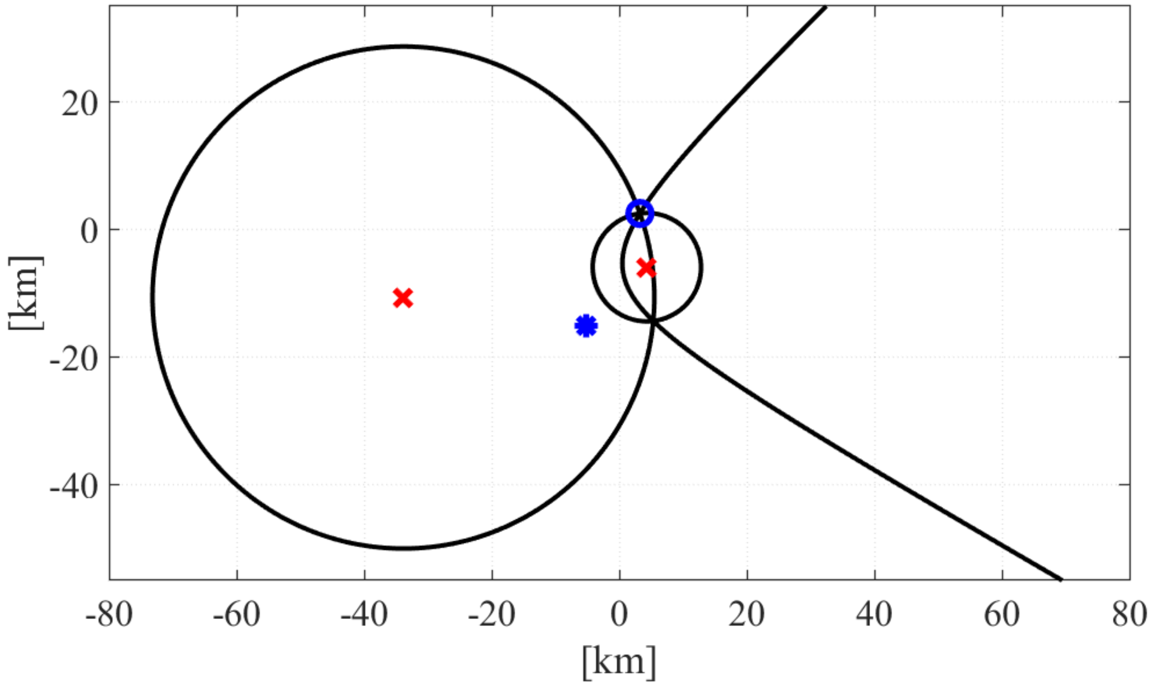

Figure 26. Localisation curves with triple intersection points with true Tx_2 position for the measurement number 4.

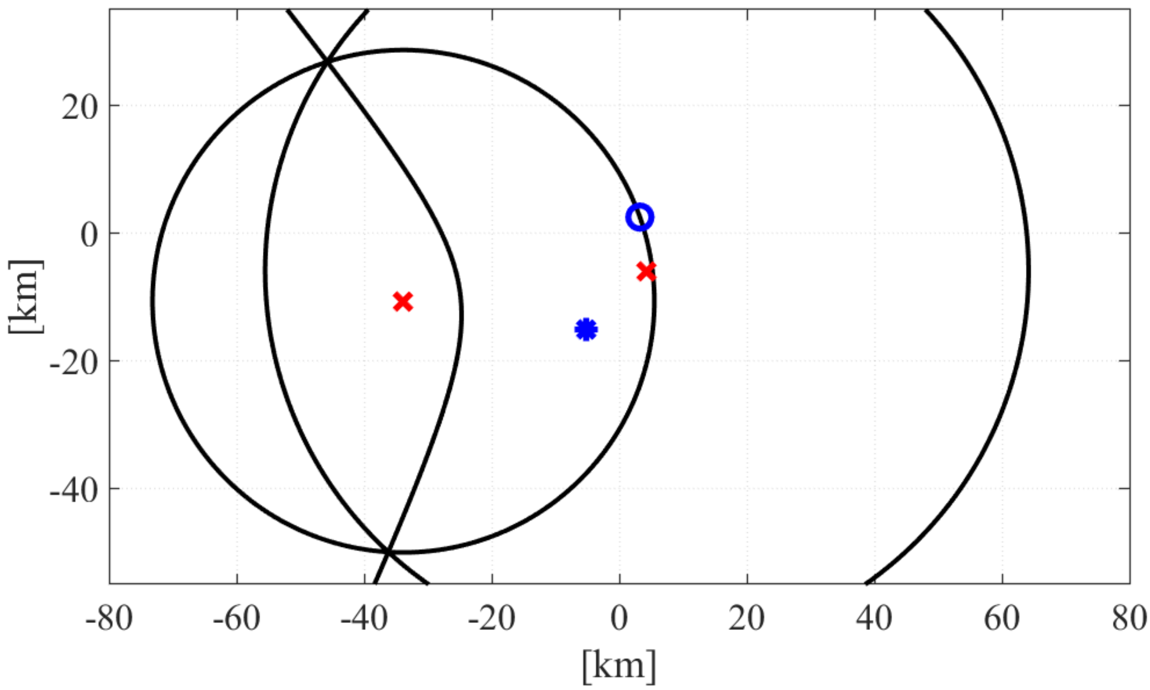

Figure 27. Localisation curves with triple intersection points with bogus Tx_2 position for the measurement number 4.

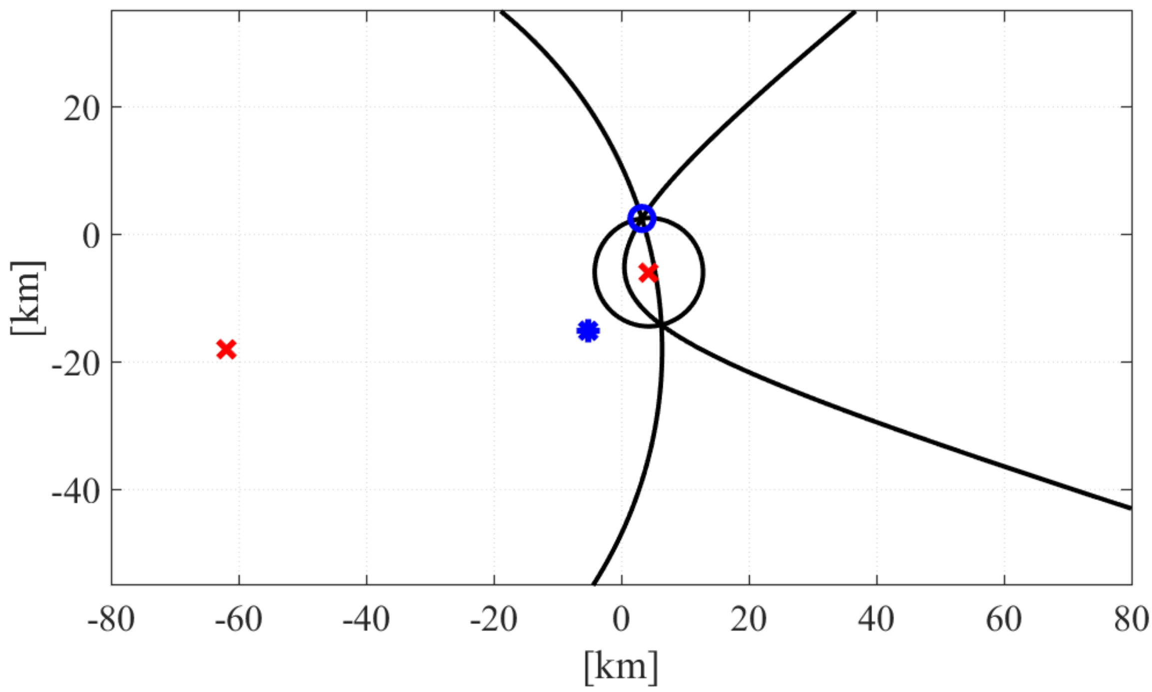

Figure 28. Localisation curves with triple intersection points with true Tx_2 position for the measurement number 7.

5.4.3. Scenario 2

Since in scenario 2 there are four receivers, three pairs are chosen. For each pair, the following steps were taken:

- A cross-correlation was calculated (algorithm step from Chapter 4.1.1)
- All four peaks were identified in the plot via the peak detection method described in Chapter 5.3.1. and the peak corresponding with TDOA caused by a known transmitter (Tx_1) was discarded (algorithm step from Chapter 4.1.2).
- Six permutations of the three remaining peaks were determined. In every permutation, each of the peaks was assumed to have a different "role" i.e., one peak was assigned as the second TDOA peak (caused by Tx_2) and the other two as ghost peaks. Surprisingly, in this geometry, all pairs had only one permutation with triple intersections (algorithm step from Chapter 4.1.3).

Again, no AOA measurements were made, hence, no further elimination of plausible solutions was possible (algorithm step from Chapter 4.1.4).

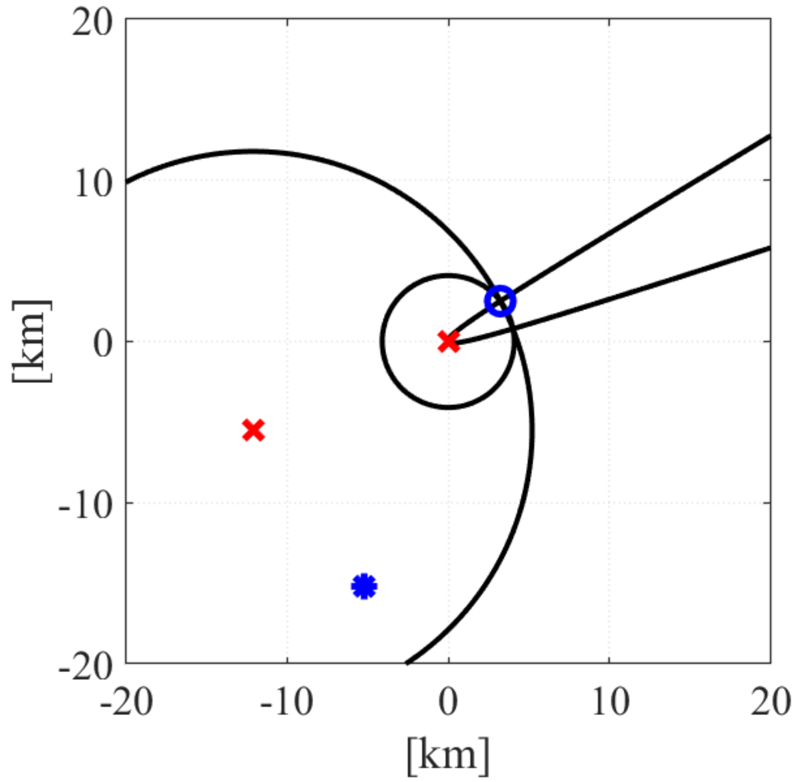

Figure 29. Localisation curves with triple intersection points with true Tx_2 position for the Rx_1-Rx_2 pair.

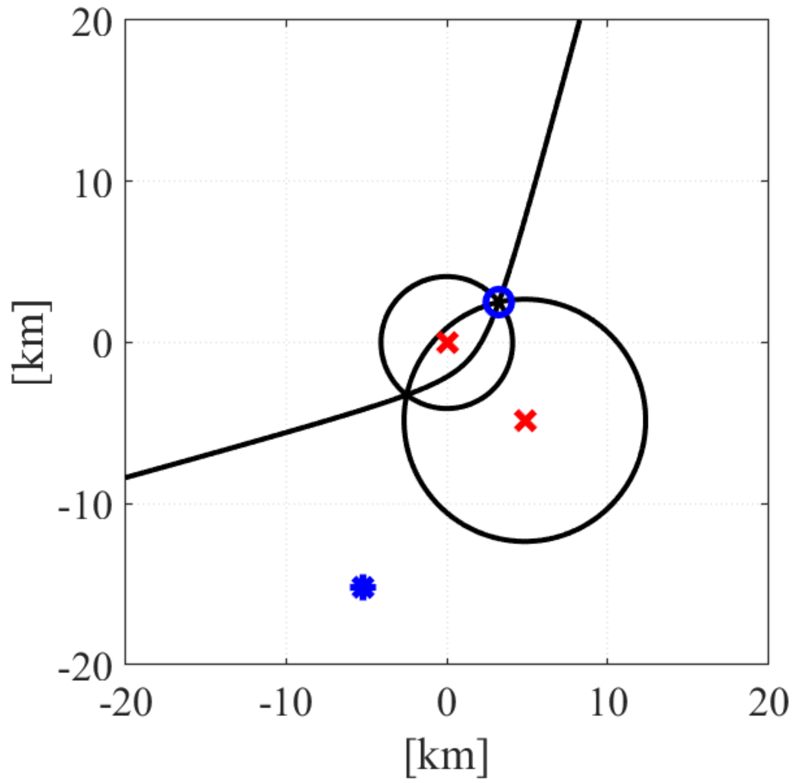

Figure 30. Localisation curves with triple intersection points with true Tx_2 position for the Rx_1-Rx_3 pair.

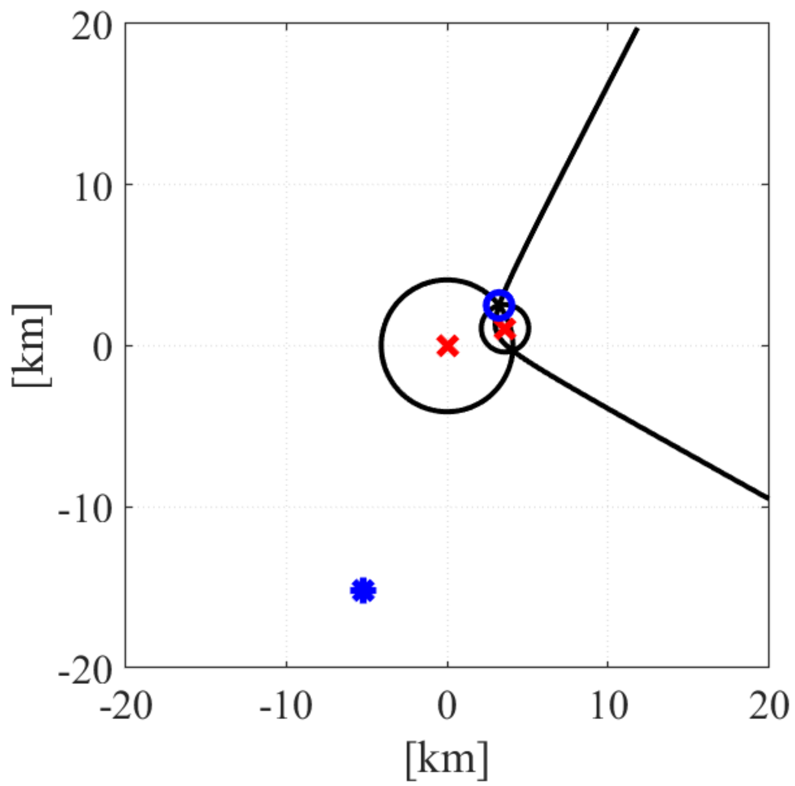

Figure 31. Localisation curves with triple intersection points with true Tx_2 position for the Rx_1-Rx_3 pair.

Similarly to the situation in scenario 1, by comparing the intersection points acquired from all three pairs, a single common point was found. As expected, the distance between Tx_2 position and this point was below 1 m, making it a satisfying estimate of Tx_2 localisation.

5.5. Desynchronisation calculation

In this chapter, the method presented in Chapter 4.4 will be verified using simulated data. The full algorithm requires multiple receivers to calculate the emitter's position (as described in Chapter 4.4.3), therefore scenario 2 will serve as the basis for verification. Three simulations were conducted with different desynchronisation errors: 0µs, 4µs, and 10µs. In each simulation, a number of steps were taken for each pair:

- A cross-correlation was calculated (algorithm step from Chapter 4.4.1). Example results for different desynchronisation values are presented in Figure **32**, Figure **33**, and Figure **34**.
- Using known transmitter and receiver locations, the positions of both TDOA peaks (P_1 and P_2) on the cross-correlation plot were calculated using (96) and (97). TDOA peaks were identified in the cross-correlation plot using those positions. Other two peaks were classified as ghost peaks (P_3 and P_4).

- Using TDOA peaks and the localisation method from Chapter 3.5.5, the estimated positions of both transmitters was calculated. Since no TDOA measurement error was introduced, results are different from Tx_1 and Tx_2 only by numerical errors (<1 µm).
- Using the estimated localisation of Tx_1, Tx_2, and receivers known localisation, positions of P_3 and P_4 ghost peaks were calculated using (98) and (99).
- Lastly, by comparing the measured positions of ghost peaks with their calculated positions, a desynchronisation estimate was acquired.

The results of the simulation were very encouraging. With no introduced error in TDOA measurement results of the algorithm were nearly perfect: ~0µs, ~4µs, and ~10µs, respectively. The differences varied at the level of the numerical error. Intermediate and final results for simulation with desynchronisation error set as 4µs are presented in the tables Cross-correlation of Rx1-Rx2 pair for all desynchronisation errors (Figure **32**, Figure **33**, and Figure **34**) show migration of ghost peaks with accordance to value of desynchronisation.

Table 3. Coordinates of transmitters and receivers in the scenario 2.

Coordinates	Tx_1	Tx_2	Rx_1	Rx_2	Rx_3	Rx_4
X [m]	6933.6	15317.1	0	16955.2	15684.4	12088.1
Y [m]	-9643.8	8056.3	0	723.8	6631.7	5539.4
Z [m]	329.9	210	0	-9.2	0.2	4.1

Table 4. TDOA peaks.

TDoA peaks [µs]	P_1 calc.	P_1 meas.	P_1 diff.	P_2 calc.	P_2 meas.	P_2 diff.
Rx_1-Rx_2	8.467	8.467	~0	-32.633	-32.633	~0
Rx_1-Rx_3	21.996	21.996	~0	-52.737	-52.737	~0
Rx_1-Rx_4	13.851	13.851	~0	-44.028	-44.028	~0

Table 5. Ghost peaks.

Ghost peaks [µs]	P_3 calc.	P_3 meas.	P_3 diff.	P_4 calc.	P_4 meas.	P_4 diff.
Rx_1-Rx_2	-14.550	-10.550	-4.000	-9.615	-13.615	4.000
Rx_1-Rx_3	-34.653	-30.653	-4.000	3.912	-0.088	4.000
Rx_1-Rx_4	-25.944	-21.944	-4.000	-4.231	-8.231	4.000

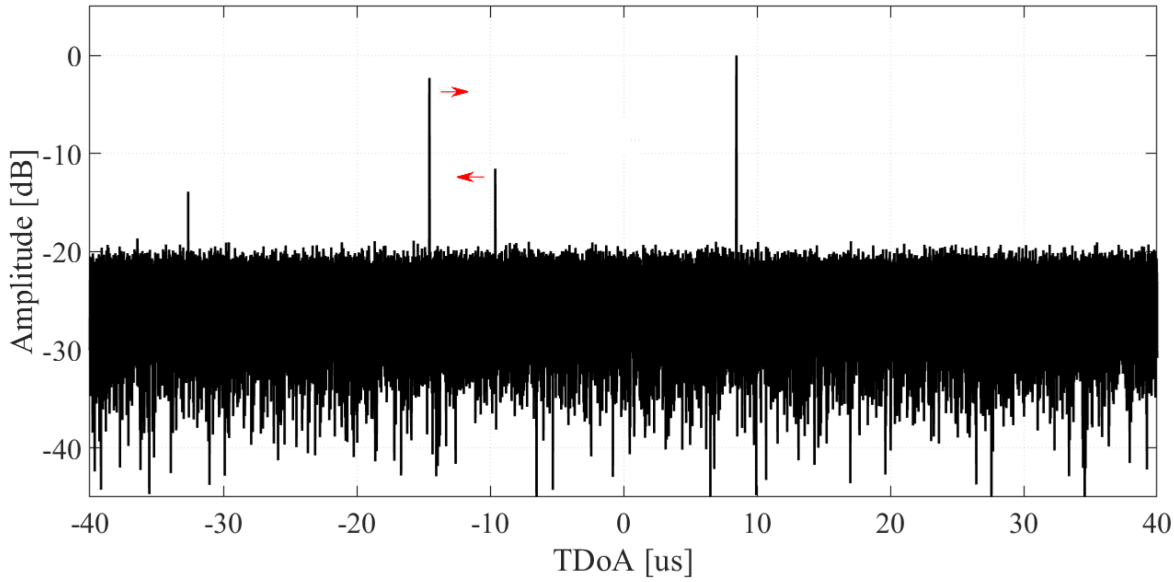

Figure 32. Cross-correlation plot of Rx1-Rx2 pair for desynchronisation error = 0μs. Red arrows indicate direction of ghost peaks migration with increasing desynchronisation error.

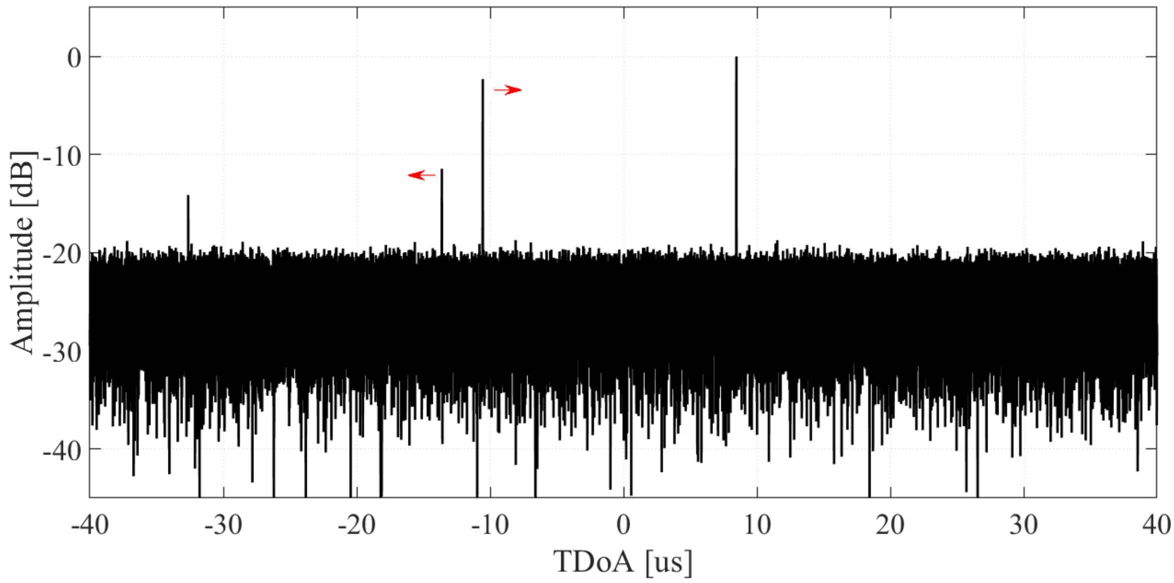

Figure 33. Cross-correlation plot of Rx1-Rx2 pair for desynchronisation error = 4μs. Red arrows indicate direction of ghost peaks migration with increasing desynchronisation error.

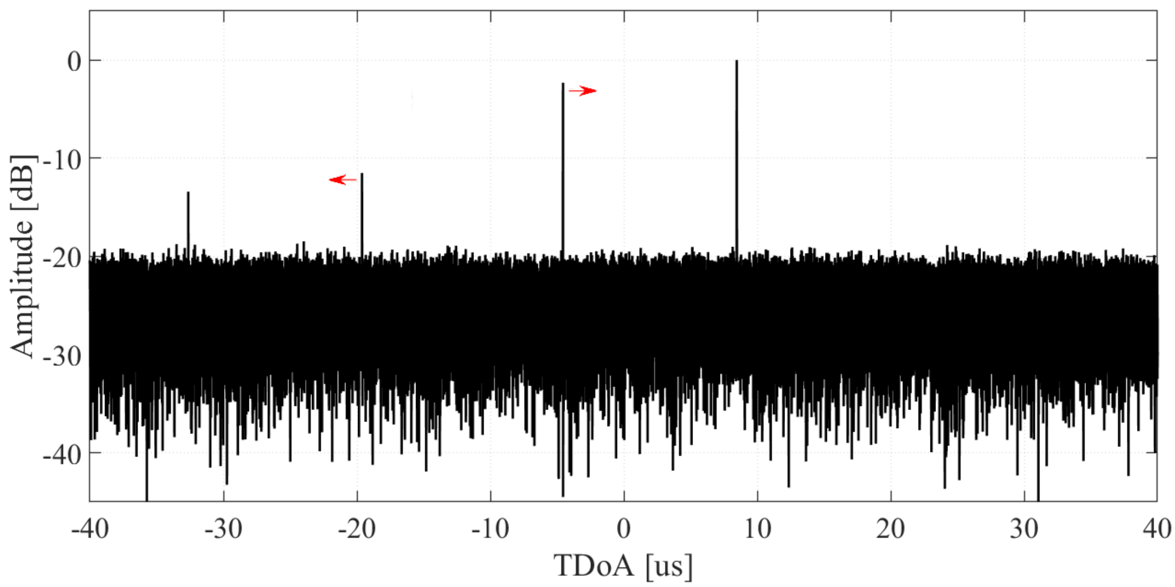

Figure 34. Cross-correlation plot of Rx1-Rx2 pair for desynchronisation error = 10μs. Red arrows indicate direction of ghost peaks migration with increasing desynchronisation error.

6. TRAILS AND EXPERIMENTS

This chapter presents the trials and experiments conducted in the study to validate simulations and proposed algorithms. The validation process will use real-life data collected from the actual SFN transmitters. The chapter provides an overview of the results of the trials and experiments, along with descriptions of the experiment setup, hardware used, and geometry employed. The subsequent sections will provide more comprehensive information on the experiments and their results.

6.1. Hardware

In order to validate the simulated results, a system of surveillance stations was developed. Basic requirements for such a system were low cost, reliability, and utilisation of remote control. Based on those requirements, the author of this thesis designed and developed a simple demonstrator of a passive radar system.

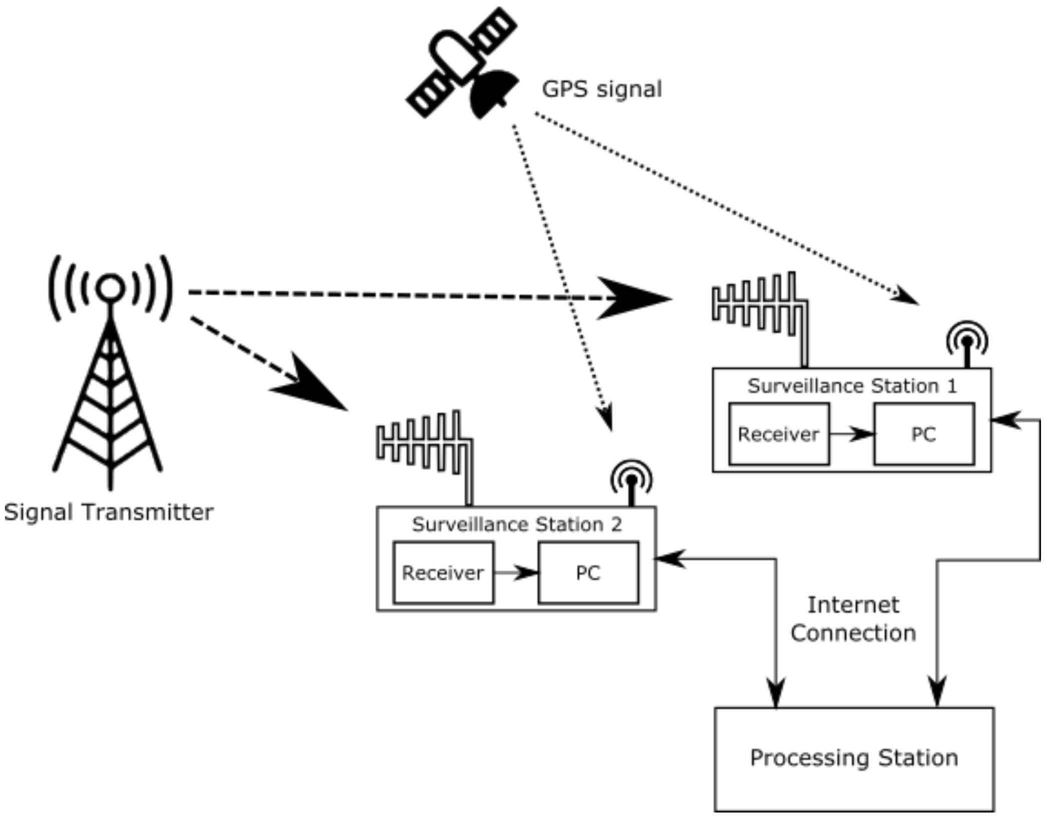

Figure 35. A simplified scheme of two surveillance stations.

The system can be divided into a number of independent surveillance stations and one processing station. Each surveillance station consists of a receiver and data storage/communication device built using a personal computer (PC). The choice of receiver implementation was conditioned by a few important factors. Firstly, the key parameter of any system based on time differentials is synchronisation. Therefore, both the device trigger and internal clock must have a function enabling adjustment to the Global Positioning System (GPS) clock. Moreover, the possibility of using GPS signal allows for easy and precise localisation of the surveillance station. Secondly, because once the stations are installed, they are difficult to reach and modify, so it was very important they work at a wide range of frequencies without any mechanical modifications, e.g., a receiver board change. Lastly, the entire station should be small and have low power consumption.

Figure 36. Surveillance station ready for measurements.

The natural choice was to construct receivers based on Software Defined Radio (SDR). SDR is a system where much of the traditional hardware components, such as filters and modulators, are replaced with software algorithms that are run on a general-purpose computer or specialised embedded system. This allows for greater flexibility and configurability of the radio system, as well as the ability to easily update or modify the system through software updates rather than physical hardware modifications. SDR technology has a wide range of applications, including military communications, wireless networks, and amateur radio.

Due to availability and previous experience, Universal Software Radio Peripheral (USRP) products were chosen. The USRP B210 is an SDR produced by Ettus Research, which is now part of National Instruments. It is designed to provide a high-performance, low-cost, and easily deployable SDR solution for various applications. The USRP B210 has a frequency range from 70 MHz to 6 GHz and provides up to 56 MHz of instantaneous bandwidth. In the designed system, the value of the instantaneous bandwidth was limited to 10 MHz. It has a 12-bit ADC and DAC, which allows for high-quality analog-to-digital and digital-to-analog conversions. The USRP B210 also includes a range of hardware features, most notably GPS synchronisation and positioning. It provided a single-board platform covering the entire DVB-T frequency spectrum.

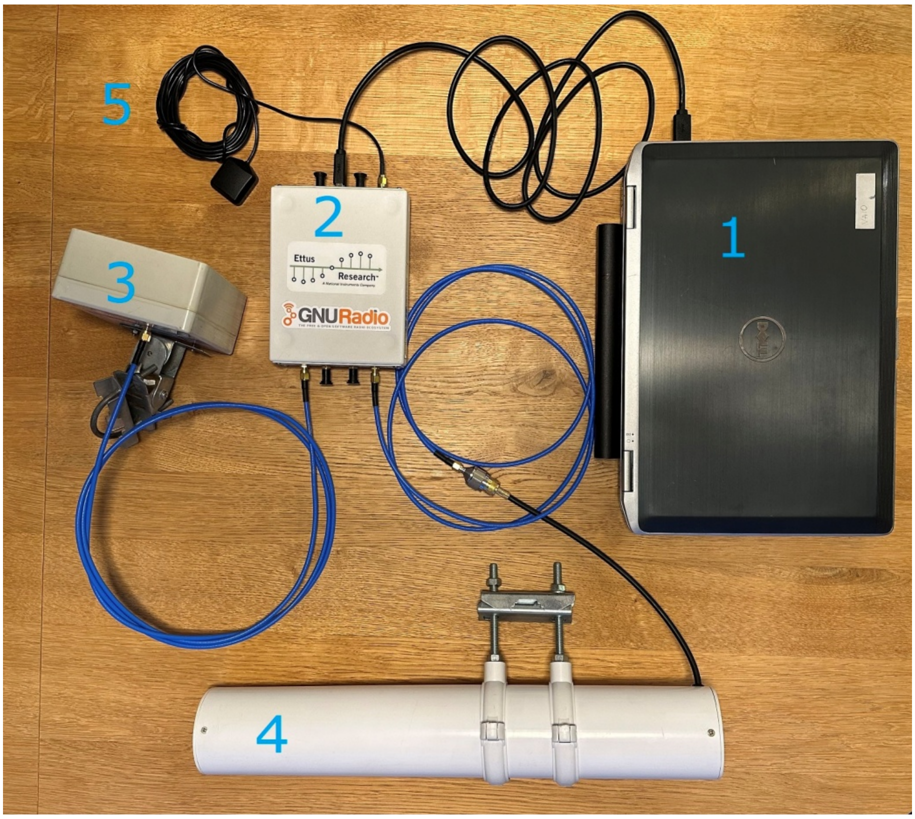

Figure 37. Surveillance station elements display. 1 – PC, 2 – USRP, 3 – sectoral antenna, 4 – directional antenna, 5 – GPS antenna.

A total of four stations were created using the B210 model. Each B210 was equipped with a GPS-disciplined crystal oscillator that provided each station with 10 MHz and 1 pulse per second reference signals synchronised with GPS. The accuracy of this synchronisation is 50 ns (root mean square 1-Sigma). PC was provided with an internet connection and was accessed by the processing station via secure shell (SSH). This connection allowed the processing station to simultaneously send commands and gather data from all surveillance stations. Each of stations was equipped with a sectoral antenna, a directional antenna, and a GPS antenna.

The system architecture is as follows: the processing station sends a request to all surveillance nodes to collect data at the desired frequency and at a precise time. After signal acquisition, raw data from all surveillance stations is transferred via internet connection to the processing station and then processed. The entire process takes several minutes from the moment of the request to receiving its final result, i.e., the localisation of the source of emission.

6.2. Geometry

To validate the simulation results from Chapters 5.4 and 5.5, two distinct measurement campaigns were carried out. In both scenarios, the same hardware was used, and the same transmitters were utilised as an illuminator of opportunity. The main difference was the geometry of the surveillance stations.

6.2.1. Transmitters

Two DVB-T broadcast towers in the vicinity of Warsaw, Poland, were chosen as transmitters. Both of those emitters transmit the same signal: MUX 1 at 770 MHz (channel 58) with an 7.8 MHz of bandwidth.

Figure 38. RTCN Raszyn by Wikipedia.org.

The first one, RTCN Raszyn (Figure **38**), is located south of Warsaw in Łazy within Piaseczno County (52.0728 N 20.8830 E). It was built in 1949 and remained one of the main sources of radio and digital television signal in Masovian Voivodeship. The mast of this transmitter is 332 metres high, but the antenna transmitting MUX 1 is 319 metres above the ground level. A total of 100 kW of power is emitted in MUX 1 by an omnidirectional antenna in horizontal polarisation (Figure **39**).

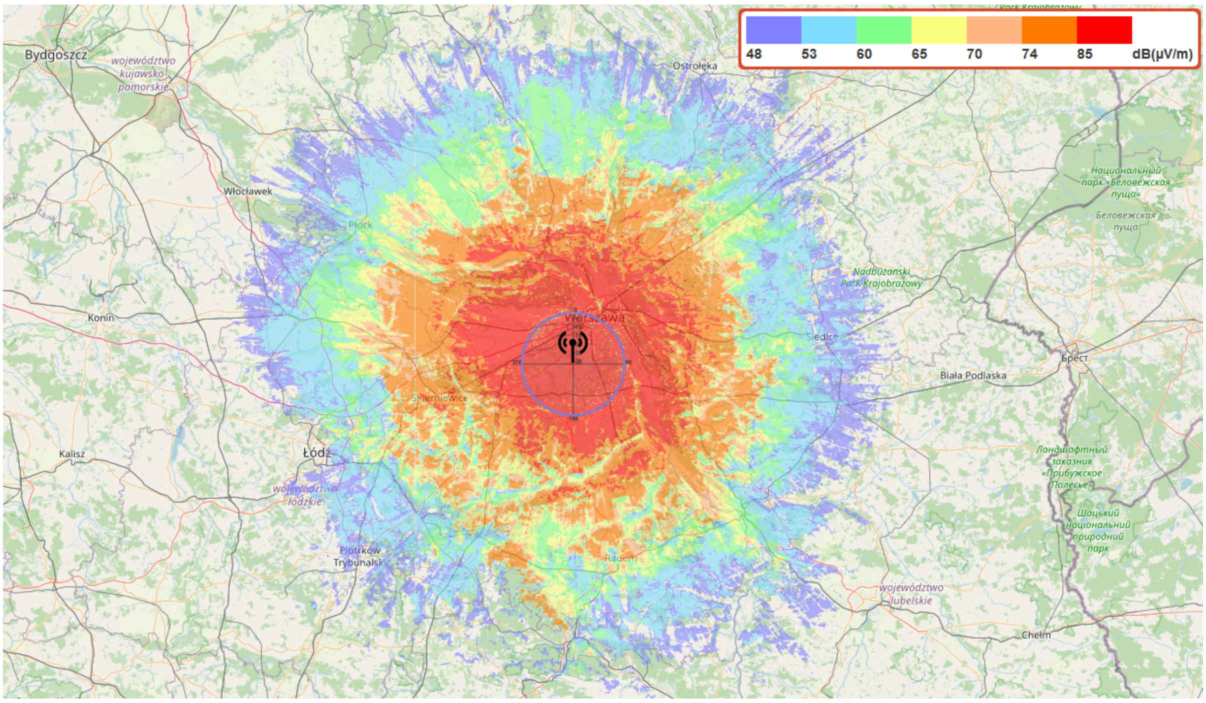

Figure 39. RTCN Raszyn coverage map [50].

The second chosen transmitter is RTCN "Pałac Kultury i Nauki" (Figure **41**), or RTCN PKiN in short. It is located in the centre of Warsaw at the top of PKiN, the highest building in Poland until 2022, built in 1955. The transmitter's mast was placed at the top of the PKiN spire one year later. Nowadays, PKiN has become an important emitter, covering Poland's capital with FM, DVB-T, and DAB signals. The directional antenna responsible for the emission of the MUX-1 signal is placed at a height of 226 metres above the ground level. Being a satellite transmitter with the main goal of covering the blind spots of RTCN Raszyn throughout Warsaw (see Figure **40**), the power of RTCN PKiN is equal to 3 kW. The main parameters of both transmitters are shown in Table **6**.

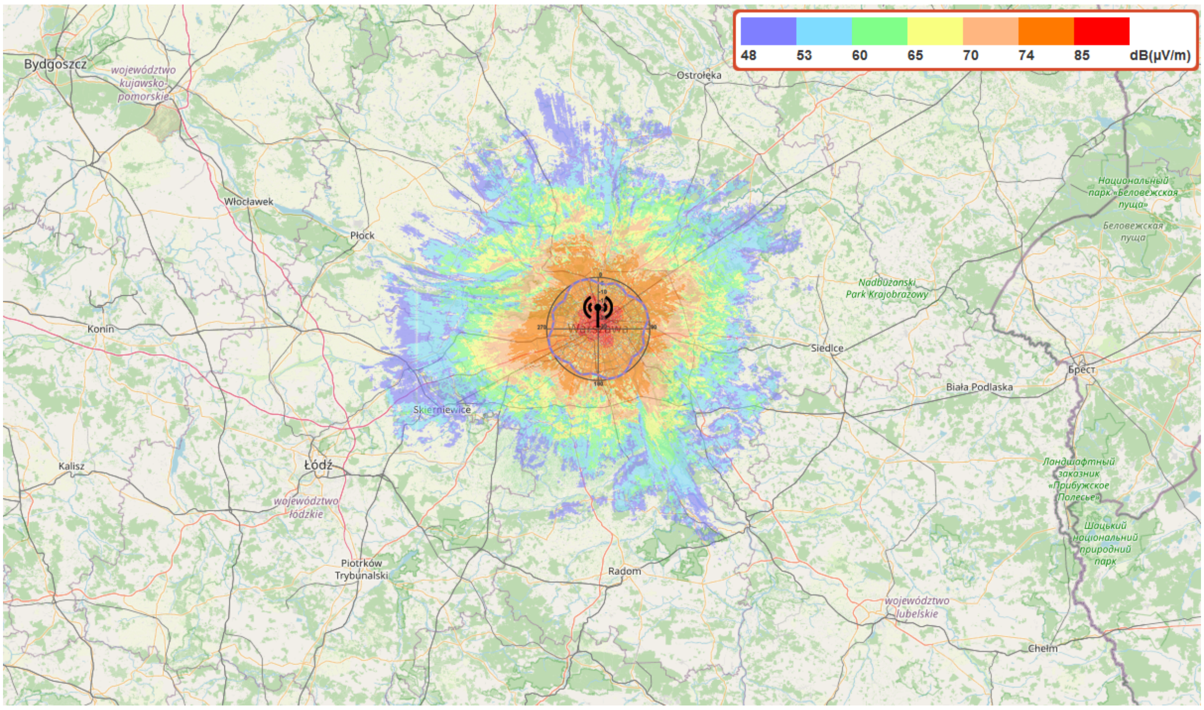

Figure 40. RTCN PKiN coverage map [50].

Figure 41. RTCN PKiN by Wikipedia.org.

Table 6. Transmitters summary.

Tx name	Latitude*	Longitude*	Channel	Power
RTCN Raszyn	52.0733 N	20.8855 E	48 (690 MHz)	100 kW
RTCN PKiN	52.2317 N	21.0064 E	48 (690 MHz)	3 kW

It is important to mention here that the precise localisation of both radio transmitter towers is ambiguous. Several sources from online databases provide different information (see Table 7). Taking the PKiN transmitter as an example, these differences can reach over 40 metres. As mentioned in Chapter 1, such an error will influence any passive radar localisation attempts. Data from Wikipedia.org was ultimately chosen as the source of the transmitters' positions.

Table 7. Transmitter localisation differences.

Source	Latitude of PKiN	Longitude of PKiN
FMSCAN.org	52.23166 N	21.00611 E

DVBTmap.eu	52.23172 N	21.00675 E
Google Earth	52.23184 N	21.00599 E
Wikipedia.org	52.23167 N	21.00639 E

6.2.2. Scenario 1

The first scenario's geometry was designed with two goals in mind. The first goal is to explore possible limitations of used hardware by separating receivers by up to 100 km apart. The second is to prove the utility of the localisation of unknown emitters method from Chapter 4.1.

Stronger transmitter (RTCN Raszyn) was designated as Tx_1 with known position (red "T" marker). The second one (RTCN PKiN) was treated as an unknown transmitter, Tx_2 (blue marker). As Rx_1 and Rx_2, two surveillance stations described in Chapter 6.1 were used. The first one with a fixed position was placed between Tx_1 and Tx_2 in the Warsaw urban area (red "R" marker). The second receiver station was mobile. Measurements were taken at a total of 9 positions of Rx_2 along the A2 highway between Warsaw and Łódź visible in Figure **42** as red markers with numbers 1 to 9.

Figure 42. Map showing position of transmitters and surveillance stations: Tx_1 - T marker; Tx_2 blue marker; Rx_1 – R marker; Rx_2 - number marker (from 1 to 9). For scale distance between Tx_1 and Tx_2 is equal to 19.6 km.

6.2.3. *Scenario 2*

A second scenario was set up to show the system's capabilities for localising sources of emission and calculating desynchronization between transmitters in SFN. Four surveillance stations were placed in different districts of Warsaw (B, C, and D markers) and Pruszków (A marker), as shown in Figure **43**. Unfortunately, due to a dense urban development and accessibility limitations, none of the four stations could be placed in a way to acquire omnidirectional reception. Nevertheless, every station could receive signals from both transmitters at acceptable levels.

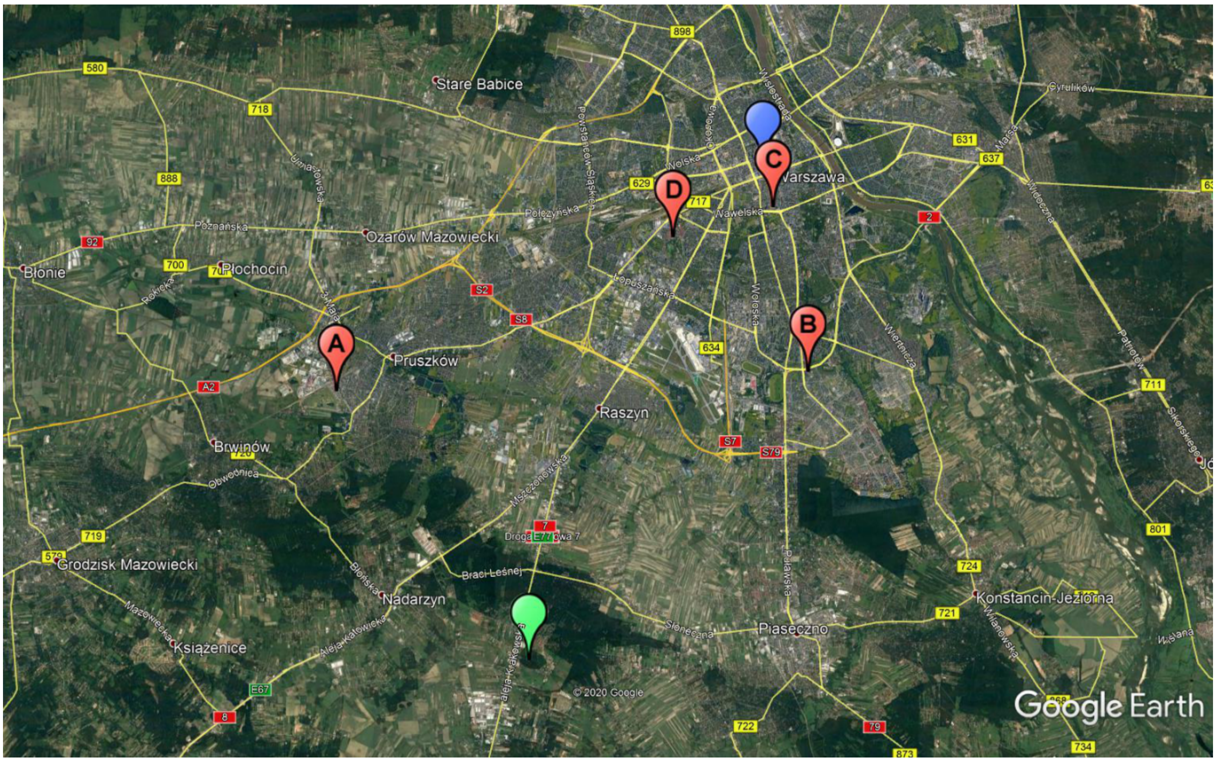

Figure 43. Map showing positions of used transmitters of opportunity (Raszyn -green marker, PKiN - blue marker) and surveillance stations (red markers). For scale distance between green and blue markers is equal to 19.6 km.

6.3. Signal analysis

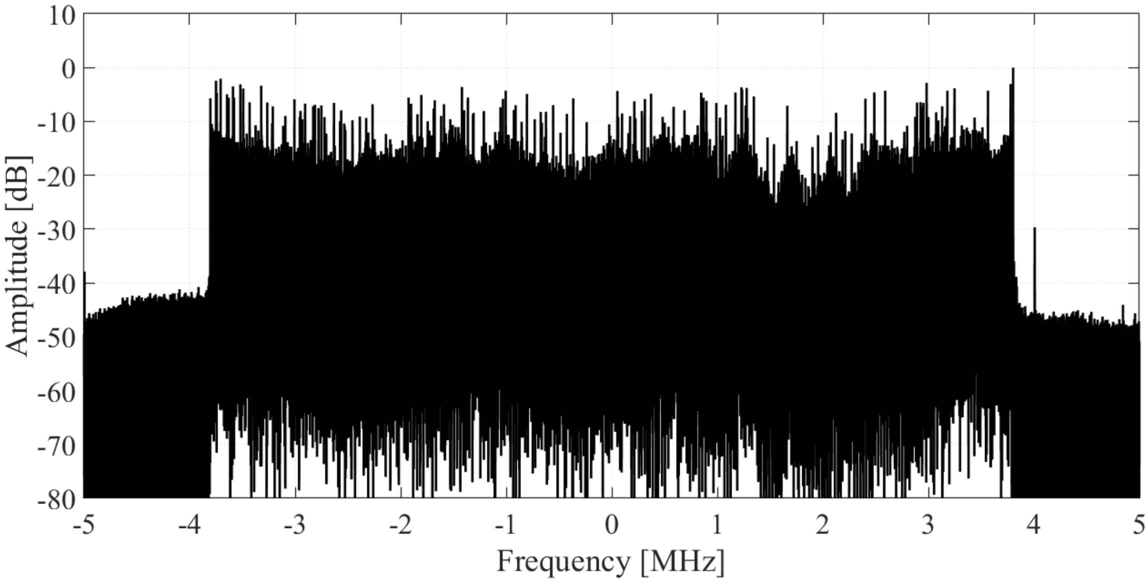

Figure 44. Spectral density of received signal.

A single surveillance station was positioned at the Warsaw University of Technology (marker C on Figure **43**). After choosing the transmitter's central frequency as 770 MHz and the receiver's bandwidth as 10 MHz, test data was gathered. In Figure **44**, the signal spectrum is presented with a clearly visible 7.8 MHz DVB-T channel. In Figure 45, signal autocorrelation is shown. As expected, three distinguishable peaks are visible, suggesting that SFN is present.

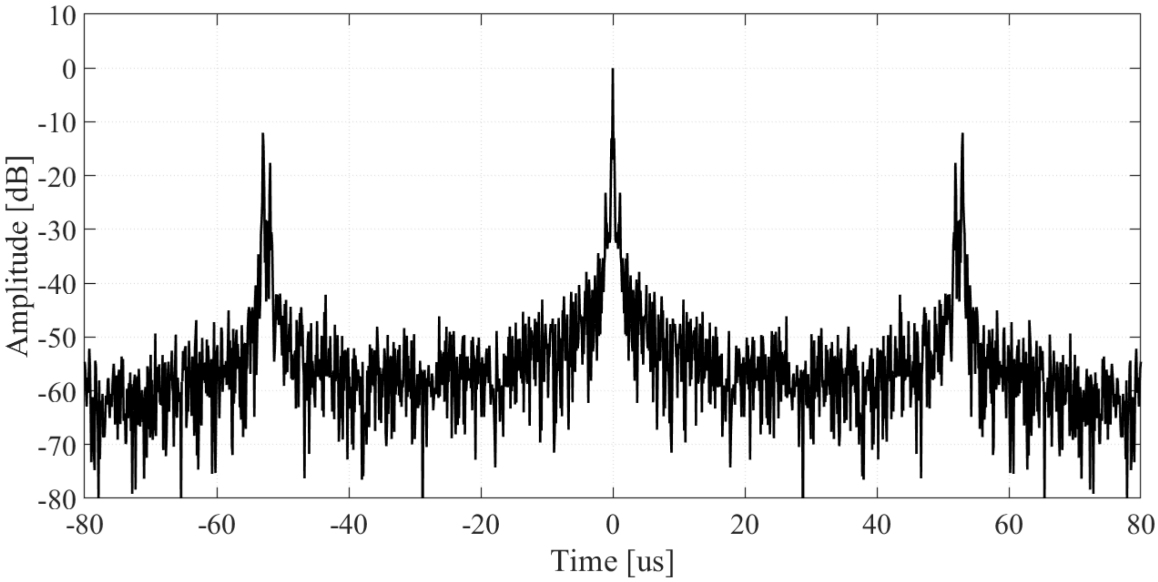

Figure 45. Autocorrelation of the received signal.

Overall, the characteristics of a real signal are comparable to those of simulated signals, although some visible differences can be observed. Most importantly, the peak on the left and its symmetric peak on the right are wider than their simulated counterparts in Figure 12. That change can be attributed to multipath phenomena. It occurs when the transmitted signal reflects from any obstacles between the transmitter and the receiver, and multiple copies of the slightly delayed original signal reach the surveillance station. The visualisation of multipath is presented in Figure **46**.

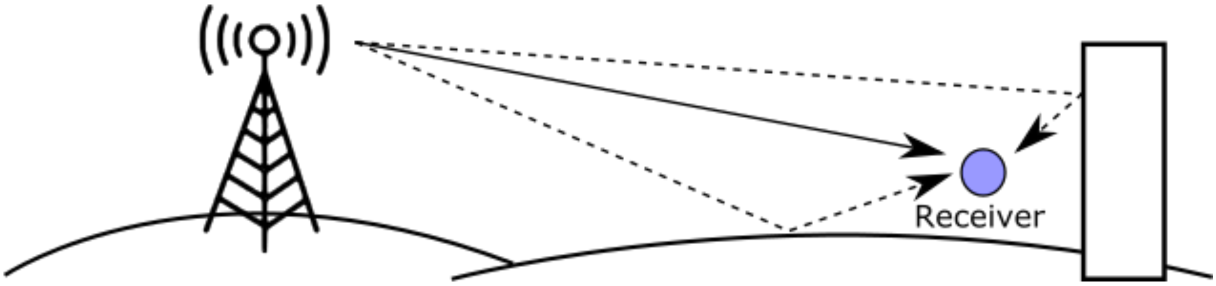

Figure 46. Visualization of multipath effect

The same effect caused by multipath will be visible in cross-correlation and can introduce some ambiguity when choosing TDOA peaks. This problem was handled using CA-CFAR, described in chapter 5.3.1, with parameters described in chapter 6.4.

Before further algorithm validation, a SNR measurement was made to make sure that the acquired signals were strong enough to perform subsequent processing. SNR was calculated as [51]

$$SNR = \frac{P_S}{P_N}, \tag{104}$$

where P_S is the received signal power and P_N is the noise power.

For scenario 1, the resulting SNR values (defined as the peak value at the noise floor level) are presented in Figure 47. In both scenarios, all measured SNR values are at an acceptable level for further processing, with the lowest value equal to 14.1 dB. The exact values of SNR are highly dependent on the used antenna radiation pattern and local terrain topography.

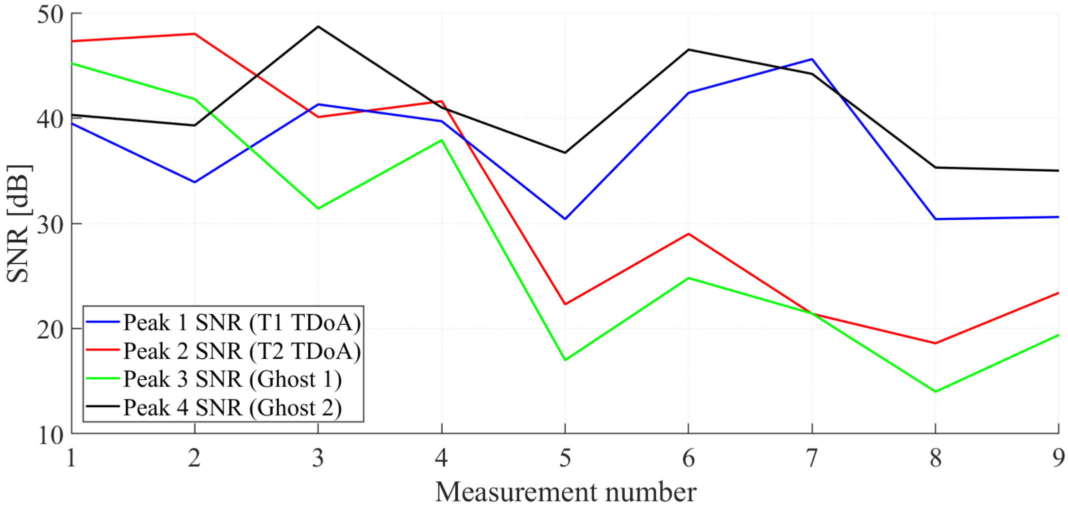

Figure 47. SNR values for cross-correlation peaks.

6.4. TDOA peak detection

The multipath effect (responsible for fluctuations of noise power level around the TDOA peak) is extremely hard to model due to its unpredictable nature and dependency on measurement geometry. Because of that fact, instead of finding a universal model for the described scenarios geometry, a number of real-life autocorrelation results were used to find α that guarantee a P_{FA} level below 10^{-5}. The ultimate CA-CFAR parameters used in this work are as follows:

- number of guard cells: 1,1
- number of cells in the reference window: 10,
- α: 22.75 dB.

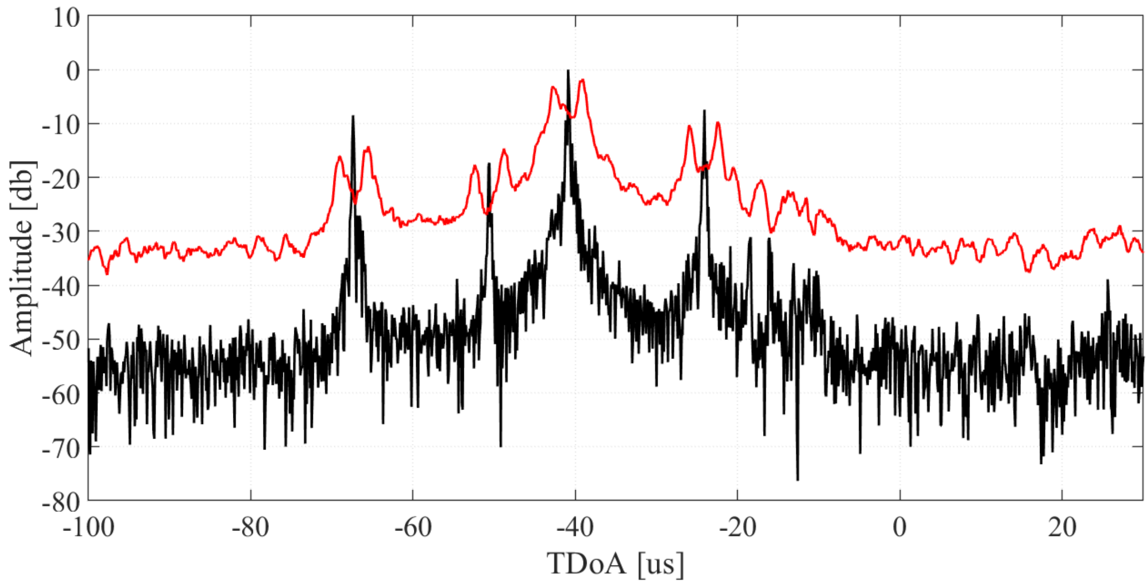

Figure 48. Cross-correlation function of real-life data (scenario 1 position 3) and CA-CFAR threshold (red).

6.5. Localisation of the unknown SFN transmitter

In order to ensure the correctness of the algorithm from Chapter 4.1 and to verify the simulation analysis, all steps of the algorithm were carried out as described in Chapter 5.4 using the collected real data. Following the proposed steps of the algorithm:

- All the data was acquired from the SDR, which performed a range of signal processing tasks such as demodulation, resampling, filtering, and synchronising with GPS. No additional digital signal conditioning was needed. The only procedure that needed to be done was the cross-correlation calculation (algorithm step from Chapter 4.1.1).
- Despite a strong multipath effect visible in the cross-correlation function, all the peaks described in Chapter 4 were found using CA-CFAR with parameters from Chapter 6.4. Figure **48** and Figure **49** show an example of this step. Just as in simulation, the peak corresponding with TDOA caused by a known transmitter (Tx_1) was discarded (algorithm step from Chapter 4.1.2).

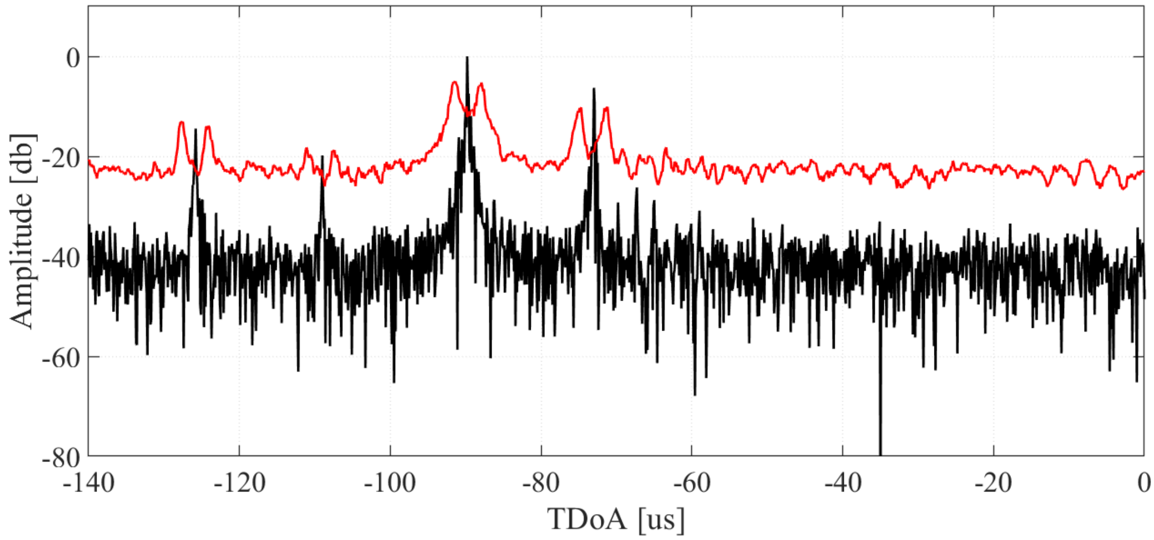

Figure 49. Cross-correlation function of real-life data (scenario 1, position 5) and CA-CFAR threshold (red).

- The next step was to create six permutations of the three remaining peaks. All of those permutations consisted of two circles (peaks P_3 and P_4) and a single hyperbola (peak P_2) as shown in Figure **50**. Permutations where those tree curves did not intersect at a single point or in close proximity were discarded. In this geometry, that constraint meant that in all measurements, four out of six permutations were rejected, leaving two permutations with two possible locations of Tx_2 (algorithm step from Chapter 4.1.3).
- Now, as the last step, some of those locations need to be dismissed. At this point, an additional set of AOA measurements was made (for every position of the mobile receiver). In a stationary station, a directional antenna was pointed towards one plausible location of Tx_2, and data was gathered from both receivers. The next cross-correlation was calculated, and the amplitude of measured peaks corresponding with P_2 (the peak corresponding with TDOA caused by Tx_2) was noted. This procedure was repeated for all plausible locations. Plausible location where P_2 had the highest amplitude becomes the estimated position of Tx_2 (algorithm step from Chapter 4.1.4).

With the end of this procedure, a single estimate of Tx_2 location was acquired for every one of the nine measurements. In Table **8**, the exact position of each peak on the cross-correlation plot and the final positioning error were shown. A visualisation of the results for measurement number 1 is shown in Figure **50**. The mean error of all measurements is 363.55 metres. It should be kept in mind that the entire algorithm is based on two-dimensional geometry due to the constraint of a single pair of receivers. After also taking into account that the height of Tx_2 is

319 metres, the true Tx_2 position is ambiguous (see Chapter 6.2.1) and the GPS synchronisation accuracy is equal to 50 ns (RMS 1-Sigma) or 15m (RMS 1-Sigma) after recalculation, such a value of the positioning error is within the experimental constraints.

Table 8. Results of localisation of unknown SFN transmitter algorithm.

Measurement number	1	2	3	4	5	6	7	8	9
P1 [μs]	-3.1	-10.8	-24.1	-53.3	-73.0	-104.0	-145.3	-182.1	-233.2
P2 [μs]	-25.8	-50.0	-67.4	-103.2	-125.8	-157.1	-199.4	-239.0	-293.5
P3 [μs]	-9.1	-33.2	-50.6	-86.5	-109.0	-140.3	-182.7	-222.3	-276.8
P4 [μs]	-19.8	-27.5	-40.9	-70.1	-89.8	-120.8	-161.2	-198.8	-250.0
Localisation error [m]	372.05	370.88	395.39	444.39	397.56	394.66	186.91	344.56	365.60

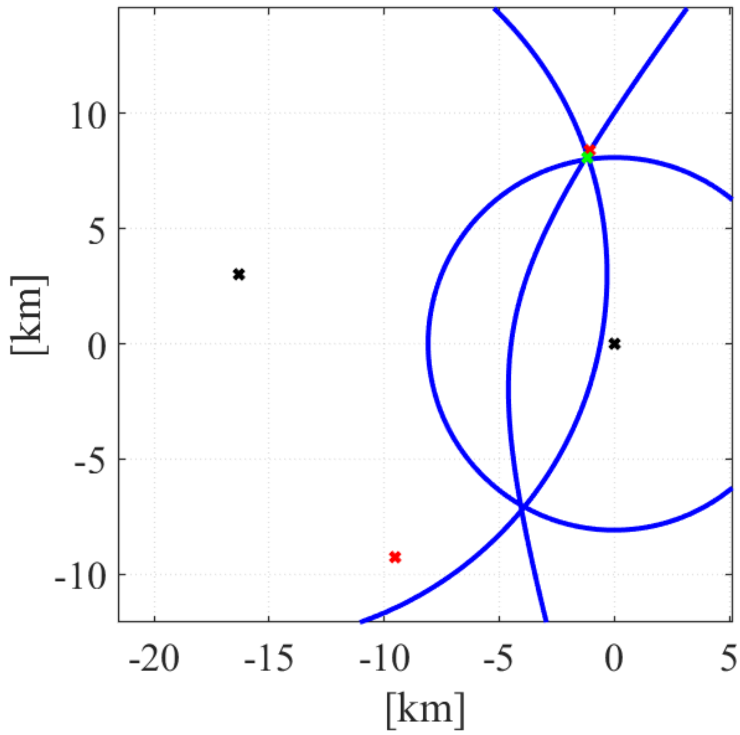

Figure 50. Localisation curves for measurement number 1. Estimated Tx_2 position is marked with a green colour, the true transmitter positions with a red colour and the receiver positions in a black colour.

6.6. Time desynchronisation calculation

In order to confirm the accuracy of the algorithm presented in Chapter 4.4 and authenticate the simulations from Chapter 5.5, the complete set of algorithmic steps were executed using real-life data:

- As in Chapter 6.5, no additional digital signal conditioning was done. A cross-correlation was calculated (algorithm step from chapter 4.4.1). Example results are presented in Figure **32**.
- Using a priori information about the transmitter and receiver's approximate locations, the positions of both TDOA peaks (P_1 and P_2) on the cross-correlation plot were calculated using (96) and (97) for all pairs of receivers. These two positions were the basis for identifying P_1 and P_2 in the cross-correlation plot. Other two peaks were classified as ghost peaks (P_3 and P_4). This fulfils the algorithm step described in Chapter 4.4.2.
- Using identified TDOA peaks from the cross-correlation plot and the localisation method from Chapter 3.5.5, the estimated positions of both Tx_1 and Tx_2 were calculated (algorithm step from Chapter 4.4.3).
- Using the estimated localisation of Tx_1,Tx_2 (and the know positions of the receivers) the positions of P_3 and P_4 ghost peaks were calculated using (98) and (99). This calculation will result in positions of P_3 and P_4 as if no desynchronisation was present. This satisfies the algorithm step described in Chapter 4.4.4.
- Lastly, the final step of the algorithm was done. By comparing the measured position of ghost peaks from the previous step with their calculated positions, a desynchronisation estimate was acquired.

Table 9. TDOA Peaks results.

TDOA peaks [µs]	P_1 true calc.	P_1 meas.	P_1 diff.	P_2 true calc.	P_2 meas.	P_2 diff.
Rx_1-Rx_2	8.47	8.10	0.37	-32.63	-32.80	0.17
Rx_1-Rx_3	22.00	21.70	0.30	-52.73	-15870	0.17
Rx_1-Rx_4	13.85	13.40	0.45	-44.03	-44.10	0.07
Rx_2-Rx_4	-5.38	-5.30	-0.08	11.40	11.3	0.10
Rx_3-Rx_2	13.53	13.60	-0.07	-20.10	-6060	0.10
Rx_3-Rx_4	8.14	8.20	-0.06	-8.71	-2520	-0.31

Table 10. Ghost Peaks results.

Ghost peaks [µs]	P_3 calc.	P_3 meas.	P_3 diff.	P_4 calc.	P_4 meas.	P_4 diff.
Rx_1-Rx_2	-14.55	-11.10	-3.45	-9.61	-12.7	3.09
Rx_1-Rx_3	-34.65	-31.3	-3.35	3.92	0.10	3.82

Rx_1-Rx_4	-25.95	-22.90	-3.05	-4.23	-8.20	3.97
Rx_2-Rx_4	-28.40	-24.50	-3.90	34.42	30.60	3.82
Rx_3-Rx_2	-43.12	-39.40	-3.72	36.55	32.80	3.75
Rx_3-Rx_4	-48.51	-44.70	-3.81	47.94	44.10	3.84

The results for each pair of receivers are presented in Table **9** (for P_1 and P_2) and Table **10** (for P_3 and P_4). In Table **9**, the second column shows the position of P_1 calculated by using Tx_1 true localisation. The third column presents the actual position of P_1 in the cross-correlation plot, and the fourth column holds the difference between those two values. The next part of Table **9** hold the same information about P_2.

Table **10** in column two holds a P_3 position calculated using estimated localisation of Tx_1, Tx_2 (instead of true positions known a priori). The next column is the actual position of P_3 in the cross-correlation plot, and the fourth column shows the difference between those two values. Again, the same information about P_4 can be found in the second part of Table **10**.

The difference between the calculated and the measured values of P_3 and P_4 can be interpreted as the value of desynchronisation between Tx_1 and Tx_2. By averaging all measurement errors, desynchronisation is estimated to be 3.63 μs. The impact of such desynchronisation on target location in passive radar is studied in Chapter 6.7.

6.7. Desynchronisation Impact on PCL

To show how desynchronisation affects passive radar localisation errors in a single reference signal scenario, a set of simulations was performed. In each of the simulations, the positions of both transmitters and all receiver stations remain the same as in scenario 2. Transmitter desynchronisation is set to a value of 3.63 μs as estimated in the experiment. Lastly, the position of the target was randomly chosen within 50 km from the midpoint of the transmitters. For each of the four receivers, a pair of ellipses can be found. Each ellipse corresponds to the signal transmitted by one of the emitters and is reflected by the target. With two ellipses, it is possible to find the point of their interception. The final result of the simulation is a distance measured in meters between the intersection point and the actual target position. When the desynchronisation of the transmitters is set to zero, this distance is shorter than 10^{-4} meters. The non-zero value is a product of numerical errors of the algorithm responsible for finding the intersection point.

A total of 10^4 simulations for each surveillance station using the Monte Carlo method were made, each with a different target position. A visual example of a simulation is presented in Figure **51**, and the simulations results are summarized in Table **11**.

7. Table 11. Simulation Results of Localisation Error.

	Rx 1	Rx2	Rx 3	Rx 4
mean error [m]	1.892e3	1.954e3	1.913e3	2.091e3
variance [m^2]	1.495e6	1.558e6	1.547e6	1.431e6

Depending on the geometry of the target and receiver, desynchronisation of transmitters equal to the measured 3.63 μs can introduce on average a 2 km error in passive radar localisation for the geometry assumed in the simulation. In extreme cases, the error can reach over 6 km. Using the proposed method, the desynchronisation error can be eliminated or greatly mitigated.

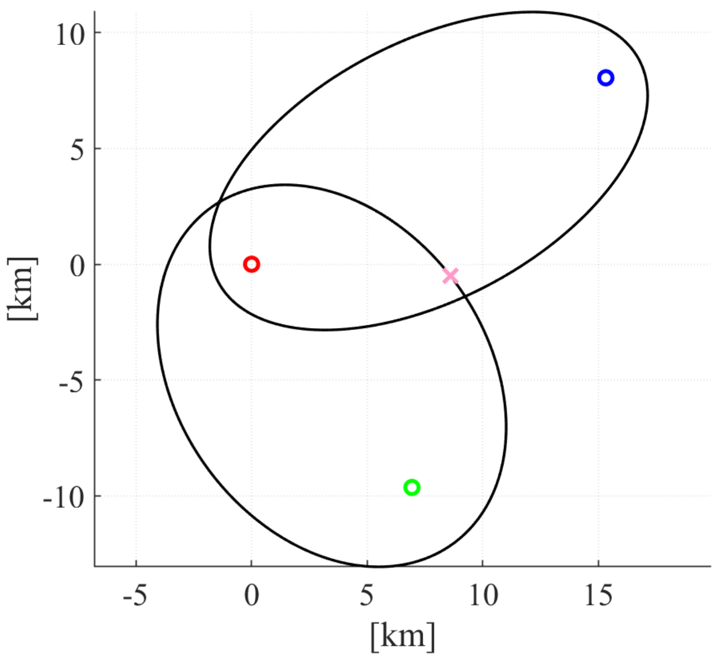

Figure 51. Visual example of a single simulation for the receiver in Pruszków (red marker) and two transmitters (Raszyn - green marker, PKiN - blue marker). Target's position (marked with pink cross) does not match the ellipses intersection point due to transmitter desynchronisation.

8. SUMMARY

The dissertation has shown the two innovative methods. The first is the method for estimating the desynchronisation of DVB-T transmitters operating in SFN. A common assumption is that SFN transmitters are time-synchronized. The author challenges that assumption and provides an algorithm that provides a desynchronisation estimate that can be used in further passive radar signal processing. The author shows that ignoring desynchronisation in passive radar processing may lead to substantial errors in target positioning. The described method can help alleviate those errors, significantly improving passive radar performance. The second of the two is the method for localising weak and unidentified transmitters operating in SFN together with strong transmitters whose existence was anticipated. Most of the analyses of passive radar systems working in an SFN focus on removing or filtering the side effects of operating in an SFN. In this thesis, another approach was taken, and a constructive use of SFN side effects was proposed that allowed the development of the algorithm that realises the second method. Passive radar users can benefit from both methods as useful tools during the mission planning phase and also while the radar is actively operating.

In this thesis the author gives an introduction to passive radiolocation basics, followed by state of the art and literature review of well-established passive localisation techniques. Then the author presents the principle of passive radar systems working in an SFN environment. The main part of the work is a detailed description of the developed algorithms, broken down into step by step explanation and followed by simulation and real-life data verification of those algorithms. The algorithms presented in this thesis were implemented in the MATLAB environment. The signal processing results obtained as the outcome of this study have shown conformity with the algorithmic possibilities envisaged in the thesis.

The author's main contributions are:

- Conducting a comprehensive TDOA transmitter localisation techniques analysis;
- Development of an novel algorithm for estimating desynchronisation of transmitters operating in Single Frequency network [21];
- Conducting a comprehensive TDOA transmitter localisation techniques analysis;
- Development of a novel algorithm for estimating time desynchronisation of transmitters operating in single frequency network [21];

- Development of a novel algorithm for localising secondary transmitters operating in Single Frequency network;
- The design and construction of a system comprising synchronized portable receivers and a central processing station. System was built using Commercial Off-The-Shelf (COTS) components and is capable of processing data in real time [22];
- Verification of the developed algorithms on simulated and experimental data [21].

8.1. Conclusions

Simulation experiments and an experiment using data gathered by a network of surveillance stations confirm both thesis stated at the beginning, that:

It is possible to estimate time desynchronisation of DVB-T transmitters operating in Single Frequency Network using only Time Difference of Arrival measurements.

It is possible to localise secondary DVB-T transmitters operating in Single Frequency Network using only Time Difference of Arrival measurements from pair of receivers.

The results of the dissertation can be used by research and development institutions and radar manufacturing industry [6][7][8] through their implementation and deployment of new algorithms in passive radars. This could be significant in promoting the innovative potential of radiolocation companies that are interested in passive radar technology and operate in both the Polish and global markets.

Just a year after publishing results of performance of algorithm for estimating time desynchronisation of transmitters operating in single frequency network [21], presented in Chapter 4.4, very similar approach of solving the same problem was successfully used in passive radar developed by Hensoldt [52].

8.2. Further work

The author of the thesis sees two main strands of further work on the algorithms proposed in this thesis. The first one is to analyse the algorithms from the perspective of networks operating in SFN in configurations of three or more transmitters. Ultimately, tools based on such algorithms could, relying on knowledge about a single transmitter, identify and locate the entire network of SFN transmitters and provide time delays between their broadcasts. Such knowledge could provide invaluable assistance in any future SFN-capable localisation technique or algorithm. At the beginning of the work on this thesis, the problem of SFN in

Poland was mainly in the vicinity of Warsaw, where there were two DVB-T transmitters in Raszyn and PKiN, which were used for the study. Due to the rapid expansion of the network of transmitters, now there are many places in Poland where it would be possible to carry out a scenario with the necessary transmitters.

The second is to adapt the solutions proposed in this work to existing research and commercial platforms. Such an opportunity would allow further research and modification of the algorithms so that they become universal tools working optimally regardless of the type and capabilities of the platform on which they are implemented. It seems clear that the rapid development of passive radiolocation with the parallel expansion of commercial broadcasting networks (e.g. DVB-T and FM transmitters) and especially SFNs will make passive radar mission planning tools essential. The algorithms presented in this work seem to be an ideal foundation to start research and development of these tools. In the author's opinion, the topics covered in this work are particularly important for passive airborne radars: PCL radars and passive synthetic aperture radars. Such platforms, due to their altitude, detect signals from a larger number of transmitters and the problems of synchronising SFN transmitters are potentially much more common.

Bibliography

[1] Richards Mark A. *Fundamentals of Radar Signal Processing.* Third ed. McGraw-Hill (2022).

[2] Bar-Shalom Yaakov and Xiao-Rong Li. *Multitarget-Multisensor Tracking : Principles and Techniques* Yaakov Bar-Shalom (1995).

[3] Baker, Christopher.J. and Hugh D. Griffiths. *An Introduction to Passive Radar* (2017).

[4] Skolnik, Meerill I. *Radar Handbook, Electronics electrical engineering.* Third Edition McGraw-Hill Education, (2008).

[5] Erhart, Christian et al. *Availability Analysis of PCL Passive Radar Systems for ATC Applications.* 2022 14th German Microwave Conference (GeMiC) (2022): 128-131.

[6] Hensoldt AG. *Twinvis Passive Radar (2022)* https://dam.hensoldt.net/m/51e84e07b501246e/original/TwInvis-Passive-Radar-Datasheet-English.pdf

[7] Patria MUSCL *Passive Rader System* (2021) https://www.patriagroup.com/download/patria-muscl-brochure-2021

[8] Pitradwar. *Passive Location System* (2022) https://en.pitradwar.com/file/3ac605b0-2eb4-11e9-a3c4-ac1f6b452b8a

[9] Bok, Dominik. *Reconstruction and Reciprocal Filter of OFDM Waveforms for DVB-T2 Based Passive Radar.*2018 International Conference on Radar (RADAR) (2018): 1-*6.*

[10] Bączyk, Marcin K. and Mateusz Malanowski. *Reconstruction of the Reference Signal in DVB-T-based Passive Radar “*International Journal of Electronics and Telecommunications 57, nr 1 *(*2011):

[11] O’Hagan, Daniel W. et al. *Passive Bistatic Radar (PBR) for harbour protection applications*. 2012 IEEE Radar Conference (2012): 0446-0450.

[12] Poullin, Dominique and Marc Flecheux. *Passive 3D tracking of low altitude targets using DVB (SFN Broadcasters)*. IEEE Aerospace and Electronic Systems Magazine 27 (2012): 36-41.

[13] Polonen, Keijo and Visa Koivunen. *Measurement association in SFN passive radar systems*.” 2015 IEEE Radar Conference (RadarCon) (2015)

[14] Yan, Jun and Lenan Wu. *A passive location system for single frequency networks using digital terrestrial TV signals*. Eurpean Transactions on Telecommunications 22 (2011)

[15] Juryca, Karel et al. *DVB-T signal analysis on passive coherent location system in single frequency network.* 2016 International Conference on Advanced Computer Science and Information Systems (ICACSIS) (2016): 43-53.

[16] Daun, Martina and Wolfgang Koch. *Multistatic target tracking for non-cooperative illumination by DAB/DVB-T.* 2008 IEEE Radar Conference (2008): 1-6.

[17] Daun, Martina and Christian R. Berger. *Track initialization in a multistatic DAB/DVB-T network*. 2008 11th International Conference on Information Fusion (2008): 1-8.

[18] Yi, Jianxin et al. *Deghosting for target tracking in single frequency network based passive radar*. IEEE Transactions on Aerospace and Electronic Systems 51 (2015)

[19] Zhang, Yimin D. and Braham Himed, *Moving target parameter estimation and SFN ghost rejection in multistatic passive radar*. 2013 IEEE Radar Conference (RadarCon13) (2013): 1-5.

[20] Taufik, Imam et al. *Total War Strategy with Passive Radar Operation.* (2021).

[21] Klincewicz, Karol and Piotr Samczyński. *Method of Calculating Desynchronization of DVB-T Transmitters Working in SFN for PCL Applications*. Sensors (Basel, Switzerland) vol. 20, 20 (2020)

[22] Klincewicz, Karol. *Demonstrator of the SDR-based multistatic system for localizing different sources of emissions*. 2016 17th International Radar Symposium (IRS) (2016): 1-4.

[23] Skolnik, Merril I. *Introduction to Radar Systems,* 3rd Edition, McGraw-Hill, New York, (2001*).*

[24] Wielgo, Maciej, et al. *Doppler Only Localization in GSM-Based Passive Radar. the Concept and Simulation Results*. Proceedings of International Radar Conference 2014, edited by , Clearance Center (2014)

[25] Habaebi, Mohamed Hadi et al. *RSS Based Localization Techniques for ZigBee Wireless Sensor Network*. 2014 International Conference on Computer and Communication Engineering (2014) :72-75.

[26] Zegeye, Wondimu K. et al. *WiFi RSS fingerprinting indoor localisation for mobile devices.*" 2016 IEEE 7th Annual Ubiquitous Computing, Electronics & Mobile Communication Conference (UEMCON) (2016): 1-6.

[27] Waadt, Andreas et al. *Positioning in multiband OFDM UWB utilizing received signal strength*. 2010 7th Workshop on Positioning, Navigation and Communication (2010): 308-312.

[28] Cao, Yuan et al. *Measurement and Analysis of RSS Using Bluetooth Mesh Network for Localization Applications*. Network (2021).

[29] Richards, Mark A. et al. *Principles of Modern Radar : Basic Principles.*(2010).

[30] Klemm, Richard and Nickel Urlich, Gierull Christoph, Lombardo Pierfrancesco, Hugh D. Griffiths, Wolgang Koch,. *Novel Radar Techniques and Applications* (2017).

[31] Koç, Arzu Tuncay et al. *Direction finding with a circularly rotated antenna.* IEEE International Conference on Acoustics, Speech, and Signal Processing. Proceedings (2000).

[32] Roy, Richard H. and Thomas Kailath. *ESPRIT-estimation of signal parameters via rotational invariance techniques.* IEEE Trans. Acoust. Speech Signal Process. 37 (1989).

[33] Chen, Yinjie et al. *Theory underlying measurement of AOA with a rotating directional antenna.* 2013 Proceedings IEEE INFOCOM (2013).

[34] Friedlander, Benjamin*. A passive localisation algorithm and its accuracy analysis.* IEEE Journal of Oceanic Engineering 12 (1987): 234-245.

[35] Foy, Wade H. *Position-Location Solutions by Taylor-Series Estimation.* IEEE Transactions on Aerospace and Electronic Systems AES-12 (1976): 187-194.

[36] Fang, Bertrand T. *Simple solutions for hyperbolic and related position fixes.* IEEE Transactions on Aerospace and Electronic Systems 26 (1990): 748-753.

[37] Chan, Yiu Tong and K. C. Ho. *A simple and efficient estimator for hyperbolic location.* IEEE Trans. Signal Process. 42 (1994): 1905-1915.

[38] Schau, Harvey C. and A. Z. Robinson. *"Passive source localisation employing intersecting spherical surfaces from time-of-arrival differences*. IEEE Trans. Acoust. Speech Signal Process. 35 (1987): 1223-1225.

[39] Smith, Julius Orion and Jonathan S. Abel. *The spherical interpolation method of source localisation.* IEEE Journal of Oceanic Engineering 12 (1987): 246-252.

[40] Li, Xinya et al. *Contributed Review: Source-localisation algorithms and applications using time of arrival and time difference of arrival measurements*. The Review of Scientific Instruments 87, 4 (2016):

[41] International Telecommunication Union. *Digital Terrestrial Broadcasting: Design and Implementation of Single Frequency Networks (SFN). Report ITU-R BT.2386-2.04/2019* (2019).

[42] Wan, Xianrong et al. *Experimental Research for CMMB-Based Passive Radar Under a Multipath Environment*. IEEE Transactions on Aerospace and Electronic Systems 50 (2014): 70-85.

[43] Colone, Fabiola et al. *WiFi-Based Passive Bistatic Radar: Data Processing Schemes and Experimental Results*. IEEE Transactions on Aerospace and Electronic Systems 48 (2012): 1061-1079.

[44] Pallàs-Areny, Ramon and John G. Webster. *Sensors and Signal Conditioning* (1993).

[45] Raout, Jacques et al. *Passive bistatic noise radar using DVB-T signals*. Iet Radar Sonar and Navigation 4 (2010): 403-411.

[46] Gao, Zhiwen et al. *DVB-T Signal Cross-Ambiguity Functions Improvement for Passive Radar.* 2006 CIE International Conference on Radar (2006): 1-4.

[47] Rohling, Hermann. *Radar CFAR Thresholding in Clutter and Multiple Target Situations*. IEEE Transactions on Aerospace and Electronic Systems AES-19 (1983): 608-621.

[48] Antipov, Irina and John Baldwinson. *Estimation of a Constant False Alarm Rate Processing Loss for a High-Resolution Maritime Radar System.* (2008).

[49] Reed, Irving S. and Xiaoli Yu. *Adaptive multiple-band CFAR detection of an optical pattern with unknown spectral distribution*." IEEE Trans. Acoust. Speech Signal Process. 38 (1990): 1760-1770.

[50] Klocek, Jędrzej. *Mapy Serwisu RadioPolska.pl* https://mapy.radiopolska.pl/

[51] Budge, Mervin, Shawn R. German, *Basic Radar Analysis.* Artech, (2020).

[52] Winkler, Volker et al. *Expert Systems for Passive Radar Configuration*. 21st International Radar Symposium (IRS) (2021): 1-10.

[53] Schmidt, Ralph O. *A New Approach to Geometry of Range Difference Location.* IEEE Transactions on Aerospace and Electronic Systems AES-8 (1972): 821-835.

[54] Smith, Julius Orion and Jonathan S. Abel. *Closed-form least-squares source location estimation from range-difference measurements*. IEEE Trans. Acoust. Speech Signal Process. 35 (1987): 1661-1669.

[55] Melvin, William L. and James A. Scheer. *Principles of Modern Radar: Advanced techniques.* (2012).

[56] Scheer, James A. and William L. Melvin*. Principles of modern radar : radar applications.* (2013).

[57] Mahafza, Bassem R. *Radar Signal Analysis and Processing Using MATLAB.* (2008).

[58] Barton, David K. and Sergey A. Leonov. *Radar Technology Encyclopedia.* (1997).

[59] Griffiths, H. D. *From a different perspective: principles, practice and potential of bistatic radar* 2003 Proceedings of the International Conference on Radar (IEEE Cat. No.03EX695) (2003): 1-7.

[60] Torrieri, Don J. *Statistical Theory of Passive Location Systems.* IEEE Transactions on Aerospace and Electronic Systems AES-20 (1984): 183-198.

[61] Malanowski, Mateusz and Krzysztof S. Kulpa. *Two Methods for Target Localisation in Multistatic Passive Radar*. IEEE Transactions on Aerospace and Electronic Systems 48 (2012): 572-580.

[62] Yi, Jianxin et al. *MIMO Passive Radar Tracking Under a Single Frequency Network*. IEEE Journal of Selected Topics in Signal Processing 9 (2015): 1661-1671.

[63] Petri, Dario et al. *The effects of DVB-T SFN data on passive radar signal processing*. 2013 International Conference on Radar (2013): 280-285.

[64] Rzewuski, Stanislaw et al. *Multistatic Wireless Fidelity Network Based Radar – Results of the Chrcynno Experiment*. Radioengineering 23 (2014): 30-40.

[65] Rzewuski, Stanislaw et al. *Supersonic target detection in passive radar*. 2015 16th International Radar Symposium (IRS) (2015): 89-94.

[66] Samczyński, Piotr Jerzy, et al. *Recent Results of High Resolution Ground Image Formation Using Miniaturized C-Band Synthetic Aperture Radar*. Proceedings of EUSAR 2016: 11th European Conference on Synthetic Aperture Radar, edited by , VDE, 2016, pp. 143–147.

[67] Drozdowicz, Jędrzej, et al. *The Use of FPGA Evaluation Board as Data Acquisition and Pre-Processing System for Synthetic Aperture Radar*. Proceedings of the International Radar Symposium IRS 2015, edited by Hermann Rohling, German Institute of Navigation (DGON), CUVILLIER VERLAG, 2015, pp. 535–540.

[68] Samczyński, Piotr Jerzy, et al. *Experimental Results of DANIEL-35 SAR System Tests*. Proceedings of the International Radar Symposium IRS 2015, edited by Hermann Rohling, German Institute of Navigation (DGON), CUVILLIER VERLAG, 2015, pp. 571–576.

[69] Radmard, Mojtaba et al. *"Data Fusion in MIMO DVB-T-Based Passive Coherent Location.* IEEE Transactions on Aerospace and Electronic Systems 49 (2013): 1725-1737.

[70] Radmard, Mojtaba et al. *Spatial Diversity Gain of MIMO Single Frequency Network in Passive Coherent Location*. Scientia Iranica 21 (2014): 2186-2199.

[71] Wang, Hui et al. *Tracking Algorithm with Data Fusion in Single Frequency Network-based MISO Passive Radar*. 2018 12th International Symposium on Antennas, Propagation and EM Theory (ISAPE) (2018): 1-3.

[72] Juryca, Karel et al. *Targets detection analysis in the passive coherent location system in single frequency network*. 2016 International Conference on Advanced Computer Science and Information Systems (ICACSIS) (2016): 123-129

[73] Chongyang, He. *A De-ghosting Technique for Passive Coherent Location With Transmitter Origin Uncertainty.* (2015).

[74] Chitgarha, Mohammad Mahdi et al. *The detector's output SNR as a criterion for receiver placement in MIMO DVB-T based passive coherent location*. 2012 IV International Congress on Ultra Modern Telecommunications and Control Systems (2012): 431-435.

[75] Wojaczek, Philipp et al. *Results of Airborne PCL Under CCI Conditions Using DVB-T Illuminators of Opportunity*. 2018 International Conference on Radar (RADAR) (2018): 1-6.

[76] Kaune, Regina. *Accuracy studies for TDOA and TOA localisation*. 2012 15th International Conference on Information Fusion (2012): 408-415.

[77] Subramaniam, V. R. *Digital video broadcasting (DVB); framing structure, channel coding and modulation for digital terr.* (2001).

[78] Malanowski, Mateusz Piotr. *Optymalizacja Przetwarzania Sygnałów w Radarach z Pasywną Koherentną Lokalizacją Obiektów*. IX Seminarium z cyklu Radiokomunikacja i Techniki Multimedialne, (2008): 45–54.

[79] Radmard, Mojtaba et al. *MIMO PCL in a single frequency network*. 2011 Microwaves, Radar and Remote Sensing Symposium (2011): 280-283.

[80] Gassier, Ghislain et al. *Passive Covert Radars using CP-OFDM SFN. Reference signal recovery from blind beamforming*. (2014).

[81] Poullin, Dominique et al. *New challenges for PCL system : 3D requirements and "Optimal" resources management for PCL air traffic survey*. 11-th International Radar Symposium (2010): 1-3.

[82] Radmard, Mojtaba et al. *Data association in multi-input single-output passive coherent location schemes.* Iet Radar Sonar and Navigation 6 (2012): 149-156.

[83] Dominique, Poullin. *Passive Radar using COFDM (DAB or DVB-T) Broadcasters as Opportunistic Illuminators.* (2010).

[84] Bok, Dominik et al. *A multistatic passive coherent location system with receiver location constraints*. 2017 18th International Radar Symposium (IRS) (2017): 1-10.

[85] Choi, Sora et al. *Target tracking for multistatic radar with transmitter uncertainty*. Optical Engineering + Applications (2009).

[86] Peng, Xiaoting et al. "*Subcarrier-based tomographic imaging for single-frequency network passive radar with orthogonal frequency-division multiplexing waveform*. Iet Radar Sonar and Navigation 10 (2016): 546-552.

[87] Schüpbach, Christof et al. *Passive Radar Illuminator Identification in Single Frequency Networks.* 2019 IEEE Radar Conference (RadarConf) (2019): 1-5.

[88] Winkler, Volker et al. *Transmitter identification and single frequency network characterization for the CASSIDIAN passive radar sensor*. 2013 14th International Radar Symposium (IRS) 1 (2013): 167-172.

[89] Winkler, Volker et al. *Characterization of Single Frequency Networks for Passive Radar Applications*. 2020 17th European Radar Conference (EuRAD) (2021): 354-357.

[90] Bialkowski, Konstanty S. and I. Vaughan L. Clarkson. *Passive radar signal processing in single frequency networks.* 2012 Conference Record of the Forty Sixth Asilomar Conference on Signals, Systems and Computers (ASILOMAR) (2012): 199-202.

[91] El Gonnouni, Amina and Frédéric Lehmann. Deghosting method for multiple target tracking in a single frequency network. 2014 International Radar Conference (2014): 1-6.

[92] Ummenhofer, Martin et al. *Direction of Arrival Estimation Techniques for Passive Radar based 3D Target Localization*. 2019 IEEE Radar Conference (RadarConf) (2019): 1-6.

[93] Huang, Jamie H. et al. *Array based passive radar target localization.* 2016 IEEE Radar Conference (RadarConf) (2016): 1-6.

[94] Emitel https://emimaps.emitel.pl (2023)